Solitary chemosensory cells in the respiratory tract of man

Inaugural Dissertation

submitted to the

Faculty of Medicine

in partial fulfillment of the requirements

for the PhD-Degree

of the Faculties of Veterinary Medicine and Medicine

of the Justus Liebig University Giessen

by

Hamarsheh, Dima

from

Jordan

Giessen 2023

From the Institute of Anatomy and Cell Biology

Cardiopulmonary Neurobiology

Head: Prof. Wolfgang Kummer

Of the Faculty of Medicine of the Justus Liebig University Giessen

First Reviewer and Committee Member: Prof. Dr. Wolfgang Kummer

Second Reviewer and Committee Member: Prof. Dr. Christian Mühlfeld

Vice-chair and Committee Member: Prof. Dr. Ivan Manzini

Chairman and Committee Member: Prof. Dr. Martin Diener

Date of Doctoral Defense 24/10/2023

Table of contents

Table of contents

List of abbreviations

ACh	Acetylcholine
ASCL3	Achaete-scute homolog 3
BM	Basement membrane
CALHM1	Calcium homeostasis modulator
CDH	Congenital diaphragmatic hernia
CGRP	Calcitonin gene-related peptide
ChAT	Choline acetyltransferase
CFTR	Cystic fibrosis transmembrane regulator
DCLK1	Doublecortin like kinase 1
DCV	Dense core vesicles
D	Dorsal bronchial system
DOPA	Dihydroxyphenylalanine
DAPI	4’,6-Diamidino-2-phenylindol
E	Embryonic day
ER	Endoplasmic reticulum
EDTA	Ethylenediaminetetraacetic acid
FOXI1	Forkhead family transcription factor
GDP	Guanosine diphosphate
GTP	Guanosine triphosphate
GRP	Gastrin-releasing peptide
GNAT3	Guanine nucleotide-binding protein G (t) subunit alpha-3
HBECs	Primary human bronchial epithelial cells
HCN4	Potassium/sodium hyperpolarization-activated cyclic nucleotide-gated channel 4
5-HTP	5-hydroxytryptophan or serotonin
IP3	Inositol trisphosphate
IP3R3	Inositol 1,4,5-trisphosphate receptor, type 3
LRMP	Lymphoid restricted membrane protein

List of abbreviations

L	Lateral bronchial system
M	Medial bronchial system
nAChRs	Nicotinic acetylcholine receptors
NSE	Neuron-specific enolaze
NEBs	Neuroepithelial bodies
OE	Olfactory epithelium
PLCβ2	Phospholipase Cβ2
PGP 9.5	Protein gene product 9.5
ROBO	Human roundabout receptor
SCLC	Human small cell lung cancer
ScRNAseq	Single cell RNA sequencing
SIDS	Sudden infant death syndrome
SE	Squamous epithelium
TRPM5	Transient receptor potential cation channel subfamily M member 5 channel
TE	Transitional epithelium
TasR	Taste receptors
Tas1R	Taste receptor family 1
Tas2R	Taste receptor family 2
TM	Transmembrane domain
V	Ventral bronchial system

1 Introduction

1.1 Gross anatomy of the airways

The lower respiratory system of the mouse is divided into two functional and structural elements; the conducting and respiratory zone. The conducting part is composed of airways that allow gases to pass into and out of the lung. It is consists of trachea and bronchus down to the terminal bronchioles. The respiratory zone comprises the respiratory bronchioles, alveolar ducts, alveolar sacs, and alveoli. The mouse trachea consists of 15-18 C-shaped cartilaginous rings for airway support to protect it from collapsing. These rings are opened posteriorly and closed by a fibromuscular membrane connecting the free ends of the rings (Treuting et al. 2017). The diameter of the trachea (~1.5 mm) in mice is equal to the diameter of small airways in human lung (Rock et al. 2010). The trachea divides into right and left main bronchi at the carina. These bronchi enter the lung and divide into the intrapulmonary bronchi, which lack cartilage in mice, in a monopodial pattern. A difference between mouse and human is in that cartilage can be found in many bronchial generations in the human lung. The right intrapulmonary bronchus divisions supply cranial, middle, caudal and accessory lobes, while the left intrapulmonary divisions divides to supply the left lung (Treuting et al. 2017). At embryonic day (E) 9.5, two lung buds arise in mouse (Hogan et al. 2014) (Figure 1.1).

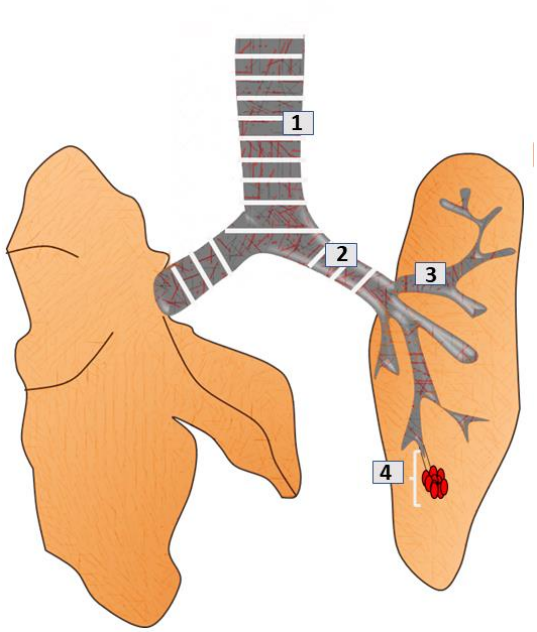

Figure 1.1: Anatomy of mouse lower airways.

The trachea (1) bifurcates into primary bronchi (2), which divide into six to eight generations of intrapulmonary airways (3). The respiratory zone is marked by (4).

The respiratory tract in pig is composed of upper and lower parts. The upper part includes the nasal cavity and nasopharynx, and the lower respiratory tract starts with the larynx and extends down to the lung. The trachea is built up by C-shaped cartilaginous rings interconnected by a fibroelastic membrane and the trachealis muscle. It bifurcates at the level of the heart. The porcine trachea is much longer than human trachea with more cartilages. The Belgian landrace pig trachea, for example, has a length of 15 to 20 cm with 32 to 45 hyaline cartilaginous rings (Judge et al. 2014). The porcine lung consists of dorsal, ventral, lateral and medial bronchial system. Additionally, one bronchus is coming from the right side of the trachea proximal to its bifurcation. This corresponds to the right cranial lobe bronchus III in human. This bronchus separates into cranial and caudal parts to supply the right upper lobe. The right middle lobe bronchus arises from the lateral bronchial system, as a first branch in this system (L1), forming the right middle lobe. Furthermore, another bronchus arises from the ventral bronchial system, as a first branch in this system (V1), and forms the accessory lobe. The right caudal lobe is formed by

bronchi from the remaining lobes of the dorsal (D2 to D6), lateral (L2 to L6), medial (M4) and ventral bronchial system (V2 to V5). So, the right lung includes cranial, middle, caudal and accessory lobes. Between cranial and middle lobe, there is a cardiac notch. On the other hand, there is an incomplete interlobular fissure located between the middle and caudal lobe. In the left lung, the left middle lobe bronchus originates from the left bronchus; this is the first bronchus (L1). It forms the lateral bronchial system, which further divides into cranial and caudal parts. This bronchus forms the left middle lobe with a deep cardiac notch. The left caudal lobe is formed by the remaining bronchi of the lateral bronchial system (L2 to L6), medial bronchial system (M4, 5) and dorsal bronchial system (D2 to D7). So, the left lung includes the bilobed middle lobe and the caudal lobe (Nakakuki 1994). There are significant differences in airway geometry between human and pig. In pig, there is an early bronchus coming from the trachea which forms the upper right lung lobe; this is not the case in human (Azad et al. 2016) (Figure 1.2).

Another difference between human and pig is in the appearance and number of airway structures in fetal and newborn lung. In pig, each terminal bronchiole branches into two or three respiratory bronchioles. Furthermore, each respiratory bronchiole divides into two alveolar ducts which at birth look like a sac containing alveoli. In human, two or three of the respiratory bronchioles are generated at birth with two or three saccules (alveolar ducts progenitors). At birth, the acinus is longer in human than in pig (1.1 mm in human, 0.5 mm in pig) (Haworth and Hislop 1981).

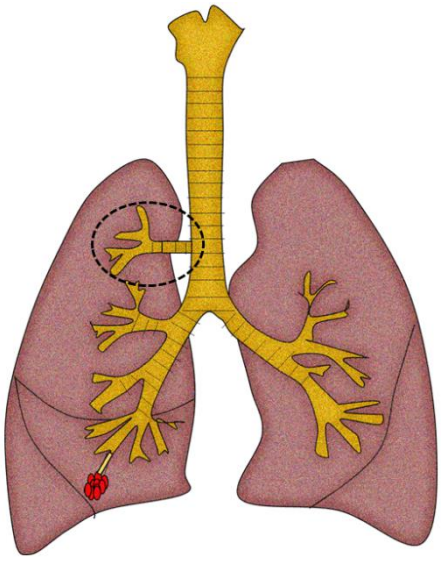

Figure 1.2: Anatomy of pig lower airways and lung.
Same as human structural organization, but in pig there is an early bronchus coming from the trachea and providing the upper right lung lobe (dotted circle).

The human nose is the gateway for the respiratory system. It is involved in smelling, air conditioning, filtering, humidifying and warming the inhaled air, so it acts as a lower respiratory tract defender. The nasal septum divides the nasal cavity into two air passages; each passage extends from the nares to the nasopharynx. The inhaled air passes through the nares into the vestibule, which is surrounded by flexible cartilage in contrast to the more distal main chamber, which is surrounded by bone. Turbinates are bony structures projecting from the lateral wall into the main chamber of the nose. There are three turbinates, termed the superior, middle and inferior turbinate. The respiratory system is divided into structural and functional parts: the conducting and respiratory zones. The conducting zone includes the trachea and bronchi and extends up to the terminal bronchioles. It is responsible for gas transport into and out of the lung. The respiratory zone includes the respiratory bronchioles, alveolar ducts, alveolar sacs, and alveoli.

The human trachea (10-13 cm long) extends from C6 vertebral level in the lower part of the neck to T4/5 vertebral level, where it divides into right and left main bronchus. The C-shaped cartilage rings (15–20) keep it open. The posterior wall of the trachea contains a

horizontally oriented smooth muscle (trachealis) (Brand-Saberi and Schäfer 2014). The carina is the end point of trachea and the starting point of the right and left main bronchus, which are also called extrapulmonary bronchi (Drevet et al. 2016; Fréchette and Deslauriers 2006). The left main bronchus is narrower, longer (5 cm) and less vertical than the right main bronchus. That is why inhaled foreign bodies tend to enter the right main bronchus (Burdett and Mitchell 2011). The main bronchus divides into lobar bronchi (secondary bronchi), and the lobar bronchi branch into segmental bronchi (tertiary bronchi), which provide the bronchopulmonary segments. The segmental bronchi within each bronchopulmonary segment divide into multiple divisions up to the bronchioles (Figure 1.3). The bronchial walls are kept open by intermittent plates of cartilage which are not present in the bronchioles (Minnich and Mathisen 2007; Treuting et al. 2017).

The human right lung consists of three lobes [upper, middle and lower] which are separated by oblique and horizontal fissures. The left lung, on the other hand, consists of two lobes [upper and lower] which are separated by the oblique fissure. The anterior-inferior part of the left upper lobe, which is located over the left portion of the heart, forms a special anatomic region called the lingula (Treuting et al. 2017). By the 16th week of intrauterine life, the bronchial tree is developed. On the other hand, the number of alveoli increases until 8 years of age with a maximal increase at 3 years of age. At birth, pulmonary arteries have thick muscular walls which decrease in thickness at the 2nd week of life, and at 4 months of age, they become similar to adult (Sieber 1971).

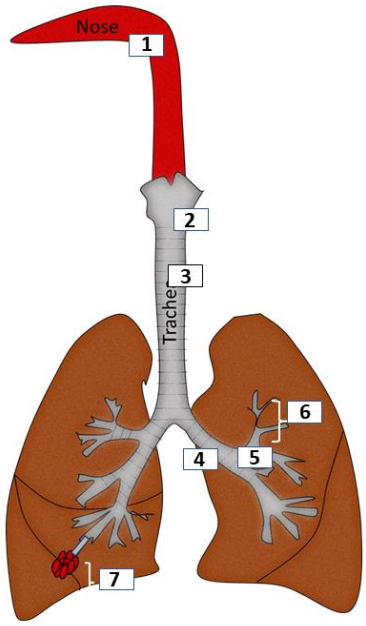

Figure 1.3: Anatomy of the airways and lungs in human.
The conducting zone starts with the nose (1) and extends further to the larynx (2) and trachea (3), which divides into two main bronchi (4). The main bronchus then divides into lobar bronchi (secondary bronchi) (5) and further into segmental bronchi (tertiary bronchi) (6), which provide the bronchopulmonary segments. The respiratory zone (7) includes the respiratory bronchioles, alveolar ducts, alveolar sacs, and alveoli.

1.2 Histology of the airways

In mice, there are differences in the cellular components and structure of the epithelium from proximal to distal airways. The tracheal and main bronchus epithelium is a pseudostratified epithelium, while a simple epithelium is lining the smaller bronchi and bronchioles (Treuting et al. 2017; Rock et al. 2010). The epithelium lining the conducting airways consists of different types of cells, including secretory, ciliated, basal and rare cells. These rare cells include pulmonary ionocytes, solitary cholinergic chemosensory cells (tuft or brush cells), solitary neuroendocrine cells, and neuroepithelial bodies (Plasschaert et al. 2018; Montoro et al. 2018; Rock et al. 2010; Hogan et al. 2014) (Figure 1.4).

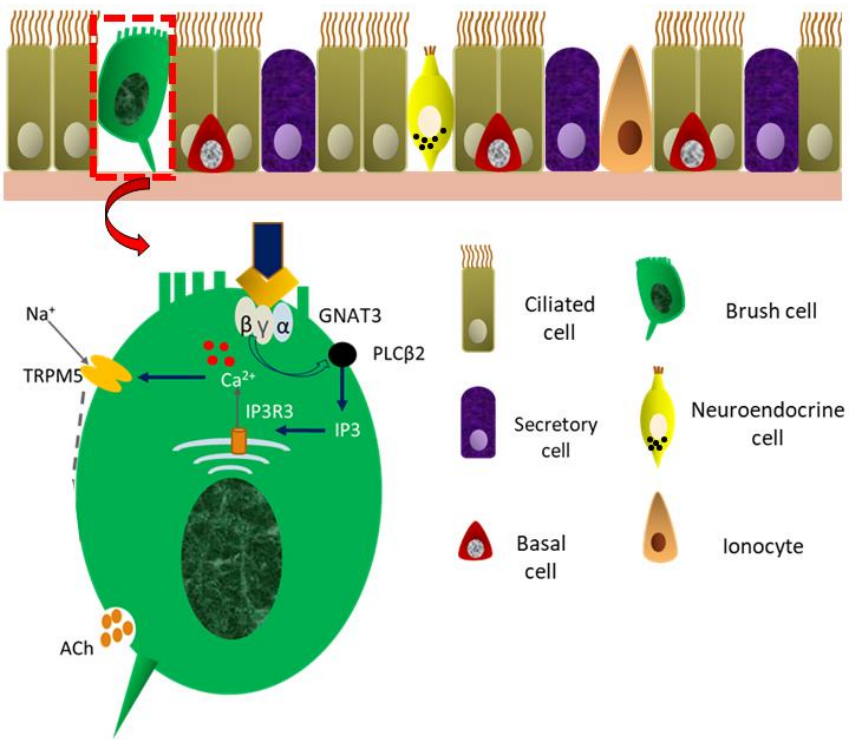

Figure 1.4 Histology of mouse lower airways epithelium.
This figure shows the different types of epithelial cells including ciliated, secretory, basal and rare epithelial cells, which are ionocytes, neuroendocrine cells and brush cells. Brush cells (red dotted rectangle) have the taste transduction signal cascade markers: When a tastant binds to the receptor, β and γ subunits of the coupled G-proteins bind to the membrane-bound enzyme phospholipase $C_{\beta}2$ (PLCβ2). PLCβ2 generates inositol trisphosphate (IP3). IP3 induces IP3 receptor, type 3 (IP3R3)-dependent Ca^{2+} release from the endoplasmic reticulum (ER), which in turn causes Na^{+} influx into the cell through the transient receptor potential cation channel subfamily M member 5 (TRPM5). These events induce depolarization at the cell level.

Previous *in silico*-analysis of single cell mRNA sequencing (scRNAseq) data of pig small and large airways revealed that the epithelium consists of ciliated cells (highest percentage in small (66.2%) and large (92.6%) airways), followed by basal (21.2% in small and 4.9% in large airways), and then secretory cells (11.9% in small and 1.8% in large airways). The rare cells group (less than 1% including small and large airways) includes brush cells and ionocytes (Figure 1.5); the latter are found only in large but not in small airways (Pezzulo et al. 2021). Additionally, neuroendocrine cells were reported using

immunohistochemistry in pig lung including the alveolar, bronchial and bronchiolar epithelium (Lauweryns et al. 1987) and in the ducts and acini of newborn pig (Yu et al. 2022).

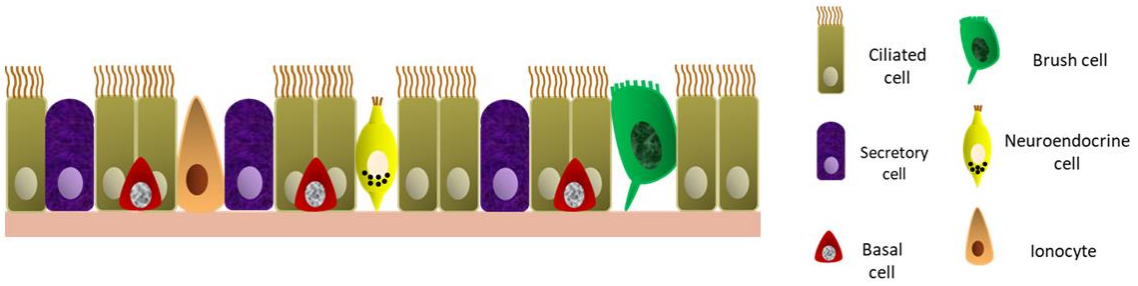

Figure 1.5 Histology of pig lower airway epithelium.
Different types of cells in pig airways epithelium; ciliated cells, followed by basal and then secretory cells. The group of rare cells includes brush, ionocytes and neuroendocrine cells.

In human, the epithelium of the nose consists of four differently build regions: 1) the squamous epithelium lining the nasal vestibule; 2) respiratory epithelium (RE), the ciliated, pseudostratified, cuboidal/columnar epithelium located in the main chamber and nasopharynx; 3) transitional epithelium lies between SE and RE in the proximal part of the main chamber; and 4) olfactory epithelium (OE), situated in the dorsoposterior part of the nasal cavity (Treuting et al. 2017; Patel 2017). The epithelial lining of the human trachea is a pseudostratified columnar epithelium. The majority (60%) of cells lining the trachea are ciliated columnar cells, 20% are basal cells, and 20% are goblet cells (Bustamante-Marin and Ostrowski 2017) (Figure 1.6). In the lung, as the bronchi divide, this involves histological changes in which the epithelium reduces in height and becomes simple columnar with a bit of pseudostratification. Goblet cell numbers also decrease while secretory cell numbers increase. In the alveoli, there are two types of epithelial cells: alveolar type I and alveolar type II. Alveolar type I cells promote exchange of gas, and alveolar type II produce surfactant, which consists of lipids (90%) and proteins (10%). The main function of pulmonary surfactant is to reduce the surface tension at the air-liquid interface (Iwasaki et al. 2017; Treuting et al. 2017; Griese 1999).

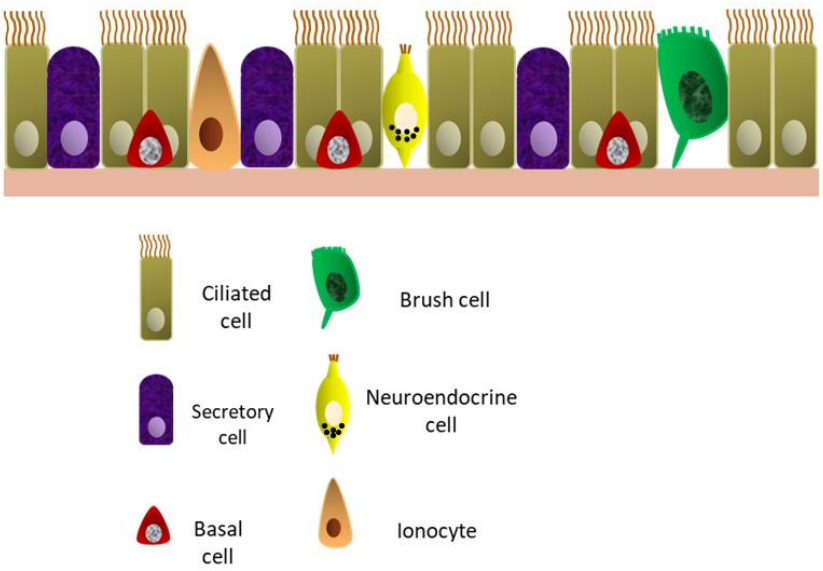

Figure 1.6 Histology of human airway epithelium.
This figure represents the different types of epithelial cells; ciliated, secretory, basal and rare cell groups (ionocyte, brush and neuroendocrine cells).

1.3 Rare epithelial cells

Beside the well known basal, secretory and ciliated cells, there are at least 3 rare cell types: 1) ionocytes, 2) neuroendocrine cells, 3) brush cells which are also called tuft or chemosensory cells (Plasschaert et al. 2018; Montoro et al. 2018; Rock et al. 2010; Hogan et al. 2014).

Ionocytes have marker genes like CFTR (cystic fibrosis transmembrane regulator, it is a chloride channel which, if mutated, causes cystic fibrosis), FOXI1 (a forkhead family transcription factor) and ASCL3 (achaete-scute homolog 3). Neuroendocrine cells are characterized by the presence of small intracytoplasmic granules called dense core vesicles (DCV). They are found as solitary cells or in clusters (Cutz et al. 1975; Lauweryns et al. 1970). Brush cells are defined by having no cilia, but instead microvilli (Rhodin and Dalhamn 1956).

1.3.1 Brush cells

These cells sense the luminal compartments or lining fluids for potential hazardous compounds. Once activated, they release various mediators to initiate protective reflexes, paracrine actions and immune reactions (Krasteva et al. 2011; Krasteva et al. 2012; Perniss et al. 2020).

Brush cells (also called non-ciliated) were first reported in rat tracheal epithelium by Rhodin and Dalham in 1956 using electron microscopy. These cells had brush-like apical processes. The cytoplasmic features of these cells were different from ciliated and goblet cells. These cells were elongated with tapering in the basal part and resting on the basal membrane. The cytoplasmic opacity was less than that of goblet cells. The Golgi apparatus was situated above the nucleus (Rhodin and Dalhamn 1956).

Similar cells were found in murine tracheal epithelial. They are elongated and flask-shaped with basal processes and apical processes that reach the lumen and. These cells are distributed from the trachea down to the bronchi with similar morphology to neuroendocrine cells but with no immunoreactivity to protein gene product (PGP 9.5), calcitonin gene-related peptide (CGRP) and serotonin (neuroendocrine markers) (Krasteva et al. 2011; Krasteva-Christ et al. 2015; Saunders et al. 2013). These cells are cholinergic as they express the acetylcholine-synthesizing enzyme choline acetyltransferase (ChAT) and release acetylcholine upon stimulation (Perniss et al. 2020; Krasteva et al. 2011).

They are characterized by markers of the taste signal transduction cascade including: G protein α-gustducin (GNAT3), phospholipase C isoform β2 (PLCβ2) and calcium-activated monovalent cation channel transient receptor potential cation channel subfamily M, member 5 (TRPM5) (Krasteva et al. 2011; Saunders et al. 2013; Tizzano et al. 2011). Additionally, these cells express structural microvillar proteins like villin and advillin. These cells are also characterized by ChAT expression.

1.3.1.1 Potential markers for brush cells

1.3.1.1.1 Taste signal transduction cascades

There are two families of taste receptors (TasR): Taste receptor family 1 (Tas1R) is responsible for the perception of the taste modalities sweet and umami. Taste receptors of the family 2 (Tas2R) are responsible for the perception of the bitter taste. Receptor activation stimulates the following signaling pathway, which is also called the taste transduction cascade: A heterotrimeric G protein (α, β and γ subunit) is coupled to the TasR (Margolskee 2002). Taste cells have different α-subunit of G proteins: αi-2, αi-3, α-14, α-15 and gustducin-α3 which is also known as GNAT3 (GNAT3 = guanine nucleotide-binding protein G(t) subunit alpha-3) (Kinnamon and Finger 2019). In the inactive state, guanosine diphosphate (GDP) is linked to the α-subunit. When a substance binds to TasR, this GDP is substituted by guanosine triphosphate (GTP) and this exchange causes a dissociation of the G protein into α-subunit and a β- and γ-dimer. This dimer binds to the membrane-bound enzyme PLCβ2 (Yan et al. 2001; Chaudhari and Roper 2010). PLCβ2 cleaves phosphatidylinositol-4,5-bisphosphate (PIP2) to IP3 and diacylglycerol (DAG). IP3 binds to IP3R3 in the membrane of the endoplasmic reticulum (ER). This leads to the efflux of Ca^{2+} from the ER into the cytosol (Narukawa et al. 2009; Clapp et al. 2001). This $[Ca^{2+}]$ increase leads to an opening of TRPM5. Influx of large amounts of Na^{+} through this channel results in a change of the membrane potential and, ultimately, depolarization of the cell (Dutta Banik et al. 2018). This leads to a release of ATP from type II taste cells through voltage-gated hemichannels containing CALHM1 (calcium homeostasis modulator 1) (Taruno et al. 2013). ATP serves as a transmitter and binds to P2X receptors on sensory nerve fibers. This leads to a transmission to the brain (Chaudhari and Roper 2010; Finger and Kinnamon 2011). The released ATP also binds to P2Y receptors, which are expressed by type III taste cells. This leads to a release of serotonin from type III cells and an activation of sensory nerve fibers. However, P2Y receptors are also expressed by type II cells (Chaudhari and Roper 2010). All cascade markers in taste cells are the same for brush cells, except for release of ATP via hemi-channels such as CALHM1, which only

occurs in taste cells (Figure 1.7). On the other hand, in brush cells these cascades ends up with acetylcholine (Ach) release from brush cells, which can induce paracrine effects by acting upon nearby cells (Hollenhorst et al. 2020; Perniss et al. 2020). Thus, these are the well-known signal transduction cascade markers in brush cells, but we do not know if there are further markers which might be involved in this cascade.

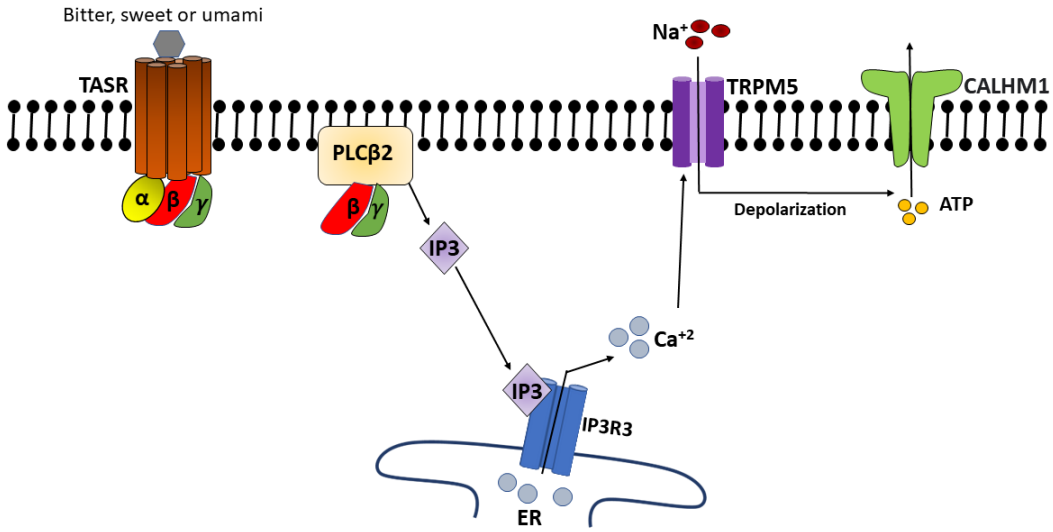

Figure 1.7: Schematic representation of the taste transduction cascade in type II taste cells. A heterotrimeric G protein consisting of α-, β- and γ-subunits is bound to the TasR. If a substance binds to the TASR, the G protein disassembles and a dimer composed of the β- and γ-subunit binds to the enzyme PLCβ2. Thereby, IP3 is released and binds to the IP3R3, which in turn induces Ca^{2+} release from the ER into the cytosol. This leads to the activation of the cation channel TRPM5, which then allows for influx of Na^{+} into the cell. This results in depolarization of the taste cell and release of ATP via hemi-channels such as CALHM1.

1.3.1.1.2 ChAT

The reaction including the transfer of an acetyl group from acetyl coenzyme A to choline in the cytoplasm of cholinergic neurons to produce acetylcholine in a single step is mediated by ChAT (Oda 1999). Five to 18% of ChAT reaches synaptic regions by fast axoplasmic transport in rat (Dziegielewska et al. 1976), while the remaining is transported

slowly from the cell body to the nerve terminal in rat and rabbit (Frizell et al. 1970). ChAT is prone to degradation and it has a short half-life time as reported in rat (Wenthold and Mahler 1975) and cat (Tandon et al. 1996). It has been found that ChAT presents in soluble and non-ionic membrane bound forms in mouse cholinergic nerve endings (Smith and Carroll 1980).

A recent review by Pan et al. (2020) considered ChAT as a marker of chemosensory cells (Pan et al. 2020). It has been shown in mice that ChAT is expressed in brush cells in the tracheal and laryngeal epithelium and tracheal and laryngeal submucosal glands. ChAT-immunoreactive cells decrease in number from the larynx to the trachea. These cells have a role in sensing infection and initiating responses like increasing the ciliary beat frequency, so they may prevent the entrance of hazardous substance into the gland (Krasteva-Christ et al. 2015).

1.3.1.1.3 Structural proteins (villin and advillin)

Villin is a microfilament-associated protein binding both G and F actin in a calcium dependent way (Bretscher and Weber 1979; Bretscher and Weber 1980). It is a characteristic structural protein of microvilli forming a brush border, although its presence is not restricted to such brush borders. Villin has been observed using immunohistochemistry in the brush border of the proximal tubule in the kidney and in the microvilli of epithelial cells in the intestine in different species including human, rat and mice (Robine et al. 1985; Gröne et al. 1986; West et al. 1988; Höfer and Drenckhahn 1992, 1996; Brown et al. 1997). Villin has been found also in the main and interlobular ducts of pancreas and in embryonic intestinal cells in human (Robine et al. 1985). Moreover, villin is expressed in the newborn pig in cell cultures of the upper airways (Delgado-Ortega et al. 2014).

Immunohistochemical studies utilized villin-antibodies to identify brush cells in mouse tracheal epithelium and glands, laryngeal glands, urethra, thymus, auditory tube and gastrointestinal tract (Horvat et al. 1990; Krasteva et al. 2011; Krasteva et al. 2012; Deckmann et al. 2014; Panneck et al. 2014; Krasteva-Christ et al. 2015; Yamashita et al.

2017). It was proposed that villin is a brush cell marker (Höfer and Drenckhahn 1992). Thus, villin was originally thought to be a brush cell specific marker, but more recent studies established advillin as a brush cell marker.

Advillin belongs to the gelsolin/villin family of proteins with more similarity to villin. It has six domain structure same as gelsolin/villin family of proteins and a carboxyl-terminal headpiece. Additionally, it shares similar amino acid sequence with adseverin and villin (Marks et al. 1998).

Single cell sequencing data revealed a high amount of advillin rather than villin in intestinal tuft cells. Advillin is more likely an intestinal brush cell marker and this raised the possibility that previous published data using villin-antibody were due to cross reactivity with advillin (Bezençon et al. 2008). Advillin and villin were colocalized with ChAT-immunoreactivity in single epithelial cell, of the human intestine, human peribiliary glands, and in the pancreatic duct (Schütz et al. 2019). Additionally, advillin expression and immunoreactivity were restricted to brush cells in the gastrointestinal tract epithelium including stomach, small intestine and colon (Ruppert et al. 2020).

1.3.1.2 LRMP (lymphoid restricted membrane protein)

The *Jaw1* gene was first detected in B-cell lines by screening for the genes both in human and mice. Its product also called LRMP (lymphoid restricted membrane protein) and *lrmp* is an alternative gene name. It is an integral membrane protein of the ER with orientation toward the cytosol with high expression in pre-T cells, pre-B cells and in mature B cells (Behrens et al. 1994). The carboxyl terminal of Jaw1/LRMP including the transmembrane domain (TM) is important for targeting to the ER (Behrens et al. 1996). LRMP was one of the BCL6 translocation partners in higher grade follicular lymphoma (Akasaka et al. 2003). It is reported to be highly expressed in human germinal center B-cells in peripheral lymphoid tissue including lymph node and tonsil, and in non-lymphoid tissues in the cerebral cortex, epithelial cells of tonsils, adrenal gland, zymogen producing cells in the stomach and epithelial cells of seminal vesicles (Tedoldi et al. 2006). LRMP is an HCN4 modulator, which is potassium/sodium hyperpolarization-activated cyclic nucleotide-

gated channel 4. This happens by inhibiting the canonical depolarizing shift in the HCN4 voltage dependence after binding to cAMP. So LRMP participates in cellular excitability regulation (Peters et al. 2020). Furthermore, LRMP has a role in taste signal transduction in bitter, sweet and umami perception. It was reported to be co-expressed with IP3R3 in the mouse taste tissue in the foliate, fungiform and circumvallate papilla (Shindo et al. 2010). The *LRMP* gene is expressed in healthy human lung tissue as shown by analyzing *LRMP*-mRNA levels using RT-PCR (Manenti et al. 2006). Using single cell mRNA sequencing certain cells that were considered as brush cells (13 brush/tuft cells) expressed *LRMP* (Deprez et al. 2020). A recent study of murine intestine reported *Lrmp* as a p53 target gene that is expressed in tuft cells with two p53 binding sites in the intron. Moreover, p53 upregulates transcription of *Lrmp* to keep its high expression in tuft cells. So, p53 loss decreases LRMP levels in tuft cells and vice versa. LRMP interacts with inositol 1,4,5-trisphosphate receptor type 2 (ITPR2) as a major IP3R expressed in tuft cells (Chang et al. 2021).

1.3.1.4 Brush cell function

Murine cholinergic chemosensory cells are distributed in the upper and lower airway epithelium, also in the tracheal and laryngeal submucosal glands (Krasteva-Christ et al. 2015). The density of these cells declines from the nose to the bronchial epithelium (bronchial diameter more than 400±100 µm). They are absent from smaller bronchioles and the alveoli. Cholinergic chemosensory cells in the nasal and laryngeal epithelium are regularly in contact with peptidergic nerve fibers, while in trachea only some of these cells are innervated. Here, 5.8% of cholinergic brush cells receive contact from $CGRP^+$ nerve fibers, while 21.7% of cholinergic brush cells receive contact from nonpeptidergic nerve fibers (PGP 9.5-positive/CGRP-negative) (Tizzano et al. 2011; Krasteva et al. 2011).

Some murine cholinergic chemosensory cells are in contact with cholinoceptive sensory nerve fibers. Such cells sense bacterial quorum sensing molecule and bitter substances in the airway lining fluid. This causes acetylcholine release, which then activates nicotinic acetylcholine receptors (nAChRs) on the nearby sensory nerve fibers. This triggers a

decrease in the breathing frequency (Krasteva et al. 2012; Krasteva-Christ et al. 2015; Tizzano et al. 2011).

Cholinergic chemosensory cells in the trachea express TAS2R family members and TAS1R3 (Tizzano et al. 2011). TAS1R3 is part of the sweet receptor (TAS1R2 and TAS1R3) and the umami receptor (TAS1R1 and TAS1R3) (Zhao et al. 2003). Accordingly, these cells express components of the taste signal transduction cascade, including: GNAT3, PLCβ2 and TRPM5 (Krasteva et al. 2011; Saunders et al. 2013; Tizzano et al. 2011).

Chemosensory cells sense the luminal contents of the airway and then transmit signals to the nearby nerves and induce inflammation by IL-25 release. Chemosensory cells express high level of IL-25, IL-25 receptor (IL17RB) and the enzymes responsible for cysteinyl leukotriene synthesis, suggesting a role in airway immune response (Bankova et al. 2018).

Formyl peptides from lung pathogenic bacteria can be detected by cholinergic chemosensory cells through the canonical taste transduction signaling pathway (PLCβ2-IPTR3-TRPM5 cascade) causing ACh release. Acetylcholine stimulates mucociliary clearance by paracrine action on ciliated cells through muscarinic M3 receptors without neuronal pathways being involved (Perniss et al. 2020).

Tracheal cholinergic chemosensory cells appear first at embryonic day (E) 18, and then substantially increase in number until post-embryonic day 78 (Perniss et al. 2021).

Skn-1a, a POU homeodomain transcription factor also known as Pou2f3, is required for the development of TRPM5-positive sweet, umami, and bitter taste cells (Matsumoto et al. 2011). Genetic deletion of *Pou2f3* leads to absence of TRPM5-positive chemosensory cells. In *Pou2f3* knockout mice no immunoreactivity toward TRPM5 and ChAT have been detected in tracheal epithelial cells. On the other hand, villin-immunoreactive cells persist. It has been reported that 38% of the villin-positive cells are TRPM5-positive, and 62% are TRPM5-negative (Yamashita et al. 2017). Another work quantifying brush cells using *Chat*-eGFP (enhanced green fluorescent protein) mice reported that 83% of villin-positive cells are ChAT-positive and 17% are ChAT-negative (Krasteva et al. 2011). Villin-positive cells with these features are not present anymore.

Pou2f3 is also critical for the generation of TRPM5-positive chemosensory cells in the alimentary tract, pancreatic duct, urethra, thymus, and auditory tube (Yamashita et al. 2017).

Using antibodies against different markers like DCLK1 (Doublecortin Like Kinase 1), TRPM5 and GNAT3, it has been shown that solitary chemosensory cells appear *de novo* in the distal airways and alveoli in the regenerative phase after epithelial damage caused by influenza (Rane et al. 2019). Tuft cells were not found in the control group (without COVID-19) in human lung, but they appeared ectopically in epithelial regeneration after COVID-19 (Melms et al. 2021).

It has been suggested that brush cells in rat are involved in absorption (Reid et al. 2005), chemosensation, regeneration, regulation of capillary resistance in hypoxia (Hijiya et al. 1977) and detoxification (Chang et al. 1986). Immunohistochemistry in rat gut epithelium using an α-gustducin antibody revealed similarity between brush cells and taste cells in the tongue using (Höfer and Drenckhahn 1996).

Four different types of cells were found ultrastructurally in pig bronchioles: ciliated, non-ciliated cells, goblet cells and brush cells. Brush cells were characterized by short microvilli protruding from the surface. They were reported in 2 pigs (9 and 16 weeks) out of 7, but they were not detected in the younger pigs (less than 5 weeks). These cells were columnar with a narrow nucleus situated in the basal part. The suggested function for these cells was in absorption. Alveolar brush cells were not detected in the alveolar epithelium (Baskerville 1970). Thus, we have very little information about the molecular characteristic of brush cells in pig respiratory tract epithelium.

An ultrastructural study of the small intestine described pear-shaped cells with a wide base, narrow apex, and a “tuft” of microvilli toward the lumen. These cells were found between enterocytes and their number increased after dietary supplementation of probiotic and zinc (Kalita et al. 2021). Cholinergic chemosensory cells in pig urethra have been shown to express TRPM5, PLCβ2 and α-gustducin, while ChAT- and villin- (50% of samples) immunoreactivity are not constantly expressed in all samples (Deckmann et al.

2015). Moreover, such cells were found in the porcine uterus (luminal epithelium and glands). No direct contact with nerve fibers was observed. These cells express markers for the canonical taste transduction cascade including TRPM5 and PLCβ2 and ChAT (Sponchiado et al. 2022).

In human, Rhodin first noted the presence of a brush cell in the tracheal mucosa and he described these cells as having many microvilli and a basal body that indicated that these cells are capable to transform to ciliated cells (Rhodin 1959). On the other hand, these cells were considered ciliated cells in the differentiation phase as there were many basal corpuscles in the apical part; their suggested role was in absorption and sensation (Basset et al. 1971). Rhodin also found microvilli projecting in between the cilia (Rhodin 1966). Furthermore, brush cells were reported in the main stem bronchus of a six years old child with no bronchogenic disease. These cells were described as having few mitochondria, few endoplasmic reticulum, many ribosomes, vesicles and vacuoles (Watson and Brinkman 1964). Microvilli were found to cover the apical surface of many cells like the neurosecretory cells with dense core vesicles, the mucous cells and also the indifferent cells in which the brush cells were thought to belong to (McDowell et al. 1978). A similar cell was described in a tracheal biopsy of a thirteen years old male patient with immotile cilia syndrome. Using electron microscopy, these cells were distinguished by straight microvilli with a filamentous core that ended in a terminal web, endocytotic vesicles and microvesicles, but with no basal body or cilia. It was concluded that these cells substituted the lost cilia (Gordon and Kattan 1984). Later DiaMaio et al. (1990) described in the trachea of a 19-20 week fetus the microscopic feature of a brush cell with straight microvilli (0.25-0.3 µm thick) and a filamentous core that ended in a terminal web. The cell had lysosomes and pinocytic vesicles, but neither basal body nor cilia, and no nerve fibers were found attached to it. These cells made up 0.5% of the total number of epithelial cells and the author suggested that these cells might have a role in absorption. DiMaio also found other cells resembling brush cells in the epithelium of trachea, bronchus and bronchiole. The difference between these cells and the cells that were only found in the trachea was that they had many and branched microvilli and few basal bodies

(DiMaio et al. 1990). So, in human we know only very little about these cells, some about ultrastructure, may be one or two single individual were reported at the time when it was unclear that there were more rare cell types.

DiMaio and co-workers observed an alveolar brush cell in a lung biopsy of a male infant, four months old, with desquamative interstitial pneumonitis. Electron microscopic studies revealed that these cells had straight microvilli with a filamentous core that did not end in a terminal web, pinocytic vesicles, microvesicles and many vacuoles. Part of this cell was covered by a pneumocyte type I. These cells were considered to participate in chemoreception and in regeneration (DiMaio et al. 1988). Thus, these previous studies pointed to brush cells based only on the presence of mirovilli on the apical surface. On the other hand, there are other cells bearing microvilli, so in these previous studies they might be referring to another cell type.

In silico-analysis of scRNAseq pointed to the presence of tuft (brush) cells, but the authors were unable to detect them in their study in human small airway. The authors explained the failure of finding these cells in small airways by assuming that they were either fragile cells or their location was discrete (Zuo et al. 2020). More recent evidence highlights ectopic appearance of tuft cells in the alveolar region of the lung after COVID-19 infection. These cells were not observed in the control lung using antibodies against ChAT and POU2F3. The suggested role of these cells is in macrophage chemotaxis. Additionally, these cells might be mobilized to participate in lung regeneration after injury of epithelium (Melms et al. 2021).

The transcription factor POU2F3 raised clinical interest as an important gene expressed in a subgroup pf human small cell lung cancer (SCLC). So, one subtype of SCLC originates from tuft (brush) cells. This subtype is different from the classical neuroendocrine high subgroup of this cancer (Huang et al. 2018).

Chemosensory cells were reported in human sinonasal mucosa including nasal septum, middle and inferior nasal concha and uncinate process. These cells were immunoreactive to the signal transduction cascade marker antibodies both in healthy and diseased

(allergic rhinitis or chronic rhinosinusitis) people (Barham et al. 2013). These cells were activated by T2R agonists like denatonium, which caused Ca^{2+} elevation through PLCβ2, IP3R3, and TRPM5 cascades. Furthermore, these cells expressed T1R2/3 sweet taste receptors which negatively affected T2R by decreasing Ca^{2+} signaling within solitary chemosensory cells (Lee et al. 2014). Although we know some details about these cells, we do not have quantitative data and overview on the spatial distribution of these cells. Nothing is known about these cells at different locations in the airways tree in the same individual. Thus, we have only fragmentary knowledge about these microvilli bearing cells.

Sensory cells (brush cells) were reported in human duodenojejunal junction with apical microvilli and a filamentous core that does not end within a terminal web. Nerve fibers were in contact with the basal and lateral aspect of these cells (Morroni et al. 2007). In 2019, Schütz and coworkers found cells with apical microvilli in the human gastrointestinal tract epithelium including stomach, small and large intestine, extrahepatic bile duct and pancreatic ductal system. Double-labeling immunofluorescence showed that ChAT is co-expressed with villin, advillin, cytokeratin 18 (CK18 is a cytoskeletal protein) , cyclooxygenase 1, 5-lipoxygenase activating protein and hematopoietic prostaglandin D synthase (Schütz et al. 2019). Additionally, cholinergic chemosensory cells have been detected in human urethral epithelium expressing taste transduction cascade markers including TRPM5, PLCβ2, α-gustducin, ChAT and villin (Deckmann et al. 2014).

Previous *in silico*-analysis of scRNA-seq data identified ionocytes, brush cells and neuroendocrine cells in three different clusters in the nose, trachea, intermediate and distal bronchi (Deprez et al. 2020). Brush cells and neuroendocrine cells were found in one cluster using HBECs (primary human bronchial epithelial cells) (Plasschaert et al. 2018). Also, three groups of cells were detected in human tracheal epithelium, including neuroendocrine cells and ionocytes, which are differentiated from tuft-like cells (no expression of GNAT3 and TRPM5). These cells form 0.8% of all epithelial cells (Goldfarbmuren et al. 2020). These three cell types were reported to originate from basal

cells (Davis and Wypych 2021). Basal cells expressing cytokeratin 5 and 14 are mainly the progenitor of brush cells after injury (Saunders et al. 2013).

1.3.2 Neuroendocrine cells

Recent studies in mouse lung reported a stem cell activity of neuroendocrine cells (Ouadah et al. 2019). Furthermore, they might play a role in mechanosensation in that physiological hypoosmotic activation of NEBs opens the Ca^{2+} channel TRPC5, which in turn increases intracellular [Ca^{2+}]. Then, this signal is transmitted from the airway epithelium to the CNS through the vagal nerve (Lembrechts et al. 2012). Finally, they take part in immunoregulation by CGRP release, which stimulates innate lymphoid cells (type 2) to secrete IL-5 which causes eosinophil recruitment (Sui et al. 2018). It has been reported that the pulmonary NEBs express Piezo2, a mechanically activated cation channel, suggesting a role of NEBs in mechanosensation (Nonomura et al. 2017). Human having compound inactivating variants in Piezo2 show difficulties in breathing throughout infancy time (Chesler et al. 2016).

It has been reported in mice that PNECs express roundabout receptor (ROBO) genes (Branchfield et al. 2016). Mutations in human ROBO genes are associated with CDH (congenital diaphragmatic hernia) (Kantarci and Donahoe 2007).

The number of neuroendocrine cells expressing CGRP is increased in allergic asthma (Sui et al. 2018). Lung diseases result in an increase of PNEC numbers. For example, in sudden infant death syndrome (SIDS) (Cutz et al. 2007) and COPD (Gu et al. 2014). Miller and Müller (1995) reported the presence of PNEC hyperplasia in bronchial and bronchiolar epithelium adjacent to carcinoid tumors (Miller and Müller 1995). On the other hand, it has been reported that, in human nose, these is no increase in the number neuroendocrine cells in asthma, tobacco smokers, and chronic hypoxia (Sieśkiewicz et al. 2007).

Clear cells (originally called “helle Zelle” in German) were first discovered in the bronchopulmonary epithelium by Froelich (1949) in man and other mammals using

hematoxylin and eosin staining. These cells were considered as part of the APUD (Amine Precursor Uptake and Decarboxylation, (Pearse 1969)) system as they exhibit some distinct cytochemical and structural properties, for example the uptake of amine precursors (dihydroxyphenylalanine (DOPA), 5-hydroxytryptophan (5-HTP)) and the ability to decarboxylase amino acids; they have argyrophilic cytoplasm (Pearse 1969).

Neuroendocrine cells are characterized by the presence of a great number of dense core vesicles (DCV) containing amines (histamine, catecholamines, 5-hydroxytryptamine and related substances) and peptides (e.g. cholecystokinin, endothelin, peptide YY, helodermin, CGRP). These cells are found either solitarily or in clusters (NEBs) (van Lommel et al. 1999).

Cutz and Conen referred to the abundance of K-type cells (Kultschitzky cells, (Bensch et al. 1965)) in the lung in the initial phases of fetal development (Cutz and Conen 1972). In the same year (1972), Lauweryns and Peuskens suggested the presence of cellular corpuscles with spherical to ovoid shape, which were called NEBs, distributed along the respiratory bronchial and bronchiolar tree of human infants. They consist of large basal cells with clear cytoplasm and many non-ciliated cells lining their apical part. Treated with silver impregnation method, they also have silver deposits (argyrophilia) at the basal side of the cell associated with free nerve terminals (Lauweryns and Peuskens 1969, 1972).

Cutz and coworkers identified one type of K-cells in human trachea in intrauterine and extrauterine stages. They were found as single cells and not as NEBs. They were elongated or pyramidal with processes reaching the lumen, a basal part resting on the basement membrane (BM), and the cytoplasm contained DCV. These cells were subjected to species variability; for instance, there are two types of these cells in the trachea of lamb and armadillo, while there is one type of this cell in human and rabbit (Cutz et al. 1975).

The number of these cells in human airways was calculated as 12.5 cells/cm BM or 0.41% of all epithelial cells using chromogranin A antibody. No significant difference in the number of these cells was observed in airways of different diameters, but no PNECs were identified in the alveoli (Boers et al. 1996). Johnson and coworkers reported the presence

of single bombesin-immunoreactive cells and clusters of cells (NEBs) from the bronchi down to the alveolar duct. These cells increased dramatically during gestation to reach the maximum at delivery. During the first month of life, these cells start to decrease (Johnson et al. 1982).

Endocrine-like cells were found in the nasal turbinate epithelium in young and adult (Thaete et al. 1981). They are triangular in shape with DCV (Petruson et al. 1984). Johnson and coworkers reported the presence of clustered PGP- and calbindin-immunoreactive cells in the nasal respiratory epithelium of human fetus and newborn. These cells had broad apical and thin basal processes (Johnson et al. 1997).

Neuroendocrine cell markers include serotonin, synaptophysin (Gould et al. 1987), calcitonin, chromogranin, neuron-specific enolaze (NSE), CGRP, enkephalin, endothelin, gastrin-releasing peptide (GRP) (Wharton et al. 1978), somatostatin, cholecystokinin and substance P (Adriaensen and Scheuermann 1993).

In human, these cells are considered to have a role during fetal development (Johnson et al. 1997) and to participate in chemoreception by which neuroendocrine contents are released from neuroendocrine cells after exposure to chemical reagents (Gu et al. 2014; Lauweryns and Peuskens 1972).

1.3.3 Ionocytes

Ionocytes were first identified in fish on the gills or skin. These cells were reported to have specific transporters in order to achieve transepithelial active uptake of Na^+, Cl^- and Ca^{2+} (Garciaromeu and Maetz 1964). These cells were also called chloride cells and mitochondrion-rich cells (MRCs). Airway ionocytes show high expression of CFTR, which is a glycoprotein, situated at the apical part of epithelial cells. The function of CFTR is to regulate the transport of ions (chloride ions and bicarbonates) and the homeostasis of fluids. The mutation of this gene leads to cystic fibrosis (Bergeron and Cantin 2019). They comprise 0.5–1.5% of epithelial cells along the conducting airways in human. CFTR is also expressed in other cell types like secretory cells, which constitute around 80% of $CFTR^+$ cells. Additionally, ciliated cells constitute around 5.6% of $CFTR^+$ cells (Okuda et al. 2021).

Ionocytes also specifically express FOXI1, ASCL3 and proton-secreting V-ATPase (Plasschaert et al. 2018). In both human nasal and bronchial epithelium, these cells showed apical immunoreactivity toward CFTR-antibody and nuclear immunoreactivity toward FOXI1-antibody. Ionocytes were highly abundant in the nasal epithelium; these cells have a 5-fold higher frequency in the nasal epithelium than in that in the bronchial epithelium (Scudieri et al. 2020). The absence of Foxi1 in mouse ionocytes causes CFTR loss. So Foxi1 loss has an indirect role in cystic fibrosis (Plasschaert et al. 2018; Montoro et al. 2018).

Murine ionocytes are characterized by having appendages from the cytoplasm. These cells were found in mouse nasal epithelium, olfactory epithelium and submucosal glands (Montoro et al. 2018). Such cells were previously identified in fish inner ear (Kwan et al. 2020) and in mouse kidney (Barone et al. 2021).

1.4 Aim of the study

Brush cells have been identified as a rare epithelial cell type monitoring the chemical composition of the lining fluid in the large airways of the mouse. They initiate protective mechanism in response to the presence of potentially hazardous compounds. While there is considerable progress in elucidating their structure and function in mice, information on this cell type in human is negligible. Thus, the present study aimed to provide an inventory of their spatial distribution in the human respiratory tract and a basic characterization expression of chemosensory signaling pathways by *in silico*-analysis of publicly available sequencing data sets, immunohistochemistry, RT-PCR. Given the substantial differences in airway anatomy and function between humans and mice, which are a commonly used model in brush cell research, we extended the study also to pigs to evaluate whether the situation in this larger mammal might better reflect that found in human. The search for markers suitable to identify such cells in human was guided by previous data collected on mice and *in silico*-analysis of publicly available sequencing data sets from human airway epithelium.

2 Material and methods

2.1 Buffers and solutions

Picric acid

30 to 50 g of picric acid (Merck, Darmstadt, Germany) are dissolved in one liter of hot water and left to stand overnight. A crystalline sediment forms. The saturated picric acid remains as a supernatant.

Zamboni fixative

Mix 50 ml of 37% formaldehyde solution (Carl Roth, Karlsruhe, Germany), 500 ml of 0.2 M phosphate buffer and 150 ml of saturated picric acid as prepared above. The solution is made up to one liter with distilled water.

18% sucrose in 0.1 M phosphate buffer

18 g sucrose (Merck) are dissolved in 100 milliliters.

Phosphate buffer 0.1 M

230 ml of 31.2 g/l sodium dihydrogen-phosphate (Carl Roth) and 770 ml of 35.6 g/l sodium hydrogen-phosphate (Carl Roth) in 1 L distilled water.

Phosphate buffered saline (PBS)

28.75 ml of 31.2 g/l sodium dihydrogen-phosphate (Carl Roth), 96.2 ml of 35.6 g/l sodium hydrogen-phosphate (Carl Roth) and 22.4 g sodium chloride (Carl Roth) dissolved in 5 l distilled water.

Histoblock

10% normal horse serum (PAA-Laboratories, Hessen, Germany), 0.5% Tween 20 (Sigma-Aldrich), and 0.1% bovine serum albumin (Thermo Fisher, Massachusetts, USA) in PBS.

PBS+S

0.005 M phosphate buffer, with 0.15 M NaCl, pH 7.4.

Carbonate-buffered glycerol

50 ml 0.5 M sodium hydrogen carbonate (Sigma Aldrich, Steinheim, Germany) and 0.5 M sodium carbonate (Merck) were mixed in a ratio of 1:1, at pH 8.6. Glycerin (Carl Roth) was added in equal amount to the buffer.

2.2 Tissue collection and preparation

2.2.1 Human

The protocols were approved by the local ethics committee (reference no. 10/06 and 129/14). Nose, trachea and lung as well as taste bud, colon and kidney serving as positive controls were dissected from human body donors (n=23) of both genders with ages between 65 and 101 years (Table 2.1), institute for anatomy and cell biology, Justus Liebig University Giessen. The corpses were fixed by intraarterial infusion of a solution consisting of 57% ethanol, 3% formaldehyde and 5% glycerin in water. In addition, lungs from organ donors (n=9) and lung resected from COPD patients in the course of lung transplantation (n=6) were collected by the institute of pathology and cytology, Wetzlar (Prof. Dr. L. Fink) and fixed in 10% formalin.

Donor internal numbers	Sex	Age	Tissue used
37-016	Male	84	Nasal concha
08-019	Female	65	Nose concha
19-019	Male	70	Nose concha Papilla vallata Lung
10-019	Male	66	Nose concha Papilla vallata Trachea
07-019	Male	75	Nose concha Lung
27-016	Male	86	Trachea
03-017	Female	101	Trachea

			Lung
10-017	Male	83	Trachea
13-017	Male	74	Trachea Lung
22-017	Male	91	Lung
40-016	Male	86	Lung Trachea
14-017	Female	96	Lung Trachea
11-019	Female	74	Papilla vallata Lung
18-017	Female	74	Lung Kidney
06-019	Female	92	Lung Papilla vallata
28-017	Female	62	Colon
16-019	Male	74	Papilla vallata Lung
18-017	Female	74	Papilla vallata Lung
20-017	Female	93	Lung
28-016	Female	90	Trachea
34-016	Female	79	Trachea
11-017	Female	95	Trachea
26-017	Female	95	Trachea

Table 2.1 Human body donor samples.

The dissected tissues were washed with phosphate buffer (0.1 M, pH 7.4) three times for three days. Tissues were then immersed first in 70% ethanol, 80% ethanol, 90% ethanol, 100% ethanol (Carl Roth), xylene twice (VWR Prolabo BDH chemicals, Fontenay-sous-Bois, France) and finally embedded in paraplast (Leica, Wetzlar, Germany) in the paraffin processing machine (TP 1020, Leica, Wetzlar, Germany) that takes 19 hours. Then the specimens were embedded in paraffin blocks in the paraffin embedding machine (4604,

Ames company division of Miles Laboratories Ltd., Slough, England). Samples were cut into 8 µm thick sections (microtome RM2255, Leica), these sections were mounted on microscope slides (superfrost plus, Menze-Glaeser, Braunschweig, Germany) and stored at room temperature until further use.

2.2.2 Mice

The protocol was registered and approved by the respective authorities (reference no. 571_M, 624_M). Wild-type C57BL/6Rj mice (n=10, Janvier Labs, Le Genest-Saint-Isle, France) and transgenic mice *Trpm5*-eGFP (Tg(Trpm5-EGFP)#Sdmk), (Prof. Dr. R Margolskee, Monell Chemical Senses Center, Philadelphia, USA) (n=13) were used in the experiments. Mice were kept in the animal facility of the Justus-Liebig-University Giessen at specific- pathogen free conditions and were tested negative for *Bordetella pseudohinzii* by fecal pellet PCR. Mice of both genders were used at least 12 weeks of age. Animal were killed by Inhalation of 5% isoflurane (Abbott, Wiesbaden, Germany) and then exsanguination by cutting the abdominal aorta.

Trachea, lung as well as taste buds (positive control) were collected for whole mount preparation and cryosectioning (n=10 C57BL/6Rj mice, n=13 *Trpm5*-eGFP, 5 for whole mounts and 8 for cryosections).

For whole mounts, tracheas were collected, opened by cutting the trachealis muscle and then pinned on a sheet of wax. These samples were immersed in Zamboni fixative overnight. Washing was done using 0.1 M phosphate buffer (three times for three days).

For cryosections, trachea and lung were collected directly (n=5, *Trpm5*-eGFP; n=10, C57BL/6Rj) or after transcardiac perfusion (n=3; *Trpm5*-eGFP) with Zamboni fixative. After an initial perfusion with a washing solution containing heparin (0.25 g; Ratiopharm, Ulm, Germany), procaine hydrochloride (5 g; Merck), 9.0 g NaC1 and 25 g polyvinylpyrrolidone (SERVA, Heidelberg Germany) in 1 L water. Afterwards, these tissues were soaked overnight at 4°C in Zamboni fixative. Washing was done using 0.1 M phosphate buffer, followed by incubating the tissue overnight in 18% sucrose (Merck) in 0.1 M phosphate buffer at 4°C. Afterwards, the tissues were embedded in OCT cryostat sectioning medium

(Sakura Finetek Staufen, Germany), freezing was performed utilizing the cooling action of liquid nitrogen on 2-methylbutane (Carlroth), and finally the tissues were stored at -20°C.

Tissues were cryosectioned into 10 µm sections using a cryo-microtome (CM-1900 cryostat; Leica). These sections were mounted on microscope slides (superfrost plus) and stored at -20°C until further use.

2.2.3 Pig

Pig trachea and lung were obtained from the butchery (Metzgerei Manz, Hüttenberg) at 4-5 months of age (n=5), all were castrated male or female. Specimens from trachea and lung were dissected and used either for cryosectioning or for RT-PCT.

Samples processed for cryosectioning were immersed in Zamboni fixative overnight at 4°C and then washed in 0.1 M phosphate buffer three times for three days. Afterwards, the specimens were incubated overnight in 18% sucrose in 0.1 M phosphate buffer at 4°C, followed by embedding in OCT cryostat sectioning medium and freezing in 2-methylbutane cooled by liquid nitrogen. Tissues were stored at -20°C until further use.

Tissues were cryosectioned into 10 µm sections using a cryo-microtome (CM-1900 cryostat; Leica). These sections were mounted on microscope slides (superfrost plus) and stored at -20°C until further use.

2.3 Hematoxylin eosin staining (H&E)

Paraffin tissue sections were rinsed twice in xylene (5 min each, VWR Prolabo BDH), then in ethanol 100% (Carl Roth) for 3 min, followed by rinses in ethanol 96% (3 min) and ethanol 70% (3 min). Sections were immersed in PBS (pH 7.4, 1-3 min), and then washed with distilled water. Slides were immersed in hemalaun (Merck) for 10 min, followed by washing in distilled water, transferred into eosin (0.1% eosin in distilled water) (Merck) for 3 min and then dehydrated on ethanol series (70%, 96%, 100%) and xylene (twice for 3 min), then sections were cover-slipped using Entellan (Merck). This procedure was done to evaluate the quality of epithelium for further use in Immunofluorescence.

2.4 Immunofluorescence

2.4.1 Indirect immunofluorescence of paraffin sections

Sections with high quality epithelium were selected and deparaffinized in xylene twice, 100% ethanol, 96% ethanol and 70% ethanol each for 5 min, and then subjected to antigen retrieval by boiling in 10 mM citric acid, pH 6 (Carl ROTH, Karlsruhe, Germany) in a microwave oven at 900 W. The slides were then left for 15 min to cool. Then the sections were rinsed in PBS and unspecific protein binding sites were saturated using histoblock for 1 h. Six sections were used for each specimen. The 1° antibodies were added singly or in combination for double-immunolabeling (LRMP&CK19, LRMP&PGP, LRMP&uteroglobin, LRMP&FOXI1 and LRMP&tubulin) overnight at room temperature; all antibodies were diluted in PBS+S, pH 7.4. 1° Antibodies used for immunofluorescence in human are described in Table 2.2 and 2° antibodies in Table 2.3. 4',6-Diamidino-2-phenylindol (DAPI) was used to label the nucleus (1 µg/ml, D9542, Sigma-Aldrich, St. Louis, USA, 1:1000) and was applied together with the 2° antibodies. The sections were incubated with the 2° antibodies for 1 hour at room temperature; afterwards the sections were washed with PBS twice for 10 min, immersed in 4% paraformaldehyde (Carl Roth) in 0,1 M PP for 10 min and again washed with PBS twice for 10 min. Then, sections were mounted using carbonate-buffered glycerol, pH 8.6.

2.4.2 Indirect immunofluorescence of cryosections

Sections were dried for 1 hour at room temperature, then treated using histoblock for 1 hour, immunofluorescence was done on the sections using different combinations of antibodies (double or triple) overnight. All antibodies were diluted in PBS+S. 1° antibodies are described in Tables 2.4 and 2.5. 2° antibodies were applied on the sections for 1 hour at room temperature and they are listed in Table 2.3. DAPI was used to label the nucleus (Sigma-Aldrich) with the 2° antibodies. Afterwards, the tissues were washed with PBS twice for 10 min and then immersed in 4% paraformaldehyde (Carl Roth) for 10 min and again washed with PBS twice for 10 min, then Sections were mounted using carbonate-buffered glycerol, pH 8.6.

Antigen	Host	Dilution	Source	Catalogue code	Marking
TRPM5	rabbit, polyclonal	1:4000	Dr. V Chubanov, München, Germany (Kaske et al. 2007)	AB-321	Brush cells
GNAT3	goat, polyclonal	1:400	Covalab	Pab 73402	Brush cells
POU2F3	rabbit, polyclonal	1:200	Sigma	A116844	Brush cells
PLCβ2	rabbit, polyclonal	1:400	Santa Cruz	SC-206	Brush cells
Advillin	rabbit, polyclonal	1:200	Novus Biologicals	NBP2-34118	Brush cells
LRMP	rabbit, polyclonal	1:500	Thermofischer, Waltham, Massachusetts, USA	PA5-53824	Brush cells
CK19	Mouse, monoclonal	1:200	Abcam, Cambridge, UK	Ab7754	Epithelial cells
PGP 9.5	mouse, monoclonal	1:400	Biotrend, Köln, Germany	BT78-6320-04 Clone 13C4	Neuroendocrine cells
Uteroglobin	mouse, monoclonal	1:500	Antibodies online, Aachen, Germany	ABIN3215473 Clone 06	Secretory cells
Foxi1	goat, polyclonal	1:200	Abcam, Cambridge, UK	ab20454	Ionocytes
β-Tubulin	mouse, monoclonal	1:1200	BioGenex, Fremont, California, USA	MU178-UC Clone ONS1A6	Ciliated cells
PGP 9.5	Rabbit, polyclonal	1:8000	Biotrend, Köln, Germany	BT78-6305-04	Neuroendocrine cells

Table 2.2 Primary antibodies used in immunofluorescence in human.

Antigen	Host	Dilution	Source	Catalogue code
LRMP	rabbit, polyclonal	1:500	Thermofischer, Waltham, Massachusetts, USA	PA5-53824

GNAT3	goat, polyclonal	1:400	Covalab, Rue Jacques Monod, Bron, France	Pab 73402
GFP	chicken, polyclonal	1:2000	Novus Biologicals, Littleton, Colorado, USA	NB100-1614
TRPM5	rabbit, polyclonal	1:4000	Dr. V Chubanov, München, Germany (Kaske et al. 2007)	AB-321

Table 2.4 Primary antibodies used in immunofluorescence in mice.

Antigen	Host	Dilution	Source	Catalogue code
ChAT	goat, polyclonal	1:500	Millipore, Burlington, Massachusetts, USA	AB144P
Villin	mouse, monoclonal	1:200	Immunotechnology, Kraemer Boulevard Brea, California	IM0258 Clone 1D2C3
Advillin	rabbit, polyclonal	1:200	Novus Biologicals, Littleton, Colorado, USA	NBP2-34118

Table 2.5 Primary antibodies used in immunofluorescence in pig.

Antigen	Host	Conjugate	Dilution	Source	Catalogue code
Rabbit Ig	donkey	Cy3	1:2000	Chemicon, Limburg, Germany	AP182C
Rabbit Ig	donkey	Alexa 488	1:500	Invitrogen, California, Carlsbad, USA	A-21206
Mouse Ig	donkey	Cy3	1:1000	Dianova, Hamburg, Germany	715-165-151
Mouse Ig	donkey	FITC	1:100	Dianova, Hamburg, Germany	715-095-151
Mouse Ig	donkey	Cy5	1:800	Dianova, Hamburg, Germany	715-175-151
Chicken IgY	donkey	FITC	1:400	Dianova, Hamburg, Germany	703-095-155
Goat Ig	donkey	Alexa 488	1:1000	Molecular Probes, Eugene, Oregon, USA	A-11055
Goat Ig	donkey	Cy5	1:400	Dianova, Hamburg, Germany	715-175-147

Table 2.3 Secondary antibodies used in immunofluorescence.

2.4.3 Indirect immunofluorescence of whole mount

Tracheas were first rinsed in PBS for 15 min and then, permeabilization was performed for 2 hours using 0.3% Triton X-100 (Carl Roth) in PBS (0.08 M NaCl, 0.005 M phosphate buffer), pH 7.4. Then, a blocking solution (1% bovine serum albumin, 4% normal horse serum in PBS) was used for 2 hours to block the non-specific binding sites. All antibodies were diluted in PBS+S, pH 7.4. 1° Antibodies were added overnight at room temperature. After washing the sample with PBS (5x30), histoblock was added to the sample for 2 hours incubation time. 2° Antibodies were applied on the sections overnight at room temperature. DAPI was used as described before to label the nucleus. After a washing step with PBS (5x30 min), postfixation in buffered formaldehyde (Carl Roth) for 10 min and again washing with PBS at room temperature (5x30 min), then samples were mounted using Mowiol 4–88 (pH 8.6; Merck).

2.4.4 Microscopy

The evaluation of the samples was done with an epifluorescence microscope (Axioplan 2, Zeiss, Oberkochen, Germany) equipped with appropriate filter sets (Table 2.6). The quality of preservation of the epithelium in H&E-stained sections was evaluated by brightfield microscopy (Leica, DM750, Wetzlar, Germany). Confocal laser scanning microscopes (LSM 710, Zeiss) was used to evaluate whole mount tracheas.

Fluorescent dyes	Excitation filter	Emission filter	Dichroic mirror
DAPI	360-370 nm	420-460 nm	400 nm
FITC	460-490 nm	515-550 nm	505 nm
Cy3	525-560 nm	570-650 nm	555 nm
Cy5	590-650 nm	665-740 nm	655 nm

Table 2.6 Epifluorescence microscope filters.

2.4.5 Controls for immunofluorescence studies

The 1° antibody was omitted to determine the specificity of the 2° antibody. In the experiments, incubation with only PBS+S on the sections was done. Human papilla vallata was used as a positive control for LRMP-, TRPM5-, PLCβ2-, GNAT3- and POU2F3-antibodies and to choose the best dilution of the antibody. Moreover, human kidney was used as a positive control for FOXI1 antibody and human lung as a positive control for uteroglobin antibody. Preabsorption with the immunizing peptide (recombinant LRMP protein with N-terminal His6-ABP tag, Novusbio, 3 mg/ml overnight at room temperature) completely prevented LRMP-immunostaining, indicating the specificity antibody for the LRMP epitope.

2.5 Cell counting

To quantify LRMP-immunoreactive cells in the human nose, trachea, bronchus and bronchiole, immunolabeling with antibodies against LRMP was performed. Six sections of the nasal concha (n=5), trachea (n=5) and lung (n=8) were done with at least 50 µm distance from each other. Counting was performed directly at the epifluorescence microscope (Axioplan 2) with 40x objective lens. The number of immunoreactive cells was counted and expressed in relation to the length of the underlying BM measured by imageJ. LRMP-immunoreactive cells in lungs from organ donors (n=9) and in lungs resected from COPD in the course of lung transplantation (n=6) were quantified in the same manner.

To quantify PGP-immunoreactive cells in the human trachea, bronchus and bronchiole, immunolabeling with antibodies against PGP was performed. Six sections of the upper trachea (n=10), lower trachea (n=6) and lung (n=6) were done with at least 50 µm distance from each other. Counting was performed directly at the epifluorescence microscope (Axioplan 2) with 40x objective lens. The number of immunoreactive cells was counted and expressed in relation to the length of the underlying BM measured by imageJ.

To quantify ChAT-, villin- and advillin- immunoreactive cells in the pig (n=5) trachea (upper part, middle part and lower part), bronchus and bronchiole, triple-labeling with

antibodies against ChAT, villin and advillin was performed. Sections of the trachea and lung were collected, 4 sections each with at least 50 µm distance from each other. Counting was performed directly at the epifluorescence microscope (Axioplan 2) with 40x objective lens, and the number of these cells was counted per millimeter BM measured by ImageJ.

To quantify TRPM5-immunoreactive cells in the lung in C57BL/6Rj mice (n=10), labeling with antibodies against TRPM5 was performed. Longitudinal sections of the lung were collected, 10 sections each with at least 50 µm distance from each other. Counting was performed manually using epifluorescence microscope (Axioplan 2) with 40x objective lens. In addition, to quantify TRPM5-positive cells of *Trpm5*-eGFP mice (n=5), labeling with antibodies against GFP (to enhance fluorescence of *Trpm5*-eGFP^{+} cells) and TRPM5 was carried out. Longitudinal sections of the lung were performed, 10 sections each with at least 50 µm distance from each other. Counting was performed directly at the epifluorescence microscope (Axioplan 2) with 40x objective lens and the number of these cells was counted per millimeter BM measured by the Axiovision software.

2.6 Reverse transcription PCR (RT-PCR)

2.6.1 RNA extraction

Samples from trachea, proximal part of lung and distal part of the lung were isolated from pigs (n=5). The tracheal and bronchial epithelial layer were scraped using the non-cutting part of a blade and added to RLT buffer (Qiagen, Hilden, Germany) supplemented with 1% β-mercaptoethanol (Sigma-Aldrich) and filtered with a QIA shredder column (Qiagen) (Figure 2.1). RNeasy kit from Qiagen company was used to isolate RNA from the samples according to the manufacturer's instructions. Yield was controlled by Nanodrop (Thermo Fisher) and RNAs were stored at -80°C until further use.

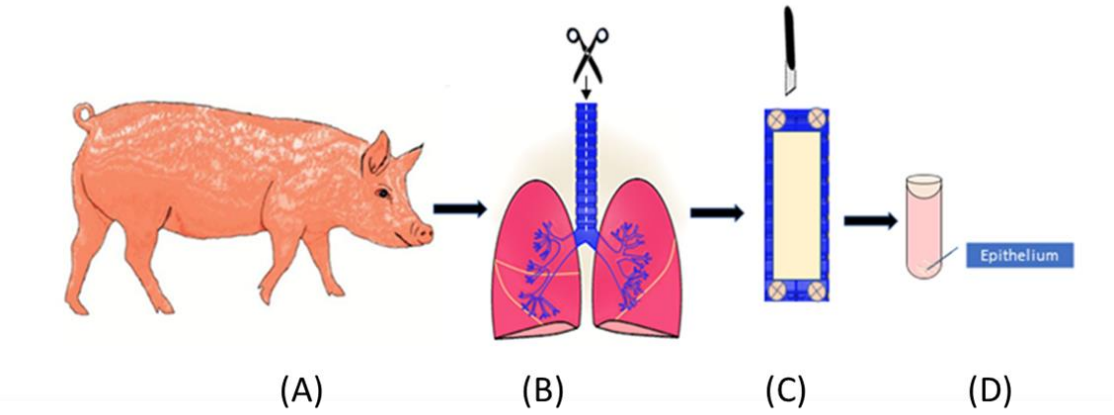

Fig. 2.1 Schematic overview of the RNA extraction in pig. (A, B) Pig trachea was opened using scissor. (C) Exposed epithelium was abraded using the non-cutting edge of the scalpel. (D) Epithelium was added to RLT and β-mercaptoethanol and stored at -80°C

2.6.2 Complementary DNA (cDNA) synthesis

For synthesis of cDNA (Eppendorf Master Cycler Personal 5332, Hamburg, Germany), 1 µl DNase (1 U/µl) and 1 µl 10x DNase reaction buffer were added to 8 µl RNA for 15 min at 25°C for degradation of contaminating DNA. 1 µl of ethylenediaminetetraacetic acid (EDTA, 25 mM) was added to each sample to inactivate DNAase (10 min incubation at 65°C), then samples were cooled for 2 min and to each sample a total of 9 µl reaction mixture including 1 µl dNTPs (10 mM), 1 µl Superscript RNase H- RT (200 U/µl), 1 µl oligo-dT (50 µM), 2 µl dithiothreitol (0.1 M) and 4 µl 5x first-strand buffer were applied to each sample. The provider for these reagents was Invitrogen, except dNTPs which were from Qiagen, and oligo-dT were from Eurofins. cDNAs were kept at -20°C until further use. Reverse transcriptase was excluded during cDNA synthesis serving as a negative control.

2.6.3 Polymerase chain reaction (PCR)

PCR (Eppendorf Master Cycler Gradient 5331, Hamburg, Germany) was done with cDNA samples using intron spanning primers (Table 2.7) for *β-actin* (housekeeping gene), *chat, villin* and *advillin*. The following protocol was used: 13.3 µl H_2O, 0.8 µl cDNA as template, 2 µl $MgCl_2$ (25 mM), 0.6 µl dNTPs (10 mM), 2.5 µl 10x PCR buffer II, 0.6 µl of primers (20 pM) and 0.2 µl AmpliTaq Gold DNA polymerase (5 U/µl) were mixed; all reagents were

from Thermo Fisher. PCR was performed using the following temperature and time: 95°C for 12 min (enzyme activation), followed by 39 cycles at 95°C for 20 s (denaturation), 60°C for 20 s (annealing), and 72°C for 20 s (extension) and a final extension for 7 min at 72°C. β-Actin was used to check for PCR efficiency, genomic DNA contamination was evaluated using water as a negative control.

Gene	GeneBank accession No	Primer	Product length (bp)
β-Actin	XR-002342206	Forward: TCTACACCGCTACCAGTTCG Reverse: CTTCTCCATGTCGTCCCAGT	274
Advillin	XM-013992155	Forward: GCTCCATTATCAAGCCTGCC Reverse: GCCTTGTTGCTACCTCTGTG	123
Chat	NM-001001541	Forward: CCGAGAAGTGTGCAAGGAAC Reverse: TACCACAGGACCATAGCAGC	130
Villin	XM-001925167	Forward: ATCTCAAGACCCATCCCAGC Reverse: GTCCCCAGAGTTTCCAAGCT	170

Table 2.7 Primers that were used in RT-PCR

2.6.4 Gel electrophoresis

Five µl loading buffer (1:5), (25 ml of glycerol (Merck), 25 ml of 1xTAE buffer, 20 mg Orange G dye (Sigma-Aldrich)) were added to 25 µl of the PCR products. Electrophoresis of the PCR products was performed using Tris-acetate-ethylenediaminetetraacetic acid buffer (1x TAE, pH 8) (for preparation of 50x TAE (242 g/l TRIS (Carl Roth), 100 ml/l of 0.5 M EDTA (Invitrogen), 57.1 ml/l glacial acetic acid (Merck), in 1 l distilled H_2O, pH 8.0) used to dissolve 2% agarose gel (20 g/l agarose, Biozym GmbH, Vienna, Austria). Afterwards, the gel was cooked in a microwave oven for 5 min (900 W) and 20 µl/l of ethidium bromide (Carl Roth) was added to the gel. In a Horizon 11-14 (peQlab biotechnology (VWR), Radnor, Pennsylvania, USA), the gel was poured into horizontal electrophoresis. 12.5 µl

of PCR products were added to the gel after 20 min. 7 µl of a 100 bp DNA ladder (Invitrogen) was used as a marker. The electrophoresis was run at a voltage of 150 V over 45 min and bands were identified by ultraviolet light using a Gel Imager (Intas, Germany)

2.7 *In silico*-analysis of published mRNA sequencing data

2.7.1 Human

Previously published single cell RNA sequencing data (Goldfarbmuren et al. 2020, dataset GSE134174; Plasschaert et al. 2018, data set GSE102580) of human bronchial and tracheal epithelial cells were downloaded from NCBI GEO dataset and analyzed. Datasets were analyzed and re-clustering was done using the Seurat R package (version 2.3.4) (Wolock et al. 2019). Principle component analysis (PCA) was done, and UMAP (Uniform Manifold Approximation and Projection) was used for non-linear dimensional reduction (Satija et al. 2015). Cells were represented in a two-dimensional UMAP plot, and clusters were identified and annotated based on the composition of typical marker genes.

2.7.2 Mice

Previously published single cell RNA sequencing data (Montorro et al. 2018, dataset GSE103354; Plasschaert et al. 2018, data set GSE102580) of murine tracheal epithelial cells (C57BL/6 wild-type) were downloaded from NCBI GEO dataset and analyzed. Datasets were analyzed and re-clustering was done using the Seurat R package (version 2.3.4) (Wolock et al. 2019). Principle component analysis (PCA) was done, and UMAP (Uniform Manifold Approximation and Projection) was used for non-linear dimensional reduction (Satija et al. 2015). Cells were represented in a two-dimensional UMAP plot, and clusters were identified and annotated based on the composition.

2.8 Pre-embedding immunoelectron microscopy

For pre-embedding immunoelectron microscopy, tracheal samples from mice were dissected and placed in Zamboni's fixative overnight at 4°C. In addition, human taste buds and lung were dissected from human body donor. Human and mice specimens were then

washed and frozen as in section 2.2.2. Then, the samples were cryosectioned at 40 µm thickness (CM-3050S cryostat; Leica).

Floating sections were immersed in PBS, and to avoid unspecific protein binding, 10% normal horse serum was used for 1 hour. Sections were then incubated overnight at room temperature with rabbit polyclonal antibody against LRMP (1:500, PA5-53824, Thermo Fisher) and with PBS (without 1° antibody). After washing with PBS (3x5 min), the sections were incubated for 1 hour using peroxidase-conjugated swine anti-rabbit Ig (1:100; P0217, Dako, Santa Clara, USA). Afterwards, the tissues were washed with PBS (1x5 min) and then with 0.05 M Tris-HCL buffer (2x5 min) pH 8.6. 4 µl of a solution containing (0.1 mg/ml 3.3'-diaminobenzidine-hydrochloride (DAB) (Sigma-Aldrich) and, to enhance staining, 15 mg/ml nickel ammonium sulfate (Honeywell, New Jersey, USA) in 0.05 M Tris-HCl buffer (pH 8.6) was added to the sections for 10 min. Afterwards, 1.2 µl H_2O_2 (30%, Fluka) were added to the solution for 45 min. Tris-HCl buffer (3x5 min) was used to rinse the samples, then specimens were incubated in 1% osmium tetroxide (Sigma-Aldrich) for 1 hour and washed in distilled water (3x5 min). Samples were stained in half-saturated uranyl acetate with distilled water (80 mg/2 ml distilled water, Merck) overnight under the hood. Dehydration was performed in a series of ethanol (30%, 50%, 70%, 90%, 96% and 2x100%, 5 min for each step, then 100% ethanol + propylene oxide were added to the samples in a ratio of 1:1 for 5 min, followed by in propylene oxide (2x5 min), and propylene oxide + epon (Agar Scientific, Essex, UK) in a ratio of 1:1 for 30 min. Samples were then penetrated by epon at room temperature overnight, then embedded flat between plastic sheets with fresh epon and sored at 60 ℃ overnight. Light microscopy (LEICA DM750, Wetzlar, Germany) was used to select the sections containing immunolabelled cells. Regions of interest were cut out with a razor blade and mounted on the top of an epon pyramid using freshly prepared epon and heating to 60° overnight. Ultrathin sections (80 nm) were cut using an ultramicrotome (Reichert Ultracut E, Leica) and collected on a copper grid without performing counterstaining.

A transmission electron microscope (EM 902 N, Zeiss, Oberkochen, Germany) equipped with a slow-scan 2K CCD camera (TRS, Tröndle, Moorenweis, Germany) was used for ultrathin sections analysis.

2.9 Statistical analysis

Statistic was performed using GraphPad Prism software version 7 (La Jolla, CA, USA) for windows. Data are shown in scatter plots indicating median ± interquartile range (IQR). Normal distribution was analyzed using the Kolmogorov-Smirnov or the Shapiro-Wilk tests. Data deviated from normal distribution were analyzed by non-parametric tests using Mann-Whitney U-test or Kruskal-Wallis test followed by Dunn's multiple comparisons test. Differences between values were considered to be statistically significant when $P \leq 0.05$.

3 Results

3.1 Brush cells in human respiratory tract epithelium.

3.1.1 The logical and first-hand approach did not work.

Taste signal transduction cascade markers (PLCβ2, GNAT3, TRPM5) [Krasteva et al. 2011, Tizzano et al. 2011, Saunders et al. 2013] and recently POU2F3 [Yamashita et al. 2017] have been considered to serve as excellent immunohistochemical markers to identify brush cells in murine tracheal epithelium. Moreover, it was previously reported that villin is a brush cell marker but nowadays it is proved that advillin is a brush cell marker. So, we used antibodies against these markers in mouse trachea and observed single positive cells in the tracheal epithelium (Figure 3.1A). Human papilla vallata was used as a positive control for the use of these antibodies on human tissue. It did not show any immunoreactivity toward TRPM5, GNAT3, POU2F3 and advillin while it showed nicely stained taste cells using PLCβ2-antibody (Figure 3.1B). These cells had processes extending from the basal and the apical part of the cells. No staining was observed in the airway epithelium using any of these markers antibodies. (Figure 3.1C).

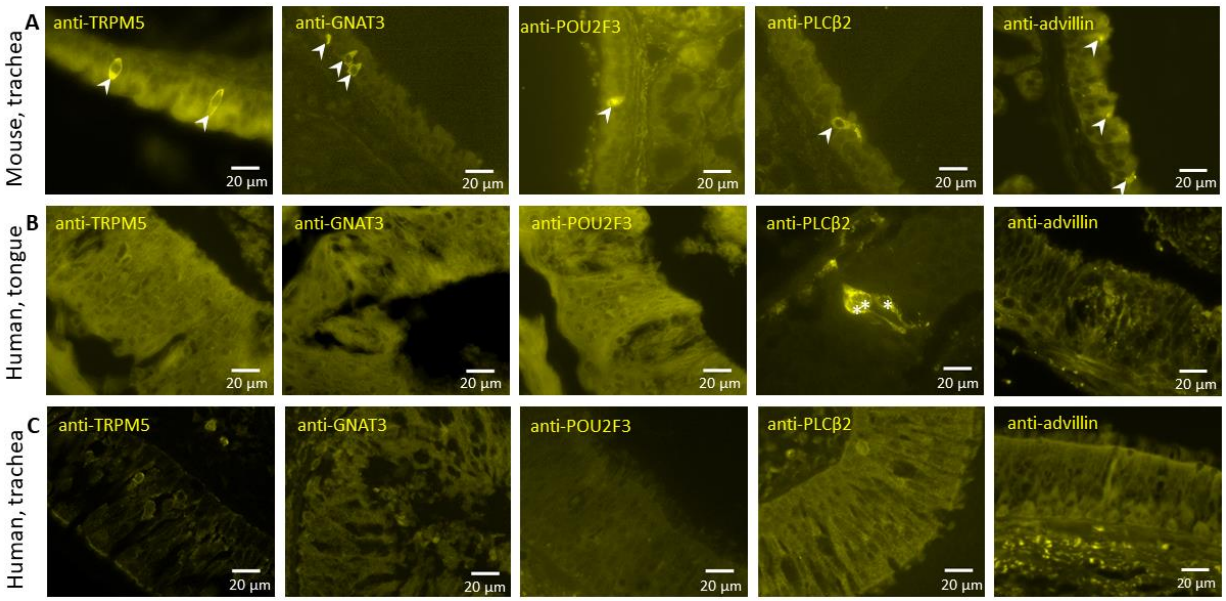

Figure 3.1: **First approach did not work on human.**

(A) Immunohistochemistry of tracheal paraffin sections from a C57BL/6RJ mouse, immunolabeled with antibodies against TRPM5, GNAT3, POU2F3, PLCβ2 and advillin showing epithelial cells with immunoreactivity toward TRPM5-, GNAT3-, POU2F3-, PLCβ2- and advillin-antibodies (arrowheads). ***(B)*** Immunohistochemistry of human taste buds, paraffin sections, showing no epithelial cells with immunoreactivity toward TRPM5-, GNAT3-, POU2F3-and advillin-antibodies but showing PLCβ2-immunoreactive cells (asterisks) (right image). ***(C)*** Immunohistochemistry of human tracheal paraffin sections showing no epithelial cells with immunoreactivity toward TRPM5-, GNAT3-, POU2F3- and PLCβ2-antibodies. Images captured with black and white camera; Image J was used to color images.

3.1.2 *In silico*-analysis of publicly available sequencing data reveals *LRMP*-mRNA expression in brush cells of human airways epithelium.

3.1.2.1 Trachea

The immunohistochemical findings were supplemented by *in silico*-analysis of published single cell sequencing data (GSE134174) of human tracheal and bronchial epithelial cells. We were able to reproduce the clustering according to the results reported by Goldfarbmuren et al. (2020) who could identify nine cell clusters, namely goblet, secretory, basal/club, ciliated, club, immune cells, basal 1, basal 2 and rare cells (Figure 3.2A). The latter were subclustered into ionocytes, neuroendocrine and brush/tuft cells (Figure 3.2B).

This analysis showed that *LRMP*-mRNA was expressed predominantly in brush cells, followed by *POU2F3*-mRNA. On the other hand, *TRPM5*- and *GNAT3*-mRNA were minimally expressed while *PLCβ2*- and *ChAT*-mRNA were not expressed at all (25 cells were used for analysis) (Figure 3.2C).

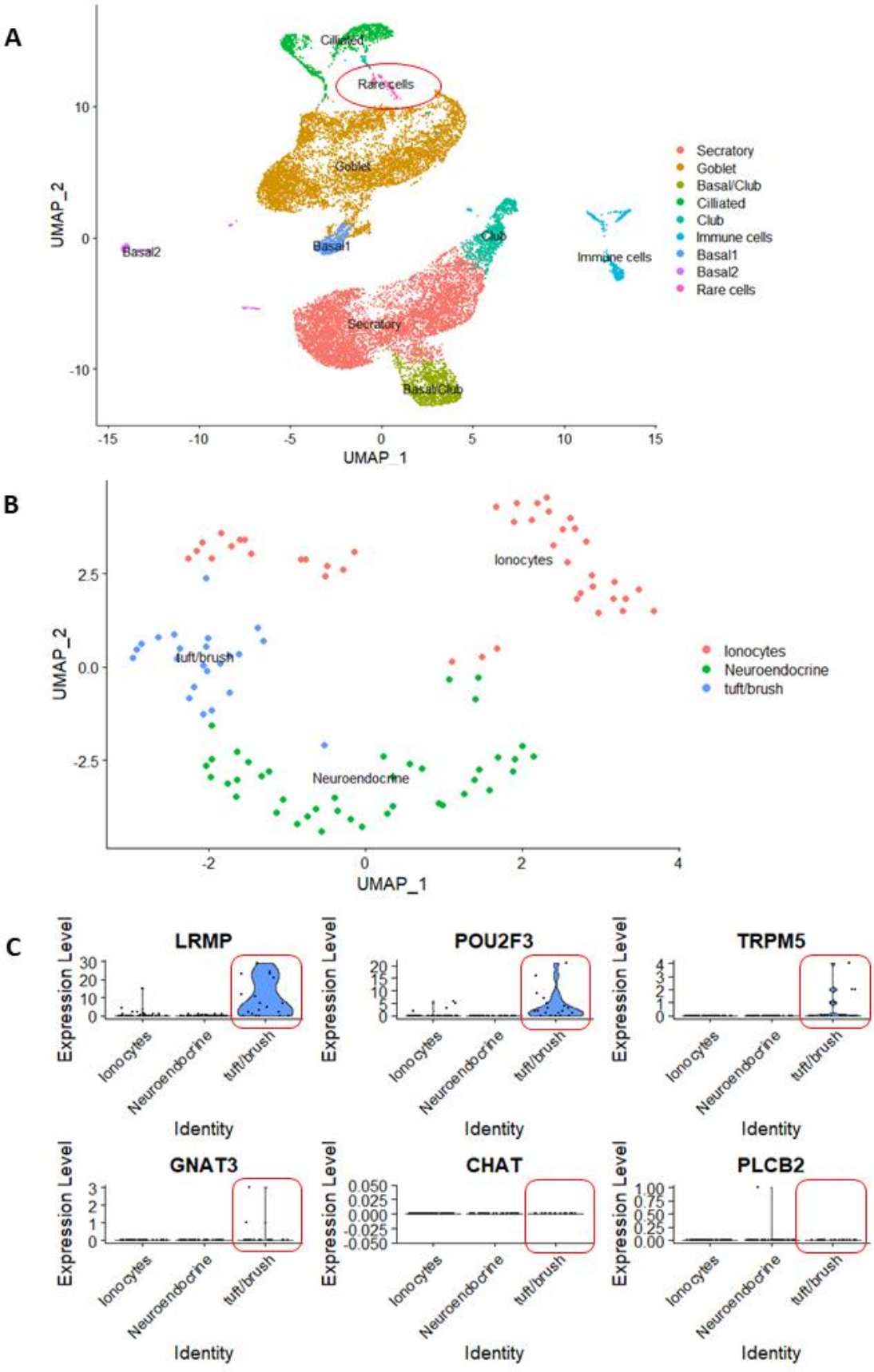
A
Ciliated
Rare cells
Goblet
Basal1
Basal2
Club
Immune cells
Secratory
Basal/Club
UMAP_2
UMAP_1
Secratory
Goblet
Basal/Club
Ciliated
Club
Immune cells
Basal1
Basal2
Rare cells
B
Ionocytes
tuft/brush
Neuroendocrine
UMAP_2
UMAP_1
Ionocytes
Neuroendocrine
tuft/brush
C
LRMP
POU2F3
TRPM5
GNAT3
CHAT
PLCB2
Expression Level
Identity
Ionocytes
Neuroendocrine
tuft/brush

Figure 3.2: *In silico*-analysis of single cell mRNA sequencing data GSE134174 reveals *LRMP*-mRNA expression predominantly in brush cells in human tracheal epithelium.
(A) SPRING plot (Uniform Manifold Approximation and Projection, UMAP) shows nine distinct cell clusters, namely goblet, secretory, basal/club, ciliated, club, immune cells, basal 1, basal 2 and rare cells. ***(B)*** The rare cell cluster was subclustered into ionocytes, neuroendocrine and brush/tuft cells. ***(C)*** Violin plots showing *LRMP*-mRNA being predominantly expressed within the chemosensory (brush/tuft) cell, followed by *POU2F3*-mRNA. On the other hand, *TRPM5*- and *GNAT3*-mRNA were minimally expressed while *PLCβ2*- and *ChAT*-mRNA were not expressed at all (25 cells were used for analysis).

3.1.2.2 Bronchus

In silico-analysis of previously published single cell RNA sequencing data from human bronchial epithelial cells (Plasschaert et al. 2018, data set GSE102580) identified seven clusters, namely secretory, basal/secretory, ciliated, club, basal, ionocytes, and cholinergic chemosensory cells (brush/tuft) and neuroendocrine cells clustered together (Figure 3.3A).

This analysis showed that *LRMP*-mRNA was predominantly expressed within the chemosensory (brush/tuft)/neuroendocrine cell cluster, followed by *POU2F3*-mRNA. On the other hand, *TRPM5-, PLCβ2*- and *ChAT*-mRNA were very minimally expressed while *GNAT3*-mRNA was not expressed at all in the combined chemosensory cell (brush/tuft)/neuroendocrine cell cluster (53 cells were used for analysis) (Figure 3.3B).

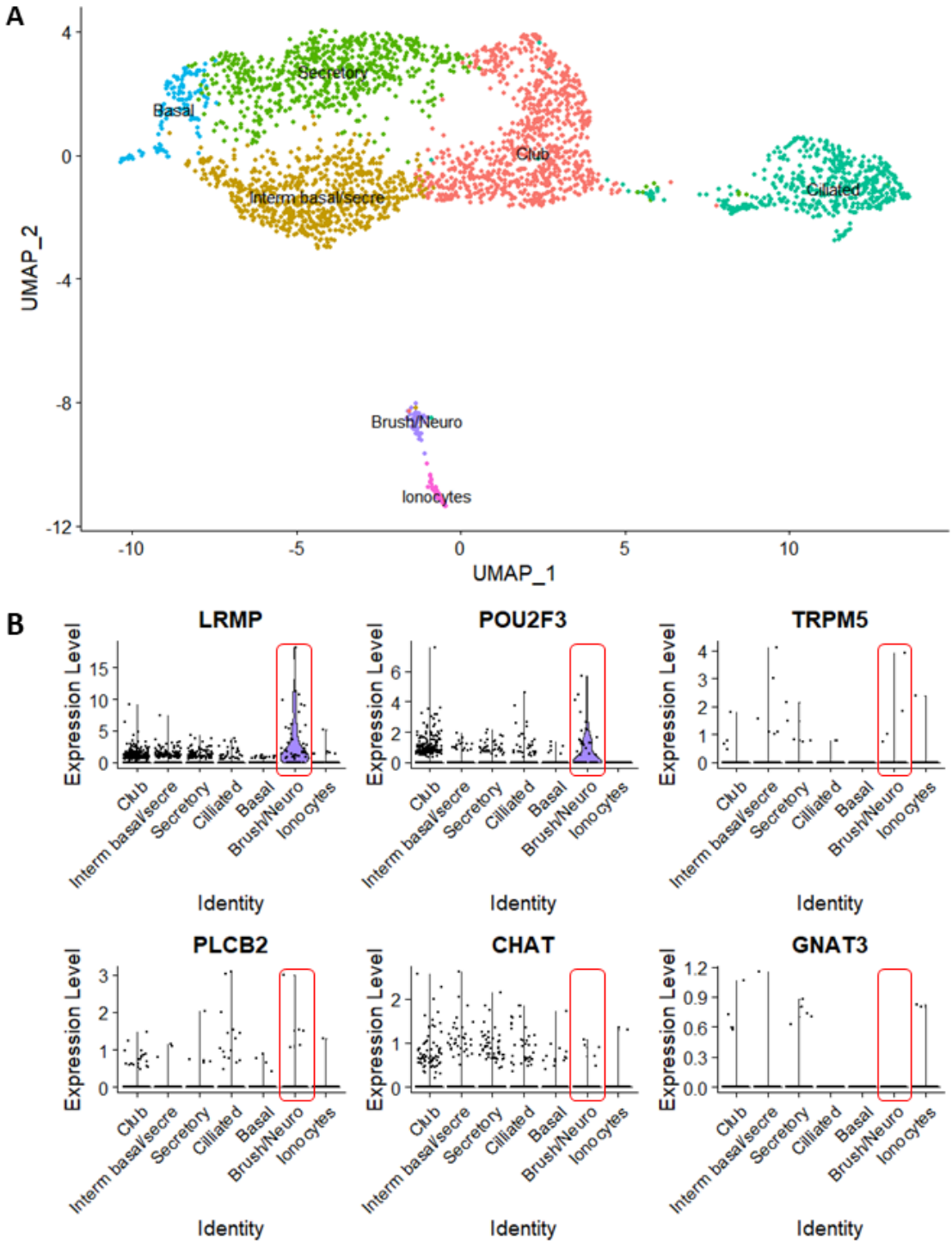

Figure 3.3: *In silico*-analysis of single cell mRNA sequencing data GSE102580 reveals *LRMP*-mRNA expression predominantly in combined brush/neuroendocrine cell cluster in bronchial epithelium.

(A) SPRING plot (Uniform Manifold Approximation and Projection, UMAP) identified seven clusters, namely secretory, basal/secretory, ciliated, club, basal, ionocytes, and

chemosensory cells (brush/tuft) and neuroendocrine cells clustered together ***(B)*** Violin plots showing *LRMP*-mRNA is predominantly expressed within the chemosensory (brush/tuft)/neuroendocrine cell cluster, followed by *POU2F3*-mRNA. On the other hand, *TRPM5-, PLCβ2-* and *ChAT*-mRNA were very minimally expressed while *GNAT3*-mRNA was not expressed at all in the combined chemosensory cell (brush/tuft)/neuroendocrine cell cluster (53 cells were used for analysis).

3.1.3 Positive controls used in the study.

Paraffin sections from human colon were immunolabelled with antibodies against LRMP; this revealed LRMP-immunolabelling of cells in human colon. These cells were flask-shaped with processes extending from the basal to the apical part of the cell (Figure 3.4A). Paraffin sections from human kidney (distal tubule) from body donors were immunolabelled with antibodies against FOXI1. This revealed FOXI1-immunolabelling of cells in human kidney. This antibody labels the nucleus of FOXI1-immunoreactive cells (Figure 3.4B).

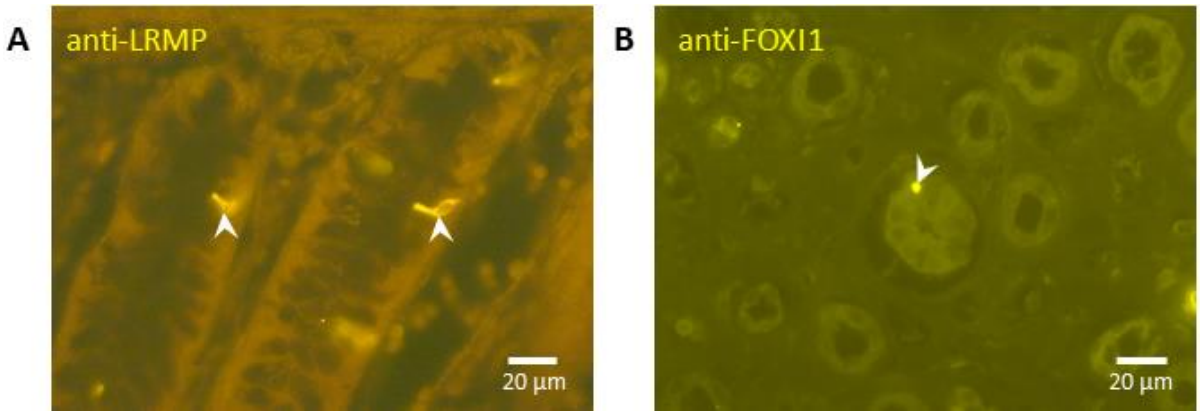

Figure 3.4: Positive controls used in the study.
(A) Immunohistochemistry of human colon paraffin sections immunolabeled with antibody against LRMP showing immunoreactivity toward LRMP (arrowheads). Image captured with color camera; true colors are shown. ***(B)*** Immunohistochemistry of human kidney paraffin section from human donor immunolabeled with antibody against FOXI1 showing immunoreactivity toward FOXI1 in the nucleus (arrowhead). Image captured with black and white camera; Image J was used to color images.

3.1.4 LRMP-immunolabelling in the taste bud in human papilla vallata

As there are similarities between taste cells and brush cells in regard to the signal transduction cascade markers, paraffin sections from papilla vallata from human donors were immunolabelled with antibodies against LRMP. This revealed LRMP-immunolabelling of cells in human taste buds. These cells were flask-shaped with processes extending from the basal to the apical part of the cell (Figure 3.5A, 3.5B).

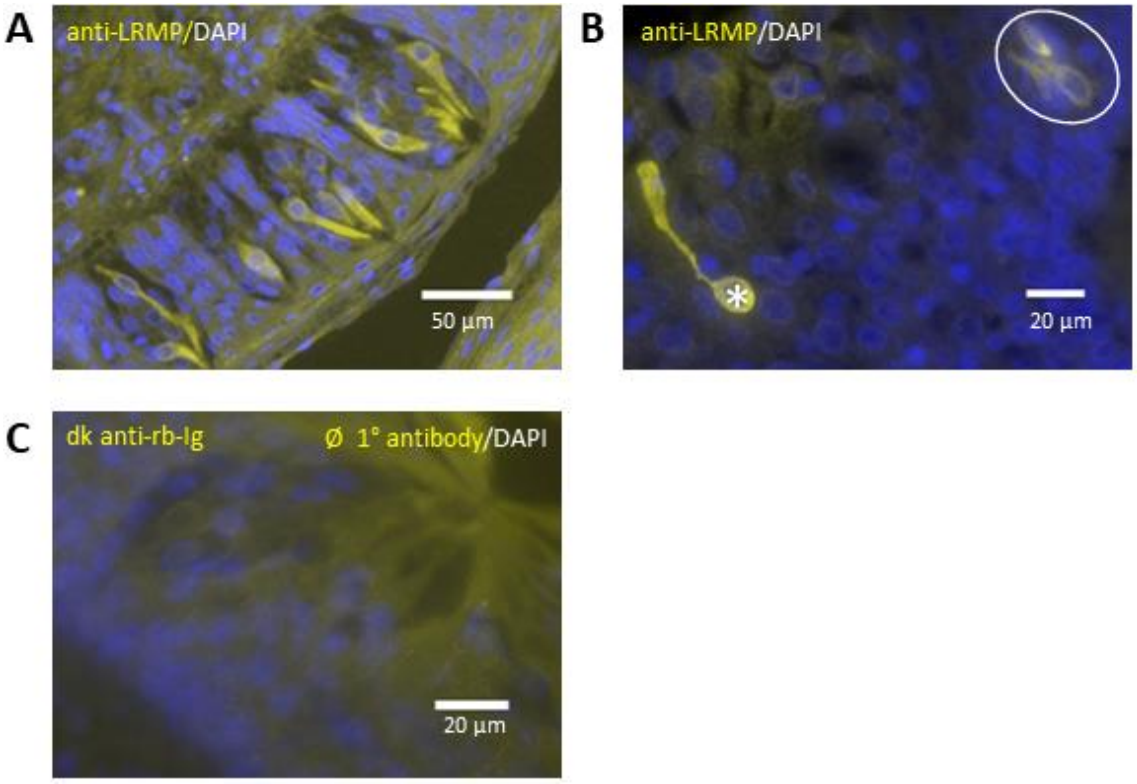

Figure 3.5: **LRMP-immunolabelling in the taste bud of human papilla vallata.** ***(A and B)*** Immunohistochemistry of human papilla vallata paraffin sections immunolabeled with antibody against LRMP showing immunoreactivity toward LRMP. ***(A)*** LRMP-immunoreactive cells in four taste buds in papilla vallata. ***(B)*** LRMP-immunoreactive cells in another taste bud at high magnification (40x objective lens) (asterisk and the circled cells). ***(C)*** No immunoreactivity was observed when the primary antibody (LRMP) was omitted. Images captured with black and white camera; Image J was used to color images and DAPI (blue) was used to label the nucleus.

3.1.5 LRMP-immunolabeling in human respiratory tract epithelium.

3.1.5.1 Nose

Nasal paraffin sections from human donors were double- and triple-immunolabeled with antibodies against LRMP and the other epithelial cell markers, including CK19 (general epithelial cell marker which labeled epithelial cells as in Figure 3.6A, central panel), PGP 9.5 (neuroendocrine cell and nerve fibers marker, Figure 3.6B, central panel), FOXI1 (ionocytes marker, this antibody labeled the nucleus, Figure 3.6C, central panel in green), tubulin (ciliated cell marker, which labels ciliated cells, Figure 3.6C, central panel in red) and anti-uteroglobin (secretory cell marker, was also applied, but this antibody did not result in any immunolabeling in these nasal sections). These incubations revealed co-localization of LRMP- and CK19-immunoreactivities, indicating that LRMP-immunoreactive cells are epithelial cells (Figure 3.6A, right panel). In contrast, no colocalization was detected between LRMP and PGP, indicating that LRMP-immunoreactive cells are not immunoreactive to PGP-antibody and, hence, are not neuroendocrine cells (Figure 3.6B, right panel). Triple-immunolabeling with antibodies against LRMP, FOXI1 and tubulin revealed that LRMP-immunoreactive cells are not immunoreactive to FOXI1- and tubulin-antibodies, indicating that LRMP-immunoreactive cells are neither ionocytes nor ciliated cells (Figure 3.6C, right panel). The LRMP-immunoreactive cells were flask-shaped epithelial cells with apical and basal processes reaching the lumen. There were cases where such a luminal process was not seen, this might be caused by the orientation of cutting.

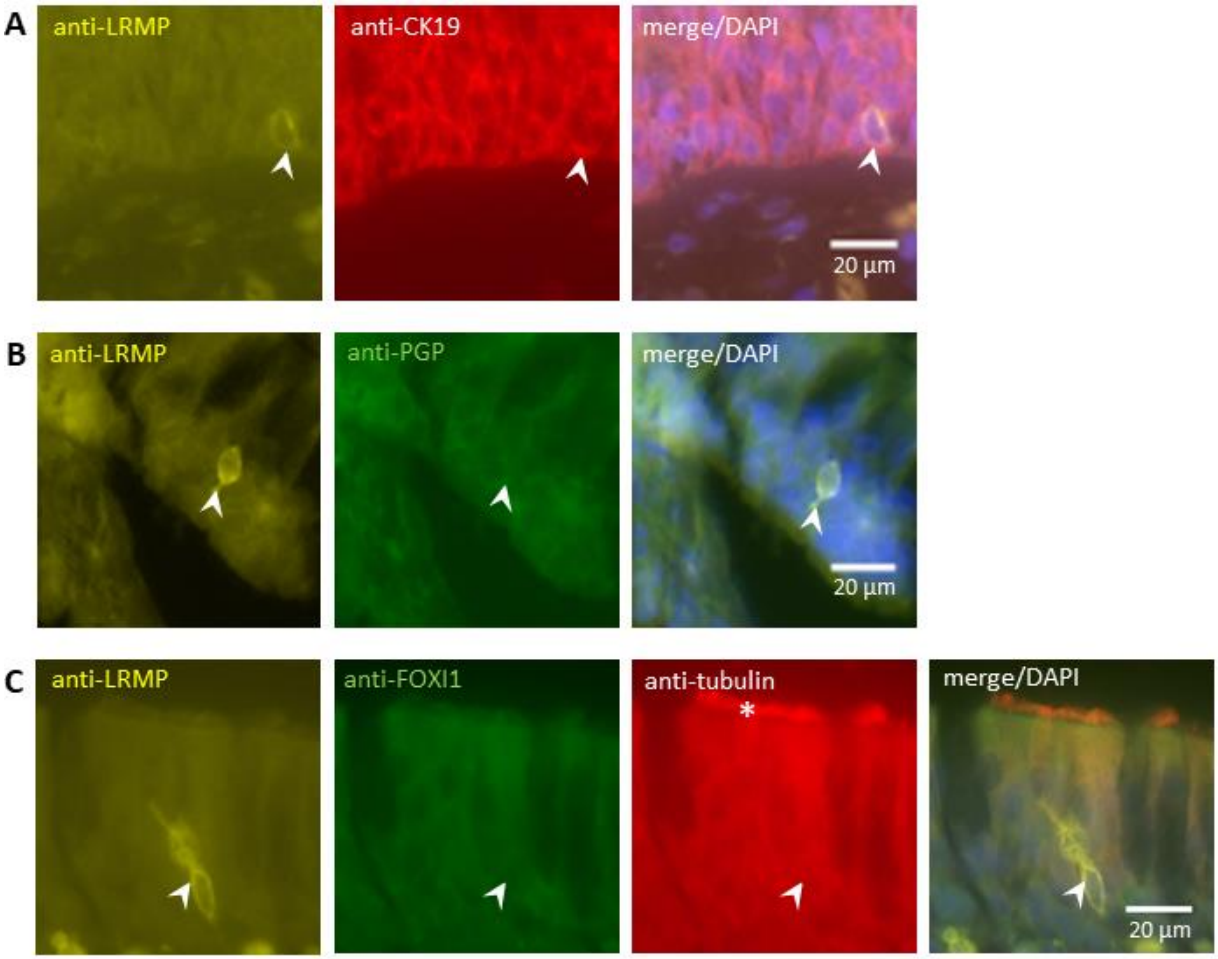

Figure 3.6: LRMP-immunolabeling in the nasal epithelium of human donor.
(A-C) Immunohistochemistry, paraffin sections of the nose. ***(A)*** Colocalization of immunoreactivities to LRMP and CK19 within the same cell (arrowhead). ***(B)*** LRMP-immunoreactive cell (arrowhead) was not labeled with antibodies against PGP 9.5 (neuroendocrine cell and nerve fiber marker), indicating that this cell was not a neuroendocrine cell. ***(C)*** LRMP-immunoreactive cell (arrowhead, right panel) was not labeled with antibodies against FOXI1 (ionocyte marker) and tubulin (ciliated cell marker, asterisk), showing that this LRMP-immunoreactive cell was neither an ionocyte nor a neuroendocrine cell. Images captured using black and white camera; Image J was used to color images and DAPI (blue) was used to label the nucleus.

Figure 3.7 shows other regions where immunoreactivities were visible and shows controls with no immunoreactivities when the antibodies were omitted.

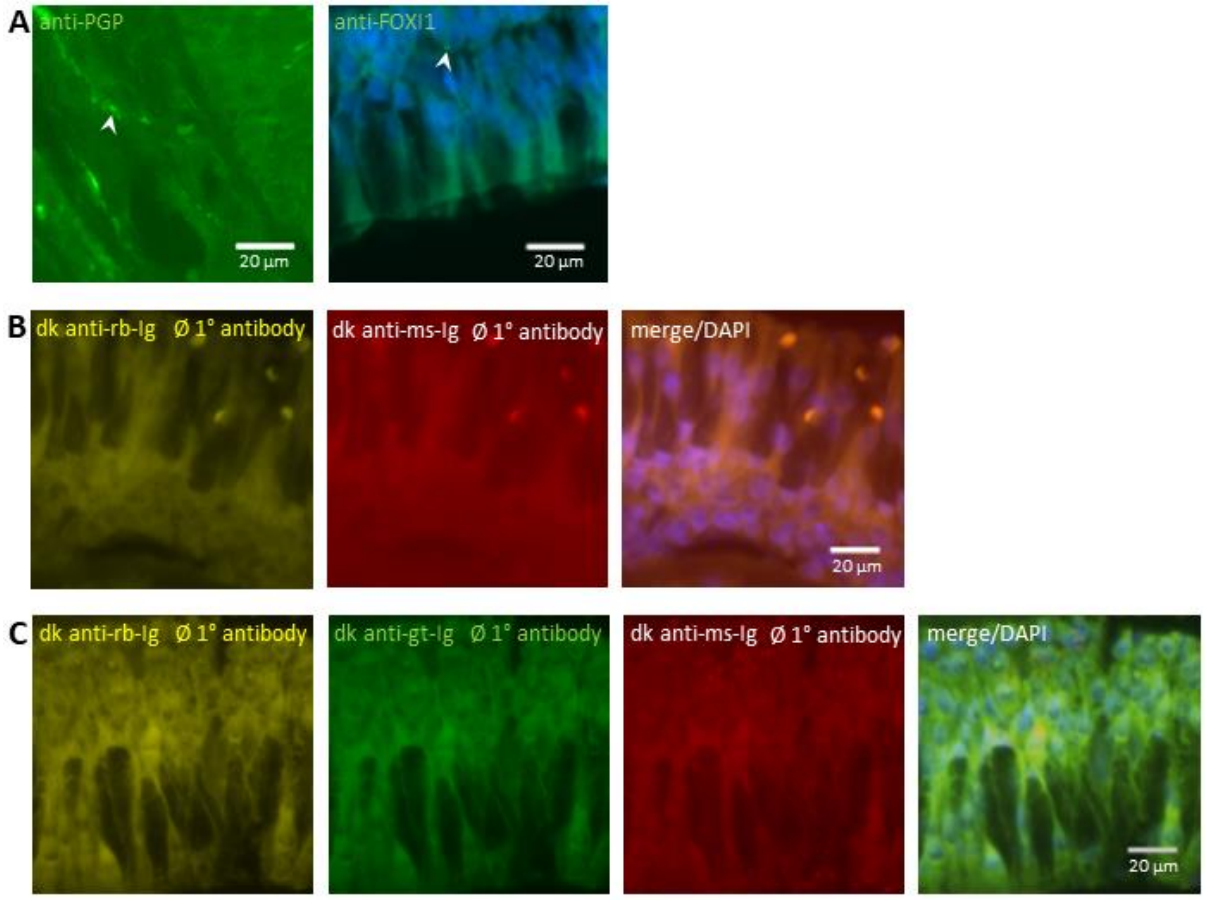

Figure 3.7: Controls used in human nose.
(A-C) Immunohistochemistry, paraffin sections of the nose. ***(A)*** PGP-immunoreactive nerve fibers (left panel, arrowhead) in the same section shown in Figure 3.6B, central panel. FOXI1-immunoreactivity labeling only the nucleus (right panel, arrowhead). ***(B)*** No immunoreactivities were observed when LRMP-antibody (from rabbit) and other antibodies (PGP and CK19; from mouse) were omitted. ***(C)*** No immunoreactivities were observed when LRMP-antibody (from rabbit) and other antibodies (FOXI1; from goat, tubulin; from mouse) were omitted. Images captured with black and white camera; Image J was used to color images and DAPI (blue) was used to label the nucleus.

3.1.5.2 Trachea

Tracheal paraffin sections from human donors were double-immunolabeled with antibodies against LRMP and the other epithelial cell markers as described in section 3.1.5.1. Double-labeling immunofluorescence revealed co-localization of LRMP- and CK19-immunoreactivities in single cells showing that these cells were epithelial cells (Figure 3.8A, right panel). Colocalization was not detected between LRMP-immunoreactivity and the other epithelial cell markers including PGP, FOXI1 and tubulin.

So, these LRMP-immunoreactive cells were not neuroendocrine cells (Figure 3.8B, right panel), not ionocytes, as there was no FOXI1-immunolabeling on the nucleus of LRMP-immunoreactive cell (Figure 3.8C, right panel), and not ciliated cells, as tubulin-immunoreactivity was not observed in LRMP-immunoreactive cells (Figure 3.8D, right panel). The LRMP-immunoreactive cells were flask-shaped epithelial cells with apical and basal processes.

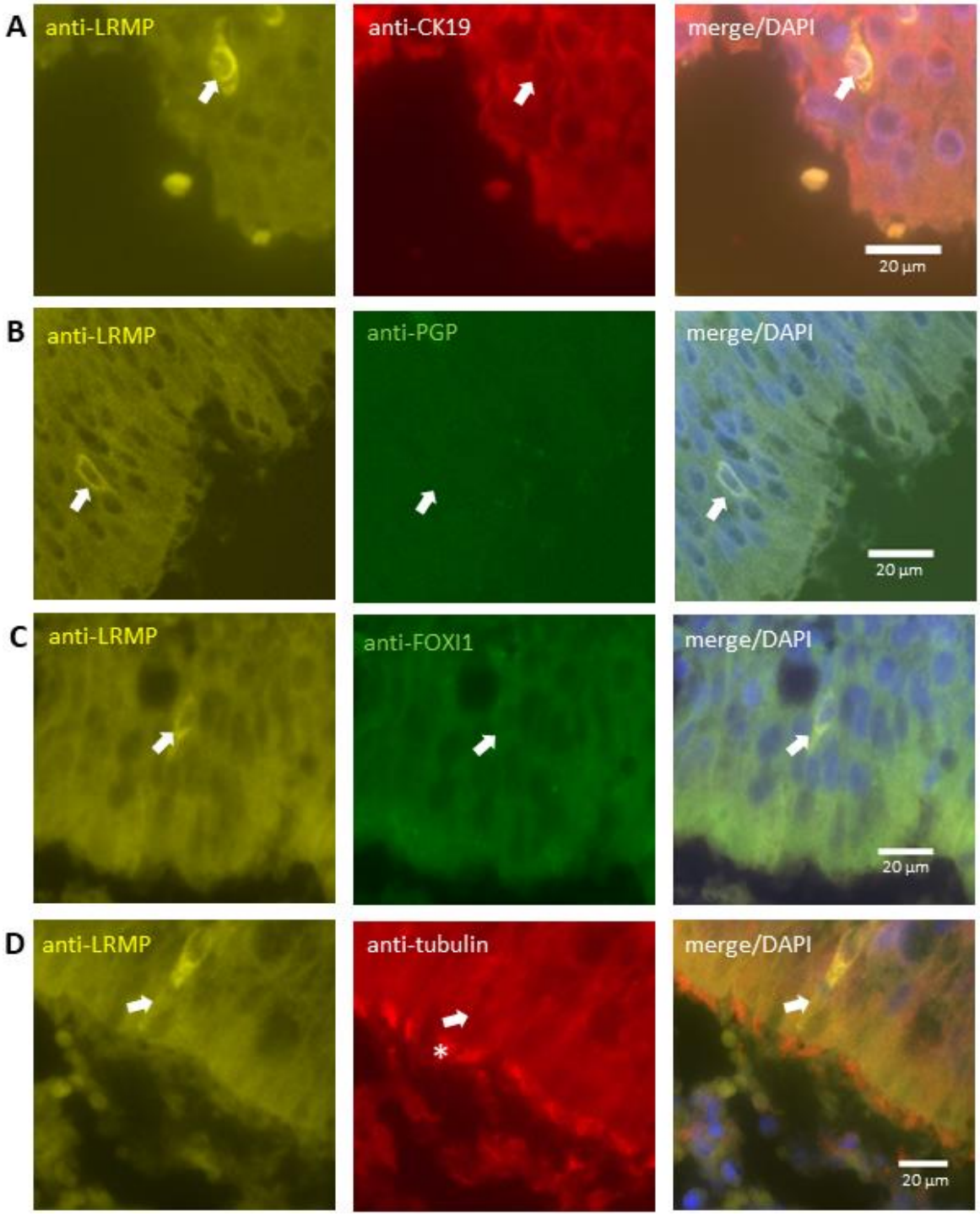

Figure 3.8: LRMP-immunolabeling in the human tracheal epithelium. ***(A-D)*** Immunohistochemistry, paraffin section of human donors. ***(A)*** Colocalization of immunoreactivities to LRMP and CK19 within the same cell (arrow). ***(B)*** LRMP-immunoreactive cell (arrow) was not labeled with antibodies against PGP 9.5 (neuroendocrine marker) (so these LRMP-immunoreactive cells were not neuroendocrine cells). ***(C)*** LRMP-immunoreactive cell (arrow) was not labeled with antibodies against

FOXI1 (ionocyte marker) (so it was not ionocyte). ***(D)*** LRMP-immunoreactive cell (arrow) was not labeled with antibodies against tubulin (ciliated cell marker, asterisk) (showing that these cells were not ciliated cells). Images captured with black and white camera; Image J was used to color images and DAPI (blue) was used to label the nucleus.

Figure 3.9 shows other regions where antibodies-immunoreactivities were visible and shows controls with no immunoreactivities when the antibodies were omitted.

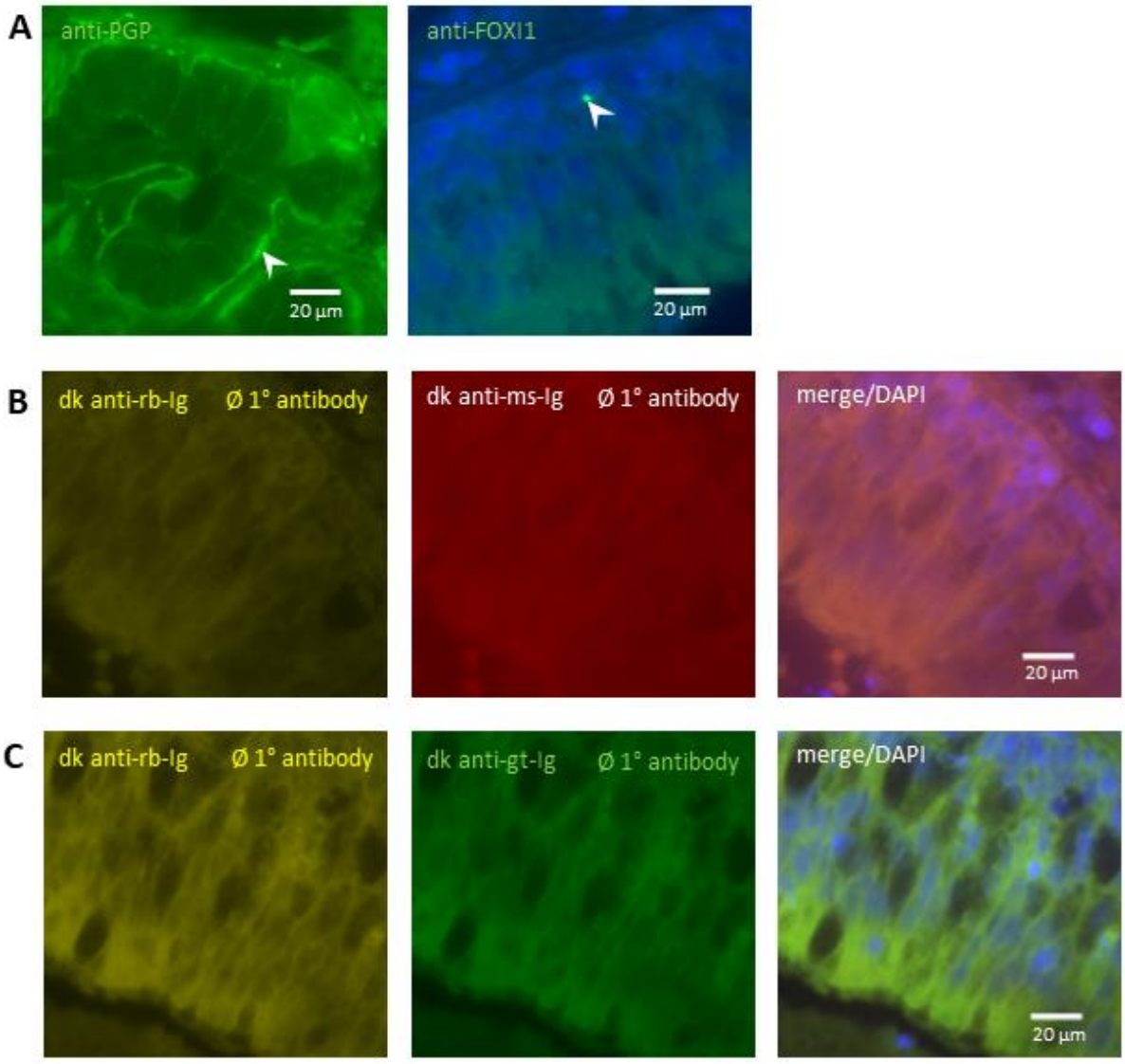

Figure 3.9: Controls used in human trachea.
(A-C) Immunohistochemistry, paraffin sections of the trachea. ***(A)*** PGP-immunoreactive nerve fibers (left panel, arrowhead) in the same section shown in Figure 3.8B, central panel. FOXI1-immunoreactivity labeling only within the nucleus (right panel, arrowhead).

(B) No immunoreactivities were observed when LRMP-antibody (from rabbit) and other antibodies (PGP, CK19 and tubulin; from mouse) were omitted. ***(C)*** No immunoreactivities were observed when LRMP-antibody (from rabbit) and other antibodies (FOXI1; from goat) were omitted. Images captured with black and white camera; Image J was used to color images and DAPI (blue) was used to label the nucleus.

3.1.5.3 Lung

3.1.5.3.1 Bronchus

Lung paraffin sections from human and organ donors and lung resected from COPD patients in the course of lung transplantation were immunolabeled with antibodies against LRMP and other epithelial cell markers (see section 3.1.5.1). Immunolabeling revealed co-localization of LRMP- and CK19-immunoreactivities in single cells the bronchi (Figure 3.10A, right panel) showing that these LRMP-immunoreactive cells were epithelial cells. In contrast, no colocalization was detected between LRMP-immunoreactivity and the other epithelial cell markers, including PGP, FOXI1 and tubulin. So, these LRMP-immunoreactive cells were neither neuroendocrine cells (Figure 3.10B, right panel), nor ionocytes, as there was no FOXI1-immunolabeling on the nucleus of LRMP-immunoreactive cells (Figure 3.10C, right panel), nor ciliated cells, as the tubulin-immunoreactivity was not observed in LRMP-immunoreactive cells (Figure 3.10D, right panel). Anti-uteroglobin labeled secretory cells in sections from organ donors and lung resected from COPD patient in the course of lung transplantation, but not in specimens taken from donor bodies processed for the dissection course (Figure 3.10E, right panel). The LRMP-immunoreactive cells were flask-shaped epithelial cells with apical and basal processes.

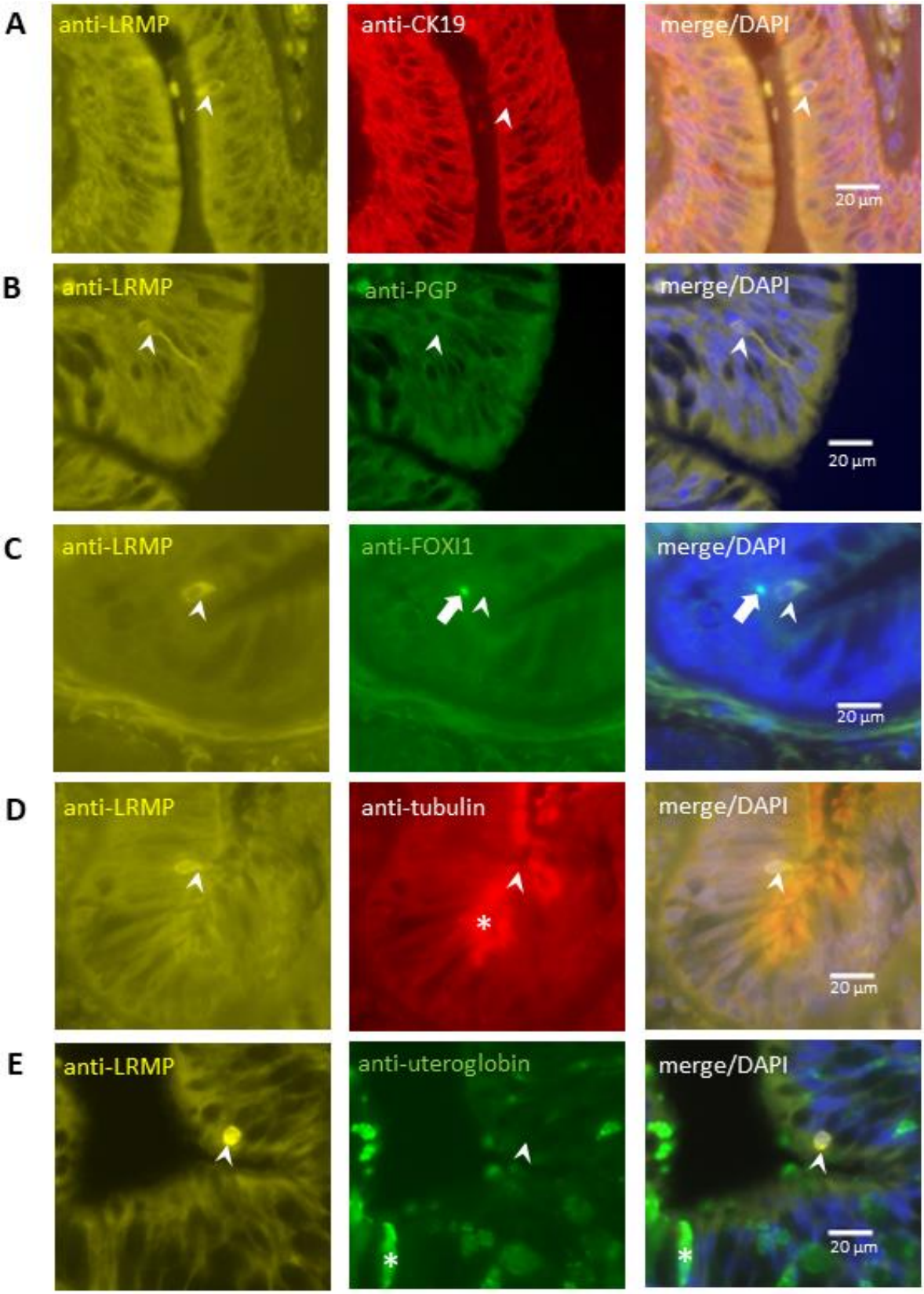
A
anti-LRMP
anti-CK19
merge/DAPI
20 µm
B
anti-LRMP
anti-PGP
merge/DAPI
20 µm
C
anti-LRMP
anti-FOXI1
merge/DAPI
20 µm
D
anti-LRMP
anti-tubulin
merge/DAPI
20 µm
E
anti-LRMP
anti-uteroglobin
merge/DAPI
20 µm

Figure 3.10: LRMP-immunolabeling in human bronchial epithelium.
(A-D) Immunohistochemistry, bronchus paraffin section from organ donors and lung resected from COPD patients in the course of lung transplantation. ***(A)*** Colocalization of immunoreactivities to LRMP and CK19 within the same cell (arrowhead). ***(B)*** LRMP-immunoreactive cell (arrowhead) was not labeled with antibodies against PGP 9.5 (neuroendocrine marker). ***(C)*** LRMP-immunoreactive cell (arrowhead) is not labeled with antibodies against FOXI1 (ionocyte marker, arrow indicates FOXI1-immunoreactivity in the nucleus of an adjacent cell). ***(D)*** LRMP-immunoreactive cell is not labeled with antibodies against tubulin (ciliated cell marker). ***(E)*** LRMP-immunoreactive cell is not labeled with antibodies against uteroglobin (secretory cell marker). Asterisk indicates uteroglobin-immunoreactive cells). Images captured with black and white camera; Image J was used to color images and DAPI (blue) was used to label the nucleus.

Controls validating the efficacy of PGP-immunolabelling and the specificity of secondary reagent (omission of primary antibodies) are shown in Figure 3.11.

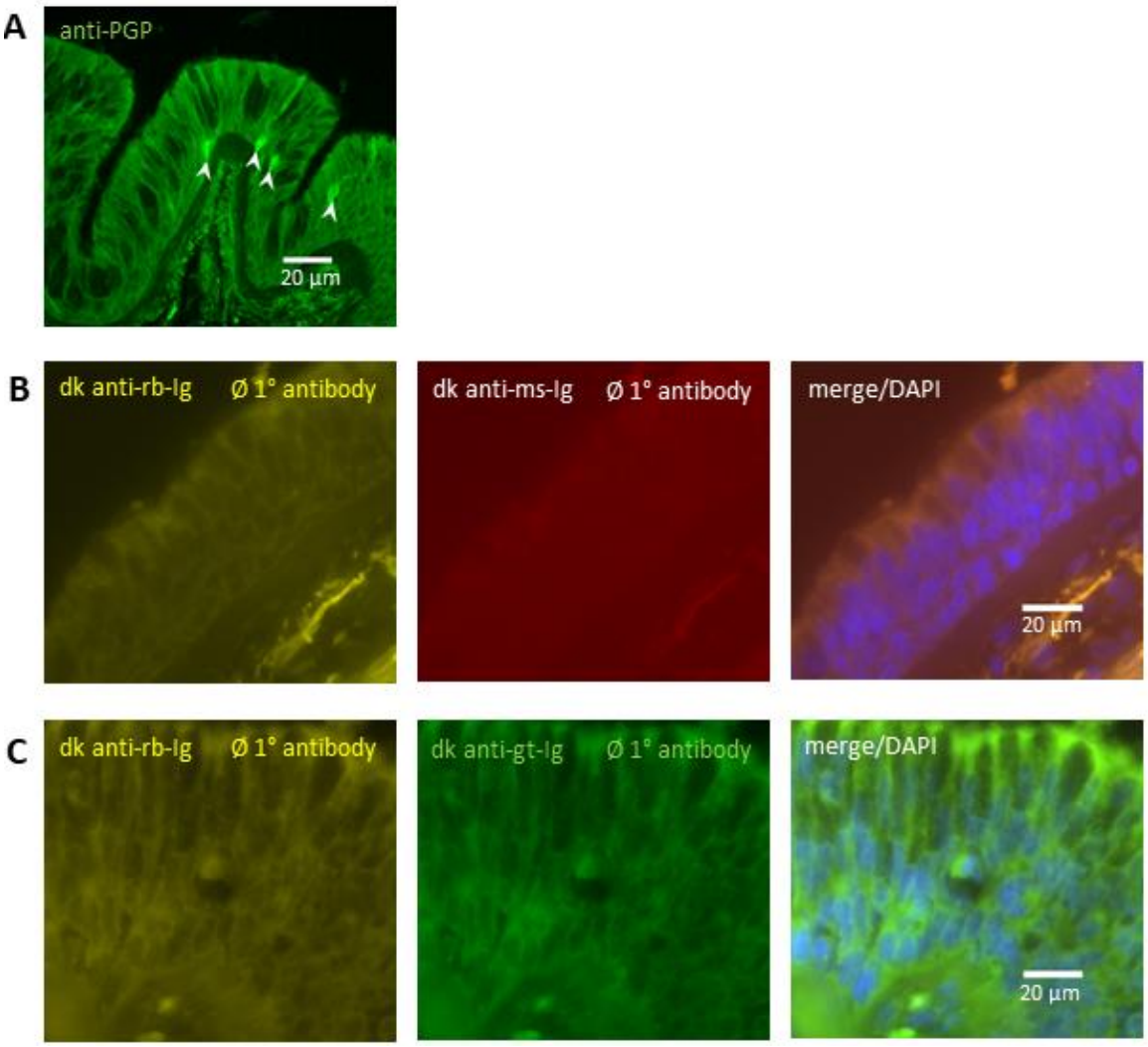

Figure 3.11: Controls used in human bronchus.

(A-C) Immunohistochemistry, paraffin sections of the lung bronchus. ***(A)*** PGP-immunoreactive cells (arrowheads) in the same section in Figure 3.10B, central panel. ***(B)*** No immunoreactivities were observed when LRMP-antibody (from rabbit) and other antibodies (PGP, CK19, tubulin and uteroglobin; from mouse) were omitted. ***(C)*** No immunoreactivities were observed when LRMP-antibody (from rabbit) and other antibodies (FOXI1; from goat) were omitted. Images captured with black and white camera; Image J was used to color images and DAPI (blue) was used to label the nucleus.

3.1.5.3.2 Bronchiole

Lung paraffin sections from human and organ donors and lung resected from COPD patients in the course of lung transplantation were immunolabeled with antibodies

against LRMP and other epithelial cell markers (see section 3.1.5.1). Immunolabeling revealed co-localization of LRMP- and CK19-immunoreactivities in single cells the bronchi (Figure 3.12A, right panel), showing that these LRMP-immunoreactive cells were epithelial cells. In contrast, no colocalization was detected between LRMP-immunoreactivity and the other epithelial cell markers, including PGP, FOXI1 and tubulin. So, these LRMP-immunoreactive cells were not neuroendocrine cells (Figure 3.12B, right panel), not ionocytes, as there was no FOXI1-immunolabeling on the nucleus of LRMP-immunoreactive cells (Figure 3.12C, right panel), and not ciliated cells, as the tubulin-immunoreactivity was not observed in LRMP-immunoreactive cells (Figure 3.12D, right panel). Anti-uteroglobin labeled secretory cells in sections from sections from organ donors and lung resected from COPD patient in the course of lung transplantation, but not in specimens taken from donor bodies processed for the dissection course (Figure 3.12E, right panel). The LRMP-immunoreactive cells were flask-shaped epithelial cells with apical and basal processes.

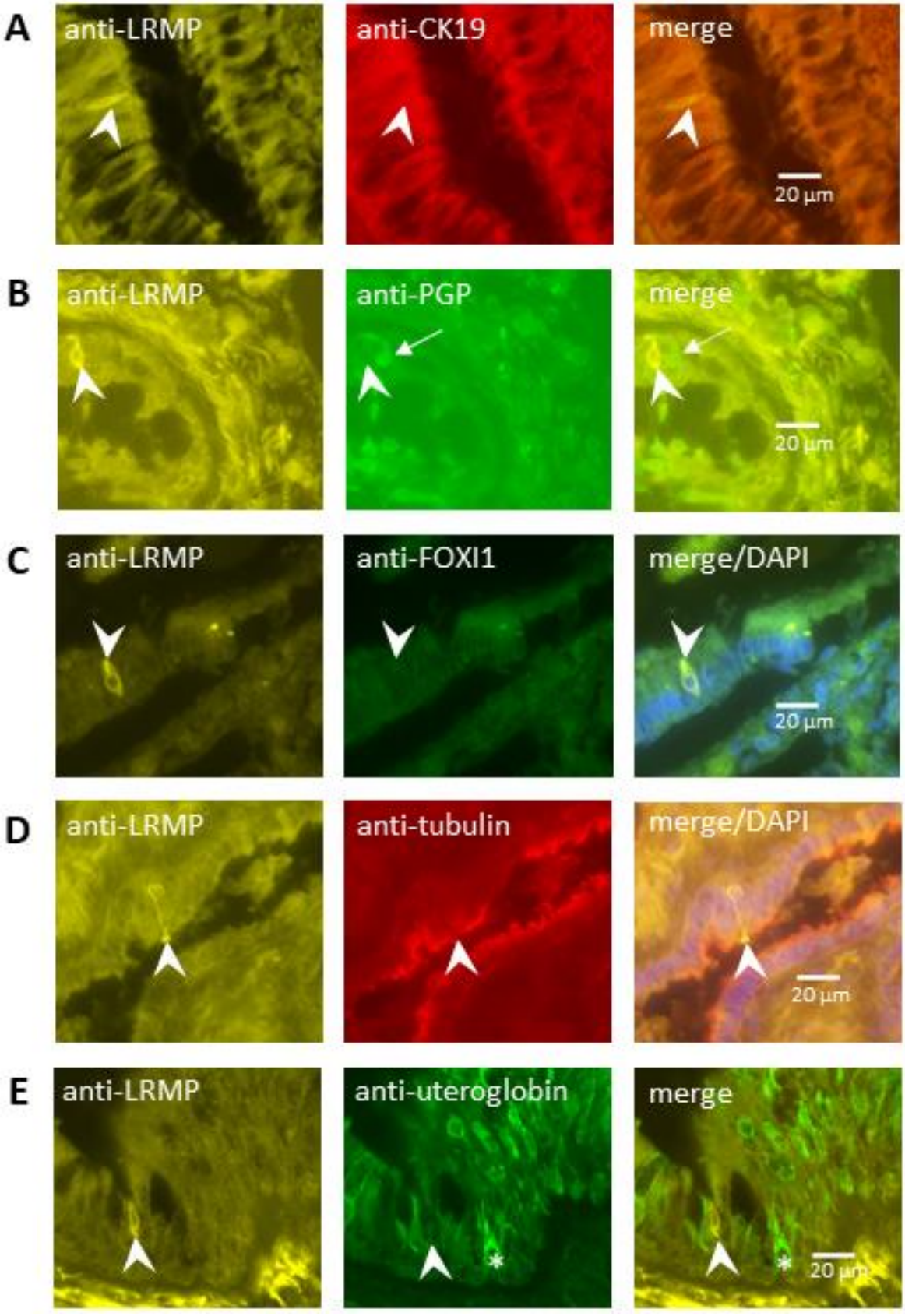
A
anti-LRMP
anti-CK19
merge
20 µm
B
anti-LRMP
anti-PGP
merge
20 µm
C
anti-LRMP
anti-FOXI1
merge/DAPI
20 µm
D
anti-LRMP
anti-tubulin
merge/DAPI
20 µm
E
anti-LRMP
anti-uteroglobin
merge
20 µm

Figure 3.12: LRMP-immunolabeling in human bronchiolar epithelium.
(A-D) Immunohistochemistry, bronchiole paraffin section from human donors (B and C) and from organ donors and lung resected from COPD patient in the course of lung transplantation (A, D and E). ***(A)*** Colocalization of immunoreactivity to LRMP and CK19 within the same cell (arrowhead). ***(B)*** LRMP-immunoreactive cell (arrowhead) is not labeled with antibodies against PGP 9.5 (neuroendocrine cell and nerve fiber marker, PGP-immunoreactive cell, an arrow). ***(C)*** LRMP-immunoreactive cell (arrowhead) is not labeled with antibodies against FOXI1 (ionocyte marker), DAPI (blue) was used to label the nucleus and is depicted in the merged image. ***(D)*** LRMP-immunoreactive cell is not labeled with antibodies against tubulin (ciliated cell marker). ***(E)*** LRMP-immunoreactive cell is not labeled with antibodies against uteroglobin (secretory cell marker, uteroglobin-immunoreactive cell, asterisk). Images captured with black and white camera; Image J was used to color images.

Controls validating the efficacy of PGP-immunolabelling and the specificity of secondary reagent (omission of primary antibodies) are shown in Figure 3.13. Furthermore, preabsorption with the immunizing peptide (recombinant LRMP protein with N-terminal His6-ABP tag) completely prevented LRMP-immunostaining, indicating the specificity of this antibody for the LRMP epitope (Figure 3.13D).

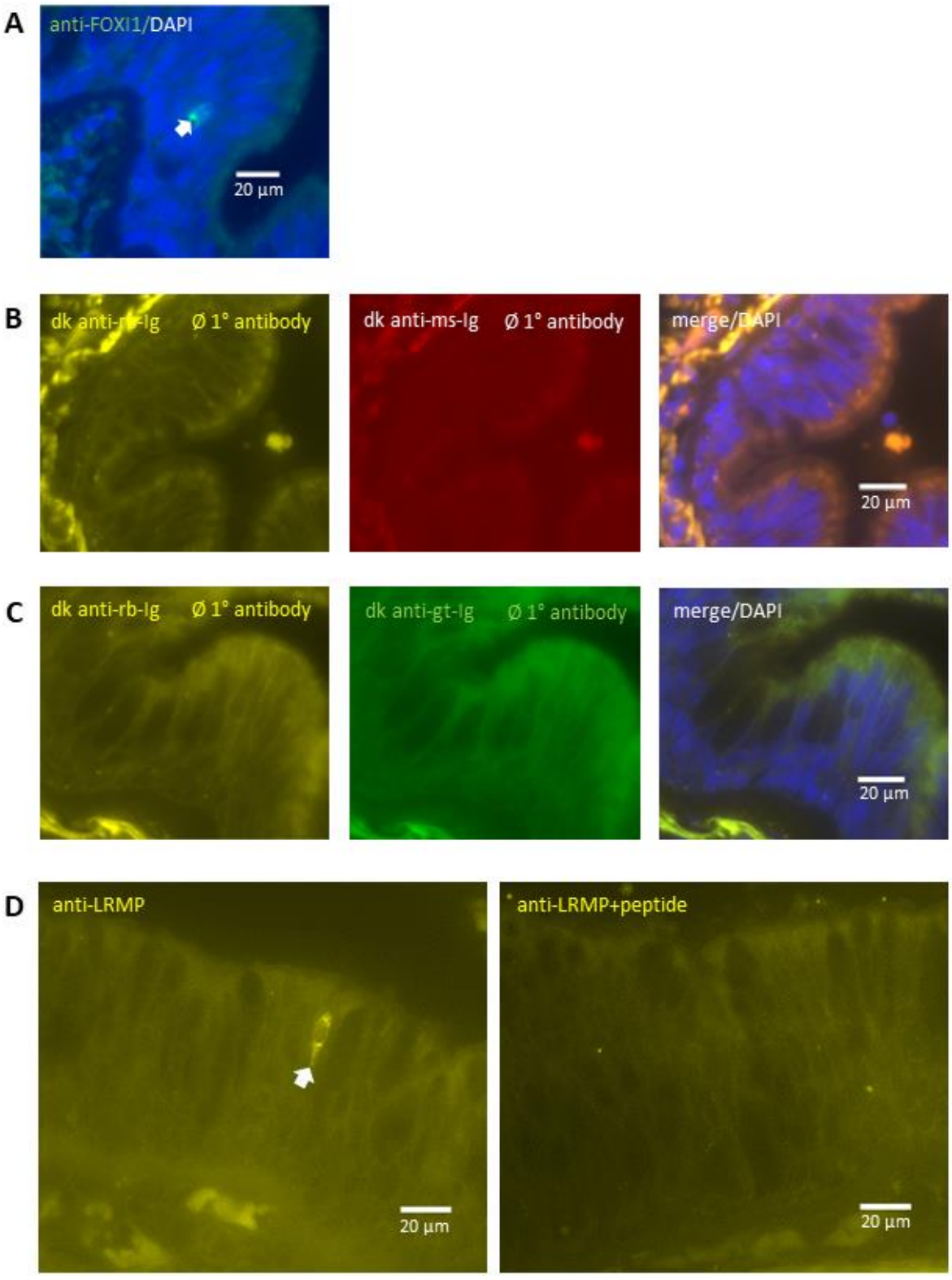

Figure 3.13: Controls used in human bronchiole.

(A-D) Immunohistochemistry, paraffin sections of the lung with bronchioles. ***(A)*** FOXI1-immunoreactive cell (arrow) labels the nucleus in the same section shown in Figure 3.8aC, central panel. ***(B)*** No immunoreactivities were observed when LRMP-antibody (from rabbit) and other antibodies (PGP, CK19, tubulin and uteroglobin; from mouse) were omitted. ***(C)*** No immunoreactivities were observed when LRMP-antibody (from rabbit) and FOXI1-antibody from goat were omitted. ***(D)*** Preabsorption control to validate the LRMP-antibody used in immunohistochemistry. Control experiment (left panel) using an antibody against LRMP, showing labeling of single cell (arrow). Preabsorption with the immunizing peptide (recombinant LRMP protein with N-terminal His6-ABP tag) completely blocked LRMP-immunolabeling (right). Images captured with black and white camera; Image J was used to color images and DAPI (blue) was used to label the nucleus.

3.1.5.4 LRMP-immunoreactive cells extend deep into the lung.

LRMP-positive cells had lowest frequency of occurrence in the trachea and their frequency increased toward the periphery. The median frequencies ranged from 0.003 (trachea) to 0.206 (bronchiole) cells/mm of BM (Table 3.1). Kruskal-Wallis test followed by Dunn's multiple comparisons test showed that this difference between trachea and bronchiole was significant (P=0.0440) (Figure 3.14).

Airway	Median cells/mm BM	Mean cells/mm BM	IQR cells/mm BM	N
Nose	0.102	0.162	0.220	5
Trachea	0.003	0.004	0.003	5
Bronchus[1]	0.078	0.203	0.070	5
Bronchus[2]	0.178	0.168	0.116	6
Bronchus COPD	0.304	0.304	0.102	2
Bronchiole[1]	0.206	0.323	0.414	6
Bronchiole[2]	0.132	0.099	0.083	3
Bronchiole COPD	0.463	0.471	0.527	4

Table 3.1: Frequency of LRMP-immunoreactive cells at different levels of the human respiratory tract. Graphical demonstration of the data in figure 3.9. IQR = interquartile range. 1: Body donors; 2: organ donors.

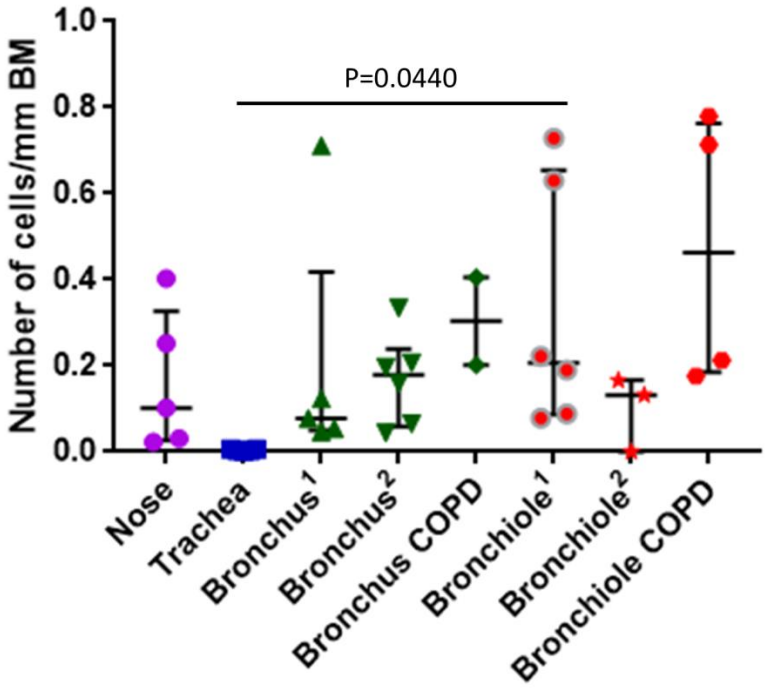

Figure 3.14: Frequency of LRMP-immunoreactive cells at different levels of the human respiratory tract.
Scatter dot plots with median and interquartile range, each dot represents the average number of LRMP-positive cells calculated from one sample. A total of 18 human donors (nose, trachea, bronchus[1] and bronchiole[1]), 9 lungs from organ donors and 6 lungs resected from COPD patients in the course of lung transplantation) was evaluated. Kruskal-Wallis test followed by Dunn's multiple comparisons test.

3.1.5.5 LRMP is detected ultrastructurally in taste and brush cells.

Ultrastructural immunohistochemistry with antibody against LRMP showed immunoreactivity in the taste cells (n=7) and in brush cells (n=4). Taste cells were detected in the tongue taste buds. In a taste bud with eight nucleated profiles, two of them had immunoreactivity toward LRMP-antibody. The DAB reaction product was densely distributed in the cytoplasm and the nucleus. The cytoplasm of these cells was darker than the cytoplasm in other cells in the taste bud indicating that these cells might be type II cells. No labeling was observed in the control where no primary antibody was added (Figure 3.15A). Because of the poor tissue preservation, we were unable to clearly discriminate organelles. LRMP-immunoreactive cells were also seen in the bronchus and

in the bronchioles. These were flask-shaped cells with oval nucleus. These cells had a narrow basal part and a narrow apical part projecting toward the lumen, although the luminal surface of the cells was not contained within the section planes. Organelles and filaments were not well preserved in our human donor samples. The DAB reaction product was densely distributed in the cytoplasm and the nucleus of these cells but it did not label ciliated or secretory cells (Figure 3.15B).

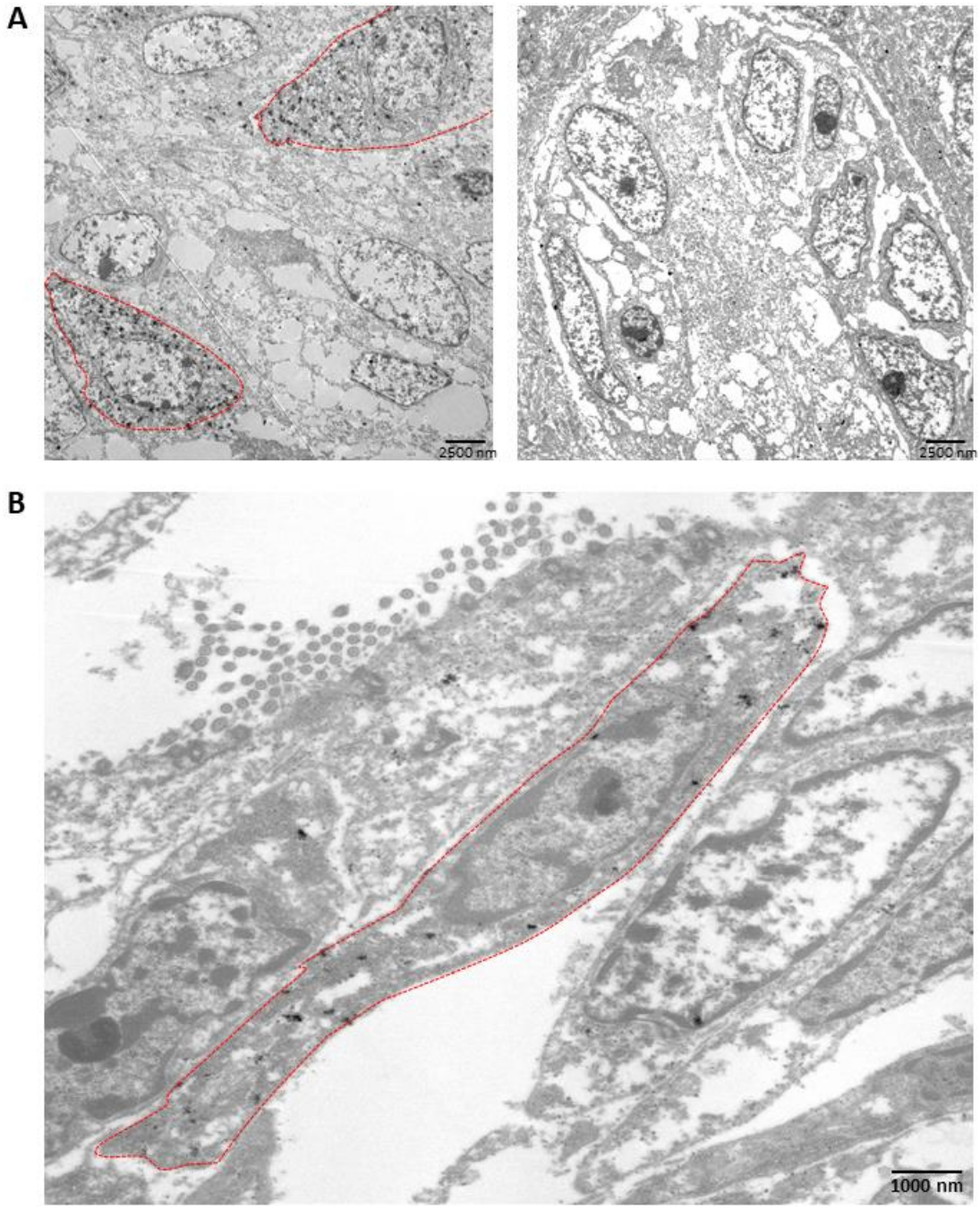

Figure 3.15: LRMP-immunoreactivity is detected ultrastructurally in human taste cells and brush cells.
Transmission electron microscopy, LRMP-immunolabeling. ***(A)*** Taste bud. Left panel: Ultrastructural immunohistochemistry with an antibody against LRMP shows immunoreactive flask-shaped taste cells with DAB distributed in the cytoplasm and nucleus (red dotted cells). Right panel: omission of the primary antibody (LRMP), no labeling is visible in taste cells. ***(B)*** Bronchiole. Ultrastructural immunohistochemistry with an antibody against LRMP shows immunoreactive flask-shaped brush cells with DAB distributed in the cytoplasm and nucleus (red dotted cells).

3.2 Neuroendocrine cells in human tracheal epithelium.

3.2.1 PGP-9.5-immunoreactivity in human tracheal epithelium.

Tracheal paraffin sections from human donors were immunolabeled with antibody against PGP. This labeling revealed PGP-immunoreactivity in epithelial cells of both upper (Figure 3.16A, left panel) and lower trachea (Figure 3.16B, left panel) and in nerve fibers surrounding glands and vessels (Figures 3.16C and 3.16D). The PGP-immunoreactive cells were flask-shaped epithelial cells with apical and basal processes, which in most of the cases reached the lumen.

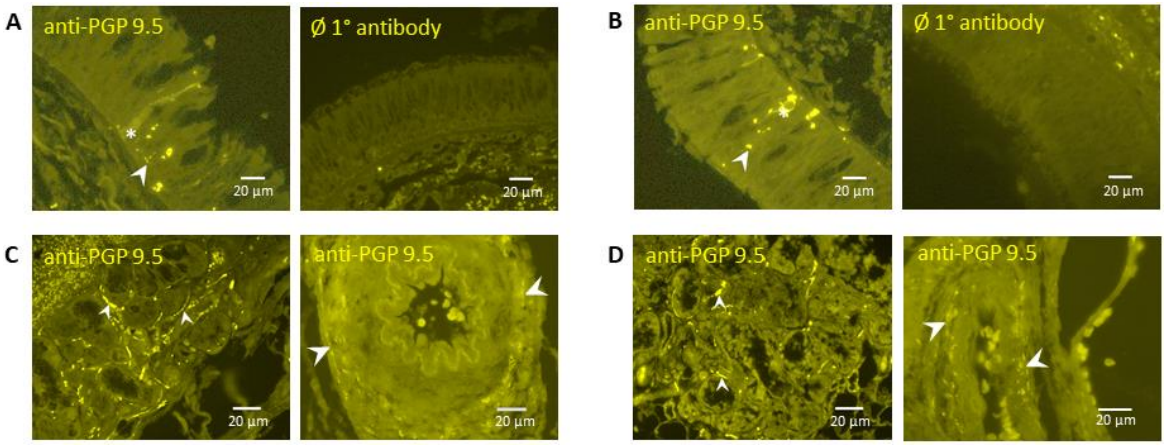

Figure 3.16: PGP 9.5-immunoreactivity in tracheal epithelium.
(A-D) Immunohistochemistry of tracheal paraffin sections from human donor immunolabeled with antibody against PGP 9.5. ***(A)*** Shows an epithelial cell positive for PGP 9.5 (asterisk) in the upper part of trachea, intraepithelial PGP-immunoreactive nerve fibers are labeled by arrowhead (left panel). No immunoreactivity is observed when the primary antibody (PGP 9.5) was omitted (right panel). ***(B)*** Shows an epithelial cell positive

for PGP 9.5 (asterisk) in the lower part of trachea, intraepithelial PGP-immunoreactive nerve fibers are labeled by arrowhead (left panel). No immunoreactivity is observed when the primary antibody (PGP 9.5) was omitted (right panel). ***(C)*** Upper part of trachea; PGP-immunoreactive nerve fibers surrounding glands (left panel) and vessels (right panel) are labeled by arrowheads. ***(D)*** Lower part of trachea; PGP-immunoreactive nerve fibers surrounding glands (left panel) and vessels (right panel) are labeled by arrowheads.

3.2.2 Neuroendocrine cells are much more frequent than brush cells in human trachea and lung.

PGP-positive cells were recorded at higher frequency of occurrence in the upper trachea (sublaryngeal) than in the lower trachea (bifurcation). Median frequencies ranged from 2.3 (bifurcation part) to 5.6 (sublaryngeal part) cells/mm of BM. This difference between sublaryngeal part of trachea and the bifurcation part of trachea was not significant (Mann-Whitney test, P=0.1417) (Figure 3.17A).

PGP-positive cells had a significantly (Mann-Whitney test, P=0.0007) 6-fold higher frequency than the LRMP-positive cells in the upper trachea (sublaryngeal). PGP-positive cells had a 5-fold higher frequency than the LRMP-positive cells in the bronchus, and a 4-fold higher frequency in the bronchiole (bronchus, Mann-Whitney test, P=0.0159; bronchiole, Mann-Whitney test, P=0.0095) (Figure 3.17B).

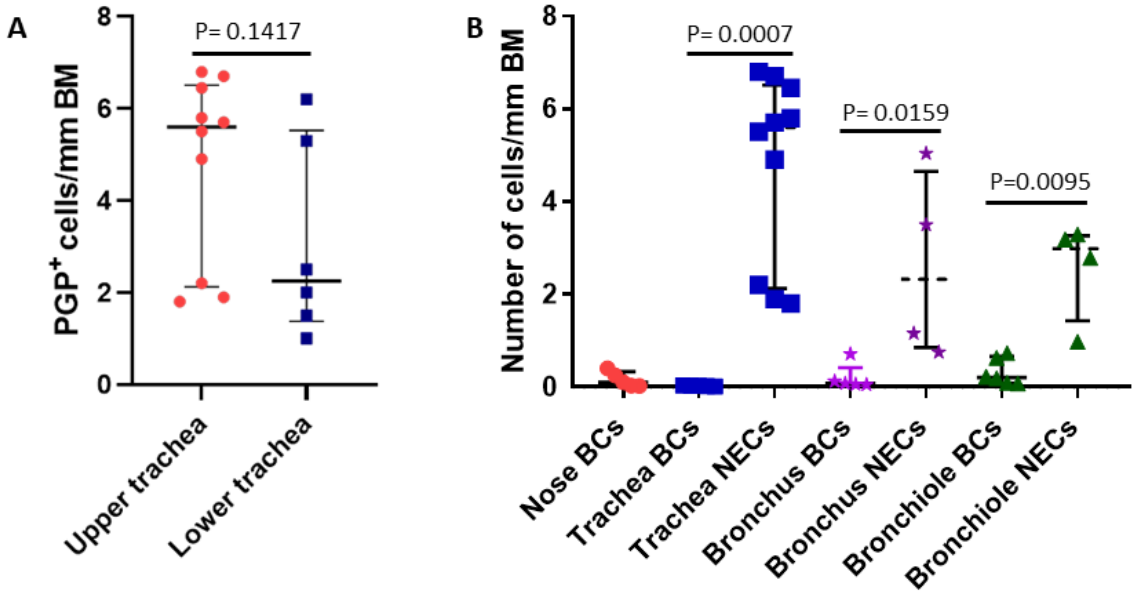

Figure 3.17: Neuroendocrine cells are more frequent than brush cells in human trachea and lung.
(A) Number of PGP^+ cells per mm of BM in the upper (sublaryngeal) and lower (bifurcation) parts of trachea (upper trachea: n=10 donors, lower trachea: n=6 donors). Scatter dot plots with median and interquartile range. No significant difference in the number of neuroendocrine cells between upper and lower tracheal epithelium (Mann-Whitney test). ***(B)*** Number of PGP^+ cells (NECs = neuroendocrine cells) and $LRMP^+$ cells (brush cells) per mm of BM in the upper (sublaryngeal) part of trachea (PGP^+ cells: n=10 donors, same data set as depicted in panel A of this figure, $LRMP^+$ brush cells: n=5 donors) and in the lung (bronchus and bronchiole, PGP^+ cells: n=6, $LRMP^+$ brush cells: n=8 donors). Scatter dot plots with median and interquartile range. Neuroendocrine cells (PGP^+ cells) were significantly more frequent in upper tracheal and lung (bronchus and bronchiole) epithelium than brush cells ($LRMP^+$ cells) (Mann-Whitney test).

3.3 Brush cells in pig respiratory tract epithelium

3.3.1 RT-PCR reveals expression of *villin, advillin* and *ChAT* in pig respiratory tract epithelium.

Villin, advillin and ChAT proteins were detected in the pig respiratory tract epithelium from the trachea to the bronchiole by immunohistochemistry (section 3.3.2.1 and 3.3.2.2). To validate the presence of *villin, advillin* and *ChAT* at the mRNA level, RT-PCR was performed on samples collected from abraded epithelium collected from the trachea, lung hilus (main bronchus) and deep in the lung (bronchus and bronchiole). RT-PCR revealed expression of *villin*-, *advillin*- and *ChAT*-mRNAs in the respiratory tract epithelium from the trachea to the bronchiole (Figure 3.18).

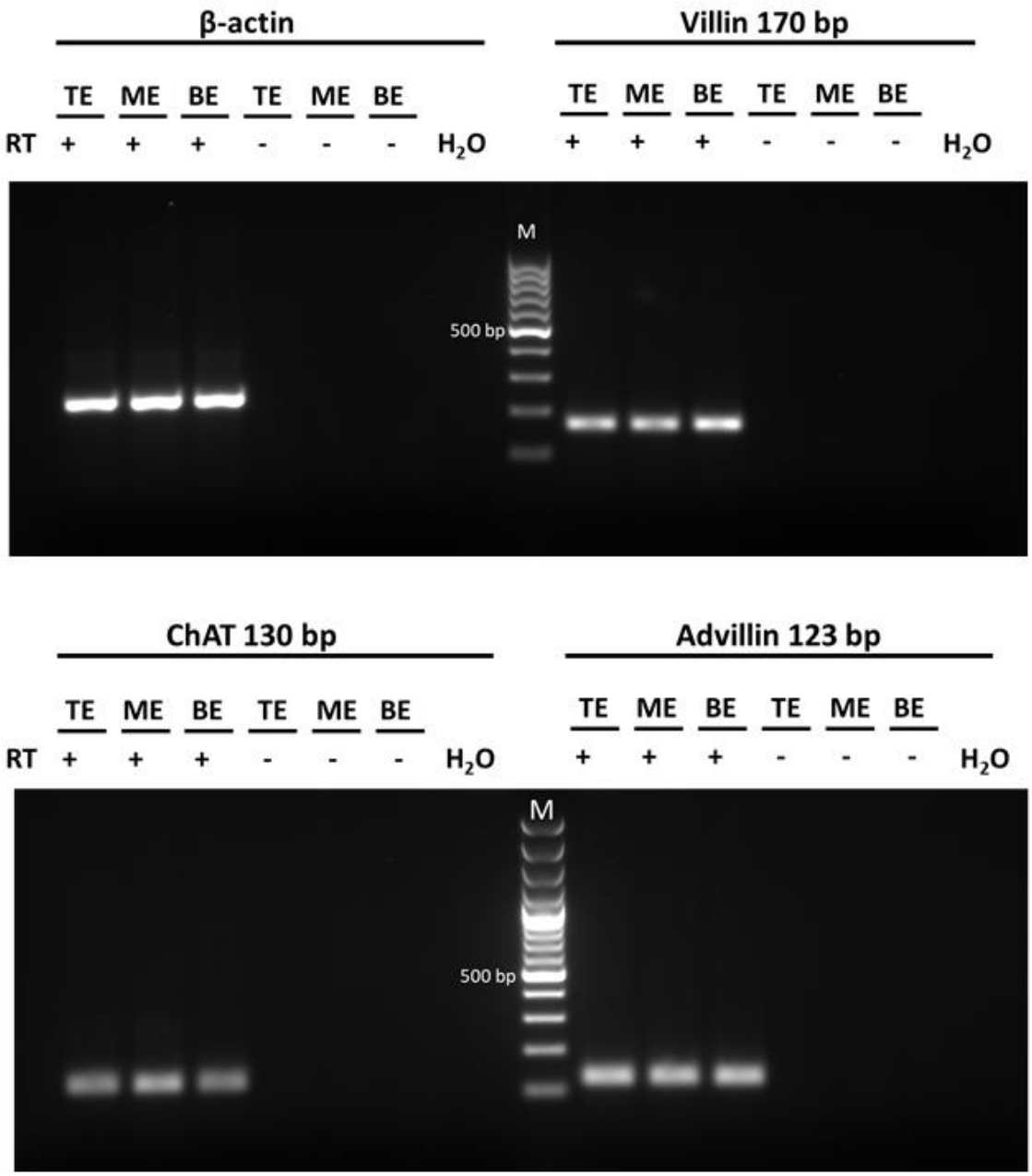

Figure 3.18: *Villin*-, *advillin*- and *ChAT*-mRNAs are expressed in the pig airways epithelium.

PCR experiments with cDNA obtained from tracheal epithelium (TE), main bronchus epithelium (ME) and bronchial epithelium (BE), representative of 5 of domestic pigs. Primers for *β-actin* (274 bp), *villin* (170 bp), ChAT (130 bp) and *advillin* (123 bp) were used. Water (H_2O) without adding cDNA and samples processed without reverse transcriptase (RT-) were used as controls. Amplicons of *β-actin* (efficacy control) and *villin*, *ChAT* and *advillin* are detected in all epithelial samples.

3.3.2 ChAT⁺ villin⁺ advillin⁺ cells in pig respiratory tract epithelium.

3.3.2.1 ChAT⁺ villin⁺ advillin⁺ cells in pig trachea and main bronchus epithelium.

Tracheal (separated in the upper, middle and lower part) and main bronchus cryosections from pig were immunolabeled with antibodies against ChAT, villin and advillin. Immunolabeling revealed the presence of three group of cells which were ChAT⁺ villin⁺ advillin⁺, ChAT⁻ villin⁺ advillin⁺ (most frequent) and ChAT⁺ villin⁻ advillin⁻ (least frequent) (Figure 3.19).

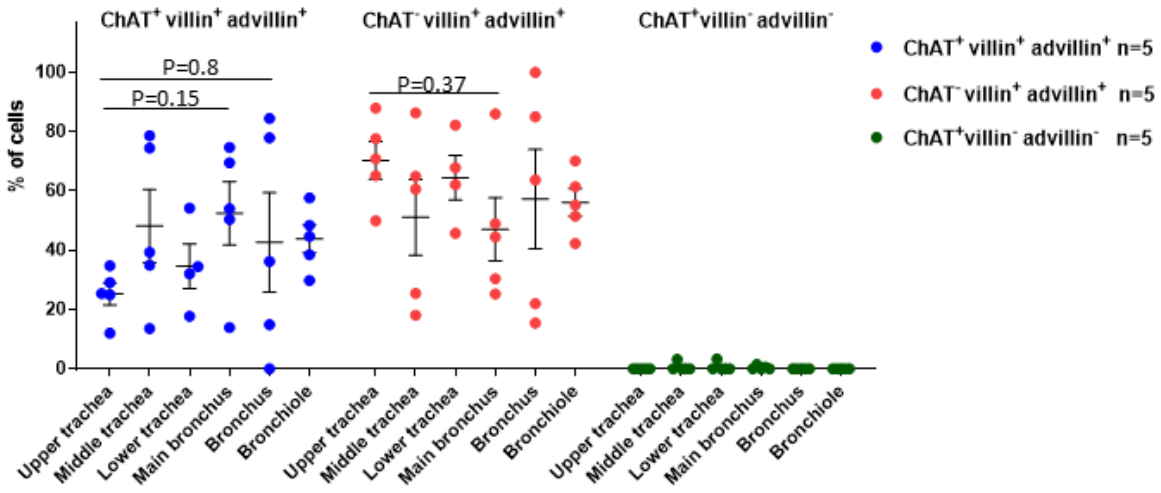

Figure 3.19: ChAT/villin/advillin cellular phenotypes in pig respiratory tract epithelium. Scatter dot plots with median and interquartile range, showing the percentages of ChAT⁺ villin⁺ advillin⁺, ChAT⁻ villin⁺ advillin⁺ and ChAT⁺ villin⁻ advillin⁻ cells in trachea, main bronchus and in the lung (4 sections for each region per specimen, Kruskal-Wallis test, n=5 pigs), indicating that there is no difference in the distribution of these cells between all regions. (P value > 0.99).

ChAT⁺ villin⁺ advillin⁺ cells were flask-shaped, slender solitary epithelial cells with basal processes and apical processes reaching the lumen (Figure 3.20A-3.20D) with a pronounced apical labeling with villin- and advillin-antibodies but not with ChAT-antibody which does not result in any apical labeling.

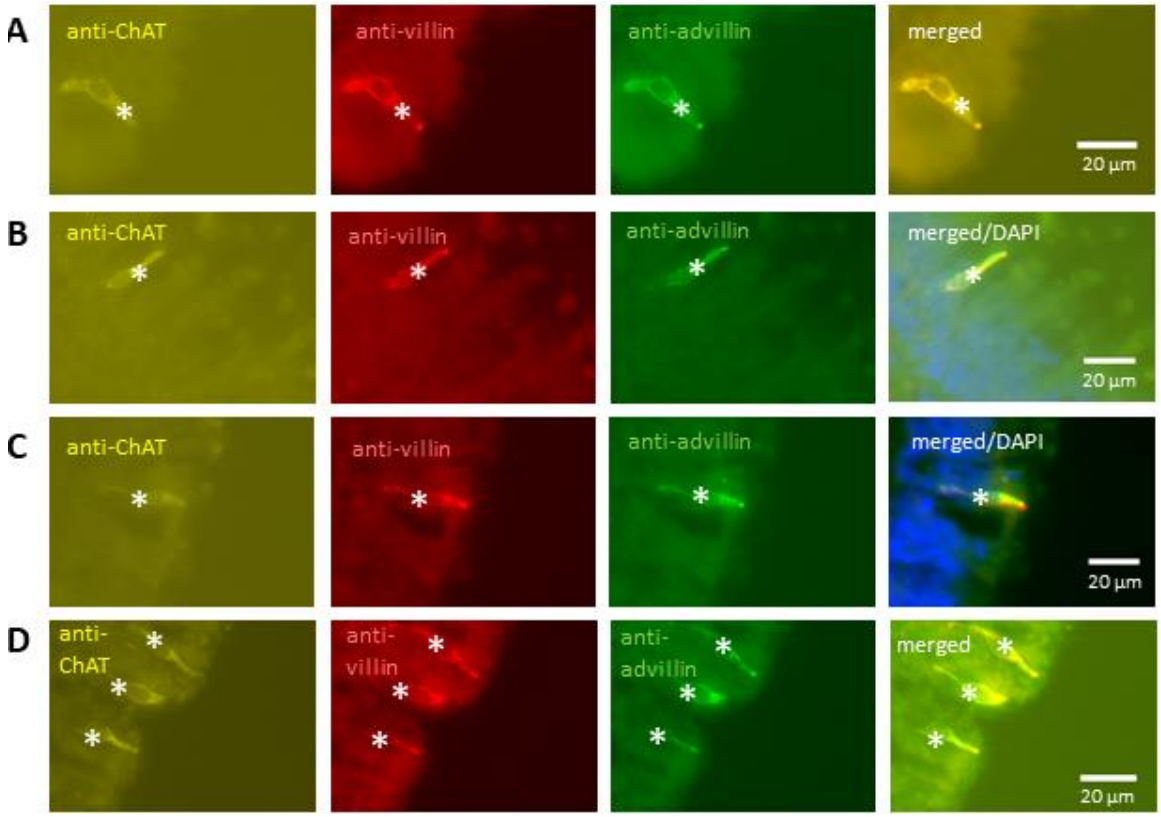

Figure 3.20: **ChAT-, villin- and advillin-immunoreactivity are colocalized in slender epithelial cells in pig tracheal and main bronchus epithelium.**
(A-D) Immunohistochemistry of tracheal (upper, middle and lower part) and main bronchus epithelium cryosections immunolabeled with antibodies against ChAT, villin and advillin. ***(A)*** Upper tracheal part. Triple-labeling of a single epithelial cell (asterisk) for ChAT (yellow), villin (red), and advillin (green). ***(B)*** Middle trachea. Colocalization of ChAT- (yellow), villin- (red), and advillin-immunoreactivities (green) in a slender epithelial cell. ***(C)*** Lower trachea. Epithelial cell (asterisk) co-labeled with ChAT- (yellow), villin- (red), and advillin-antibodies (green). ***(D)*** Main bronchus. Epithelial cells (asterisks) labeled with antibodies against ChAT, villin and advillin.
Images captured with black and white camera; Image J was used to color images.

3.3.2.2 immunohistochemistry reveals that ChAT$^+$ villin$^+$ advillin$^+$ cells extend deep into the lung down to the bronchioles.

Lung cryosections (bronchus and bronchioli) from pig were immunolabeled with antibodies against ChAT, villin and advillin. Immunolabeling revealed the presence of three group of cells with the signatures ChAT$^+$ villin$^+$ advillin$^+$, ChAT$^-$ villin$^+$ advillin$^+$ and

ChAT$^+$ villin$^-$ advillin$^-$. ChAT$^+$ villin$^+$ advillin$^+$ cells were flask-shaped, slender solitary epithelial cells with basal processes and apical processes reaching the lumen (Figures 3.21A and 3.21B).

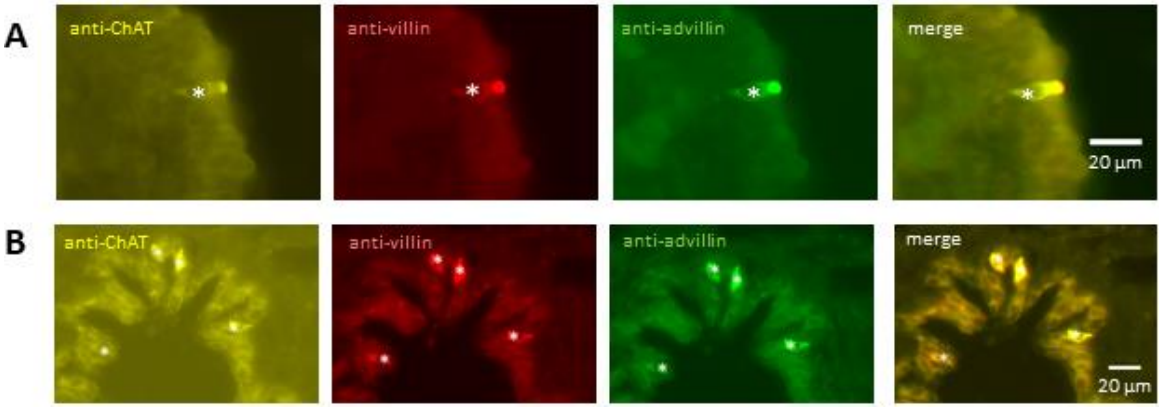

Figure 3.21: **ChAT-, villin- and advillin-immunoreactivities in pig intrapulmonary airway epithelium.**
(A and B) Pig lung cryosections immunolabeled with antibodies against ChAT, villin and advillin. ***(A)*** An epithelial cell (asterisks) in a bronchus labeled with antibodies against ChAT, villin, and advillin. ***(B)*** Colocalization of ChAT-, villin-, and advillin-immunoreactivities in 4 epithelial cells (asterisks) in a bronchiole. Images captured with black and white camera; Image J was used to color images.

The frequency of ChAT$^+$ villin$^+$ advillin$^+$ cells expressed in cells/mm BM (Table 3.2) was significantly 10-fold higher in the bronchioles (10 cells per mm BM) than in any other region (Figure 3.22).

Airway	Median cells/mm BM	Mean cells/mm BM	IQR cells/mm BM
Upper trachea	0.125	0.136	0.047
Middle trachea	0.468	0.744	0.910
Lower trachea	0.643	0.736	0.437
Main bronchus	1.490	1.290	0.807
Bronchus	0.280	0.500	0.778
Bronchiole	10.321	10.600	2.022

Table 3.2: Frequency of ChAT$^+$ villin$^+$ advillin$^+$ cells at different levels of the pig respiratory tract. Graphical demonstration of the data in figure 3.13 and 3.14:

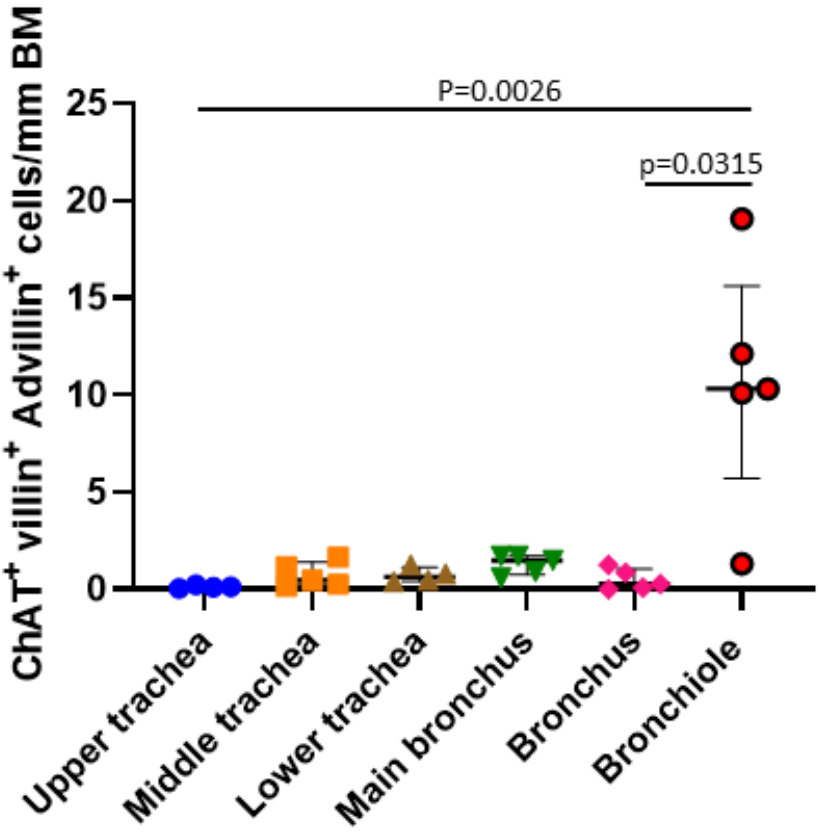

Figure 3.22: **Frequency of ChAT$^+$ villin$^+$ advillin$^+$ cells at different levels of the pig respiratory tract.**
Number of ChAT$^+$ villin$^+$ advillin$^+$ cells per mm BM in the different parts of the airway tree. Scatter dot plots with median and interquartile range for each sample (Kruskal-Wallis test followed by Dunn's multiple comparisons test, n=5 pigs).

3.3.2.3 ChAT$^-$ villin$^+$ advillin$^+$ and ChAT$^+$ villin$^-$ advillin$^-$ cells in pig respiratory tract epithelium.

3.3.2.3.1 Immunohistochemistry reveals ChAT$^-$ villin$^+$ advillin$^+$ and ChAT$^+$ villin$^-$ advillin$^-$ cells in pig respiratory tract epithelium.

As reported in sections 3.3.2.1 and 3.3.2.2, ChAT-, villin- and advillin-immunoreactivities were colocalized in approximately 40% of slender solitary epithelial cells that expressed at least one of these markers. As villin- and advillin-immunoreactivities were colocalized in a 1:1 ratio in these slender epithelial cells, double-immunolabeling revealed colocalization of villin- and ChAT-immunoreactivities (Figure 3.23A). Another group,

presented no ChAT-immunoreactivity in villin-immunoreactive cells (ChAT$^-$ villin$^+$) (Figure 3.23B). In addition, in very few cases ChAT-immunoreactive cells did not show immunoreactivity to villin- or advillin-antibodies (ChAT$^+$ villin$^-$) (Figure 3.23C).

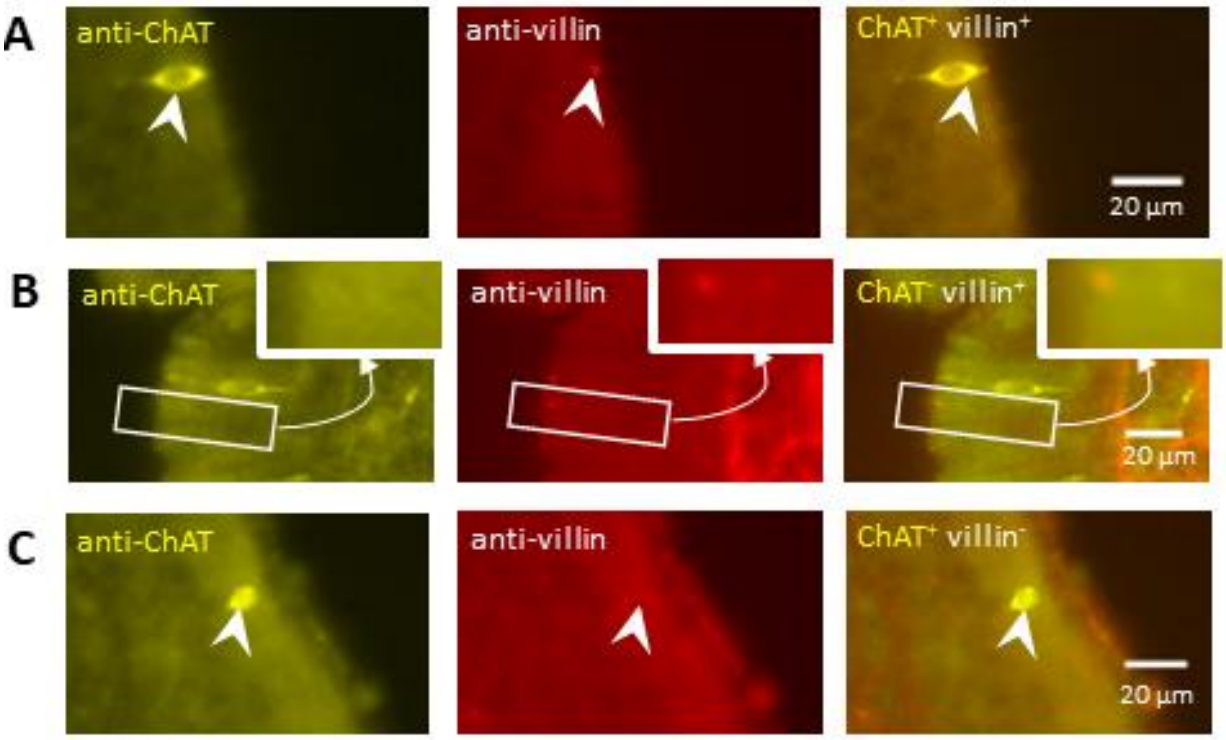

Figure 3.23: Different patterns of colocalization of ChAT- and villin-immunoreactivities in pig respiratory tract epithelium.

(A-C) Immunohistochemistry of main bronchus and intrapulmonary bronchus cryosections immunolabeled with antibodies against ChAT and villin. ***(A)*** Epithelial cells in the main bronchus labeled with antibodies against ChAT (yellow) and villin (red), colocalization of both immunoreactivities (ChAT$^+$ villin$^+$) (arrowhead). ***(B)*** Cell shows no ChAT-immunoreactivity (yellow) and only villin-immunoreactivity (red) in epithelial cell in the intrapulmonary bronchus (ChAT$^-$ villin$^+$), the boxed area shows these cells at higher magnification. ***(C)*** ChAT-immunoreactivity (yellow) and no villin-immunoreactivity (red) in an epithelial cell (arrowheads) in the intrapulmonary bronchus (ChAT$^+$ villin$^-$). Images captured with black and white camera; Image J was used to color images.

The frequency of ChAT$^-$ villin$^+$ advillin$^+$ cells expressed in cells/mm BM (Table 3.3, Figure 3.24) was 13-fold higher in the bronchiole than any other region (P=0.0095 between upper trachea and bronchiole and P=0.02 between middle trachea and bronchiole. Kruskal-Wallis test followed by Dunn's multiple comparisons test).

Airway	Median Cells/mm BM	Mean Cells/mm BM	IQR Cells/mm BM
Upper trachea	0.297	0.433	0.257
Middle trachea	0.527	0.535	0.241
Lower trachea	1.011	1.127	0.250
Main bronchus	1.579	1.619	0.967
Bronchus	0.616	1.110	1.128
Bronchiole	14.507	13.085	3.922

Table 3.3 Frequency of ChAT$^-$ villin$^+$ advillin$^+$ cells at different levels of the pig respiratory tract. Graphical demonstration of the data is shown in figure 3.23:

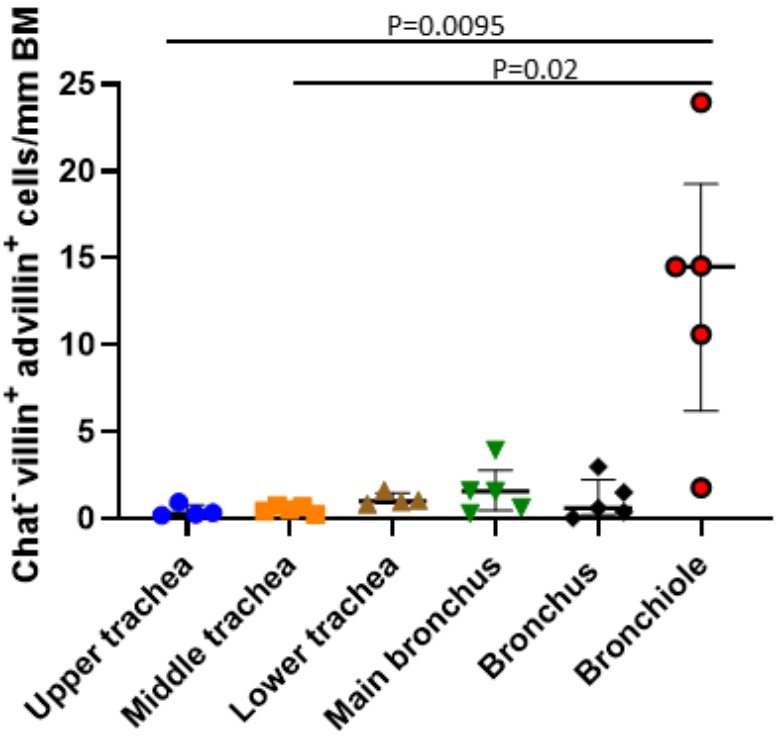

Figure 3.24: Frequency of ChAT$^-$ villin$^+$ advillin$^+$ cells in different levels of the pig respiratory tract epithelium.

Number of ChAT$^-$ villin$^+$ advillin$^+$ cells per mm BM in the different parts of the airway tree. Scatter dot plots with median and interquartile range (IQR) showing the mean value for

each sample (Kruskal-Wallis test followed by Dunn's multiple comparisons test, n=5 pigs). Median, mean and IQR provided in Table 3.3.

Controls validating the efficacy of ChAT-, villin- and advillin-immunolabelling and the specificity of secondary reagent (omission of primary antibodies) are shown in (Figure 3.25).

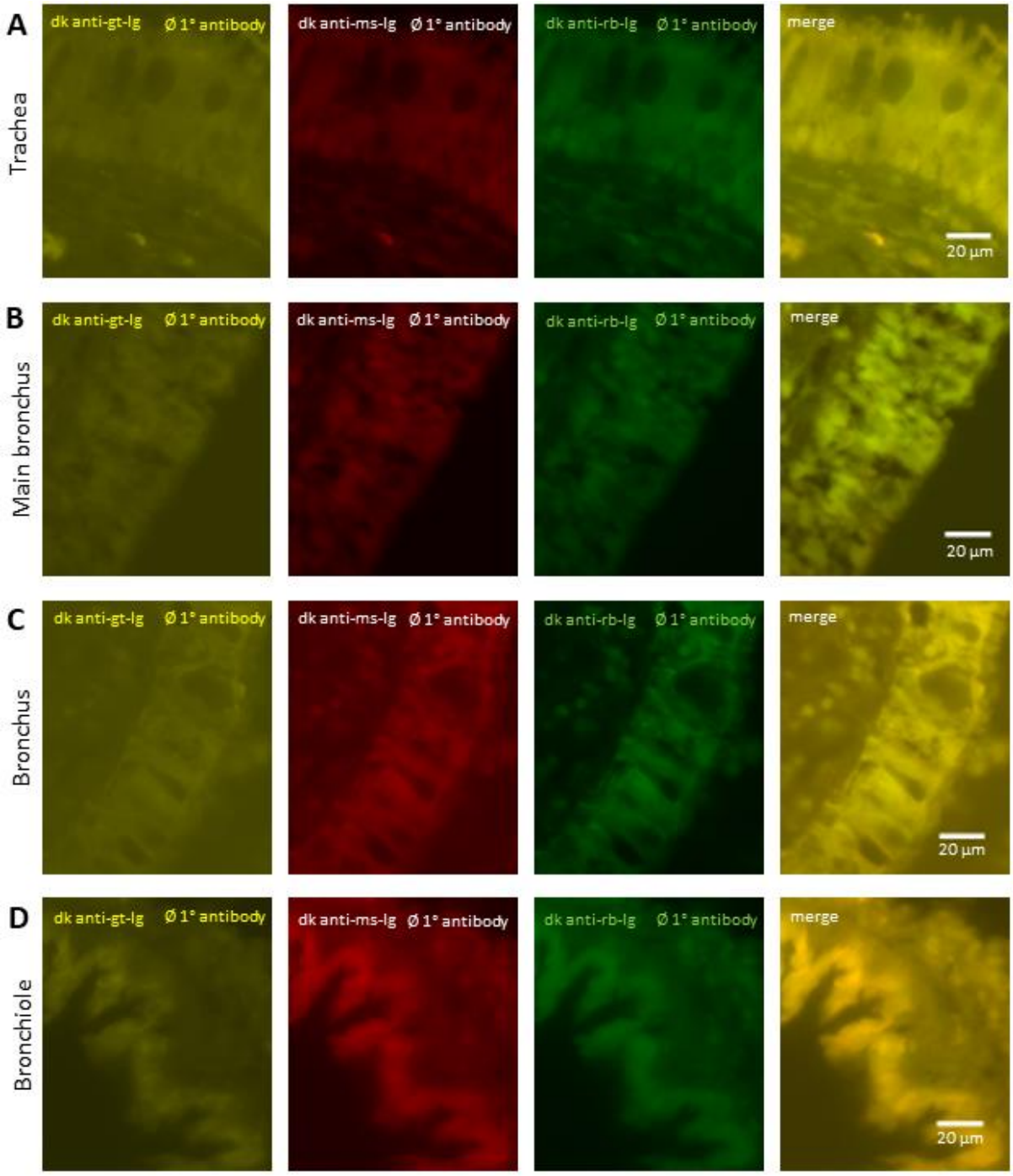

Figure 3.25: Controls used in pig airways epithelium

(A-D) Immunohistochemistry, cryosections of pig airways. ***(A)*** Pig tracheal epithelium, no immunoreactivities were observed when ChAT- (from goat), villin- (from mouse) and advillin-antibodies (from rabbit) were omitted. ***(B)*** Pig main bronchus, no immunoreactivities were observed in the epithelium when ChAT- (from goat), villin- (from mouse) and advillin-antibodies (from rabbit) were omitted. ***(C)*** Pig bronchus, no

immunoreactivities were observed in the epithelium when ChAT- (from goat), villin- (from mouse) and advillin-antibodies (from rabbit) were omitted. ***(D)*** Pig bronchiolar epithelium, no immunoreactivities were observed when ChAT- (from goat), villin- (from mouse) and advillin-antibodies (from rabbit) were omitted.

3.4 Brush cells in mouse tracheal epithelium and lung.

Brush cells were reported in mouse tracheal epithelium using antibodies against signal transduction cascade proteins including TASR, GNAT3, PLCβ2 and TRPM5 (Krasteva et al. 2011, Tizzano et al. 2011, Saunders et al. 2013).

3.4.1 LRMP is expressed in brush cells in mouse trachea.

3.4.1.1 Immunohistochemistry reveals LRMP-immunoreactivity in GNAT3 immunoreactive cells.

LRMP is expressed in mouse taste buds including papilla vallata, fungiform and foliate papillae (Shindo et al. 2010), so I used mouse papilla vallata as a positive control for LRMP-antibodies. LRMP-immunoreactive cells were observed in taste cells in the taste bud with apical and basal processes extending from the cell body (Figure 3.26A). Tracheal cryosections from wild-type mouse (C57BL/6RJ) were double-immunolabeled with antibodies against LRMP and GNAT3 (brush cell marker). Colocalization of LRMP- and GNAT3-immunoreactivities was detected in a 1:1 ratio in flask-shaped epithelial cells with apical and basal processes. LRMP- and GNAT3-immunoreactivities were detected in the whole cell (Figure 3.26B).

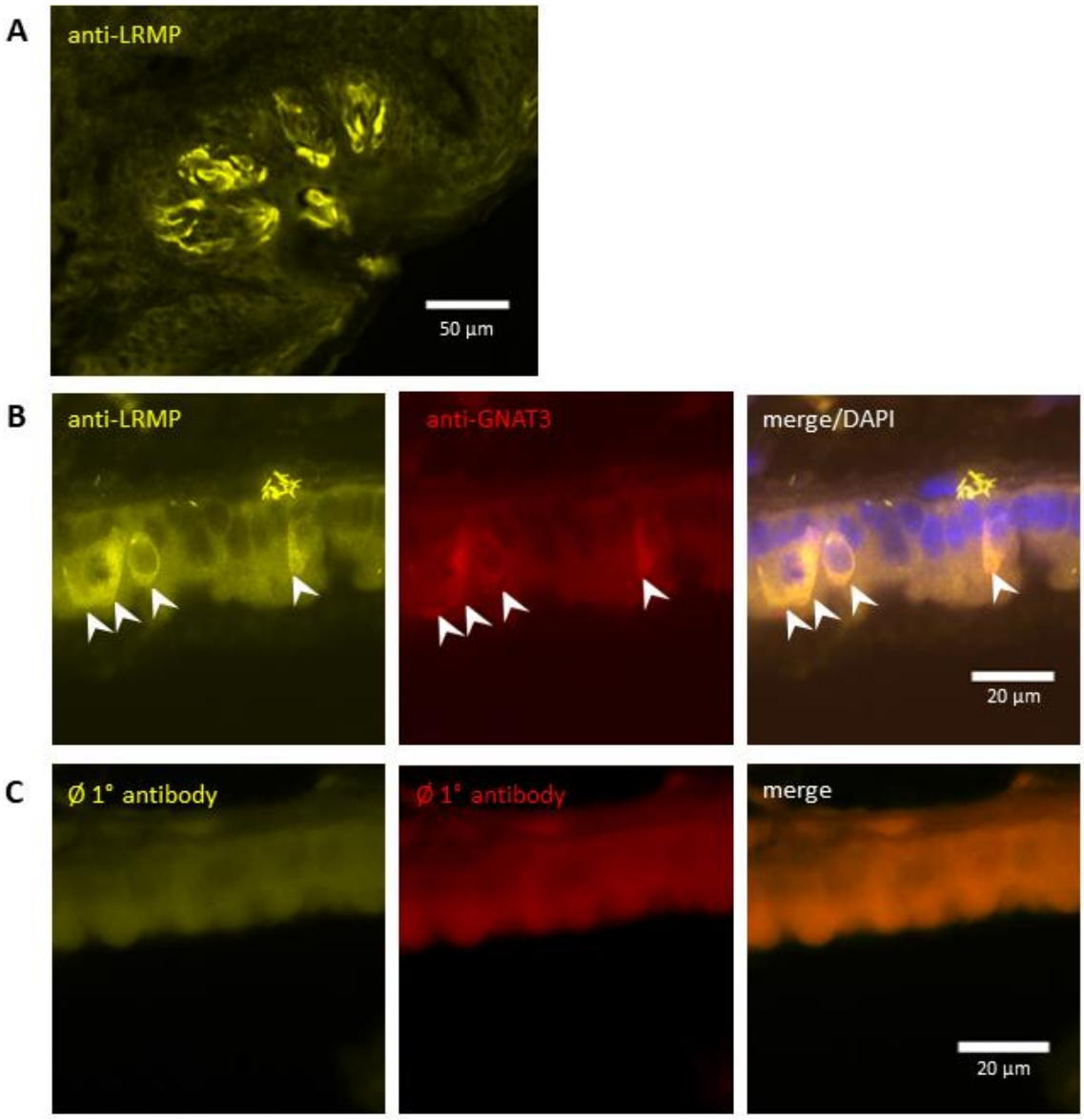

Figure 3.26: LRMP-immunoreactivities in the taste bud and tracheal epithelium in C57BL/6RJ mice.
(A) Immunohistochemistry of mouse taste bud (papilla vallata) cryosection from a C57BL/6RJ mouse, immunolabeled with antibody against LRMP, showing taste cells positive for LRMP. ***(B)*** Immunohistochemistry of a tracheal cryosection immunolabeled with antibodies against LRMP and GNAT3, showing epithelial cells double-positive for LRMP and GNAT3 (arrowheads). ***(C)*** No immunoreactivity was observed when all primary antibodies were omitted. Images captured with black and white camera; Image J was used to color images.

3.4.1.2 Immunohistochemistry reveals LRMP-immunoreactivity in GFP-immunoreactive cells in TRPM5-eGFP reporter mice.

Tracheal cryosections from 5 TRPM5-eGFP reporter mice were immunolabeled with antibodies against LRMP and GFP as enhancer. Immunolabeling showed co-localization of both LRMP- and GFP-immunoreactivities (Figures 3.27A) and this colocalization was in a ratio of 1:1. This finding was corroborated by double immunolabeling of 5 tracheal whole mounts (Figure 3.27B). The LRMP-immunoreactive cells were flask-shaped epithelial cells extending from the BM to the lumen.

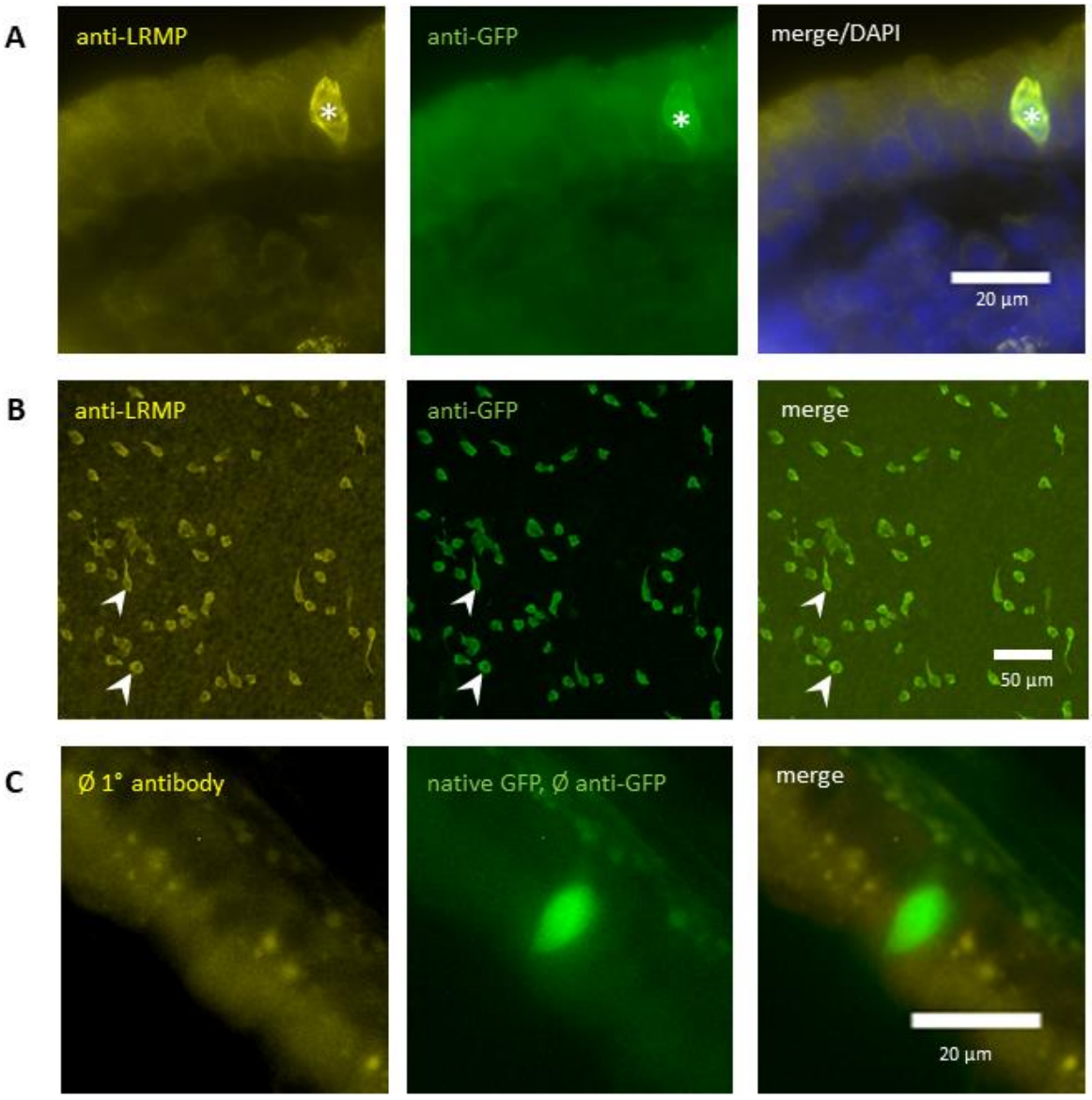

Figure 3.27: LRMP-and GFP-immunoreactivities in tracheal epithelium in TRPM5-eGFP reporter mice.
(A) Immunohistochemistry of a tracheal cryosection from a TRPM5-eGFP reporter mouse, immunolabeled with antibodies against LRMP and GFP, showing epithelial cell double-positive for LRMP and GFP (asterisks). ***(B)*** Tracheal whole mount immunohistochemistry with antibodies against LRMP and GFP, showing LRMP-immunoreactivity in GFP-immunoreactive cells (arrowheads) in a 1:1 ratio. ***(C)*** Tracheal cryosection, no immunoreactivity was observed when all primary antibodies were omitted, the green fluorescence is native GFP.

3.4.1.3 *In silico*-analysis of publicly available sequencing data reveals *Lrmp*-mRNA expression in brush cells of mouse tracheal epithelium.

The immunohistochemical finding were supplemented by *in silico*-analysis of published single cell sequencing data of mouse tracheal epithelial cells. We were able to reproduce the clustering reported by the laboratories generating the datasets. Montorro et al. (2018) could identify eight cell clusters in dataset GSE103354, namely goblet, club, basal, ciliated, tuft, neuroendocrine and ionocyte cells (Figure 3.28A). We achieved the same clustering and found that *Lrmp*-mRNA was expressed predominantly in brush/tuft cells, followed by *Gnat3*-mRNA, *Trpm5*-mRNA, *Pou2f3*-mRNA, *Plcβ2*-mRNA, and 5 cells out of 121 were expressing Chat (Figure 3.28B).

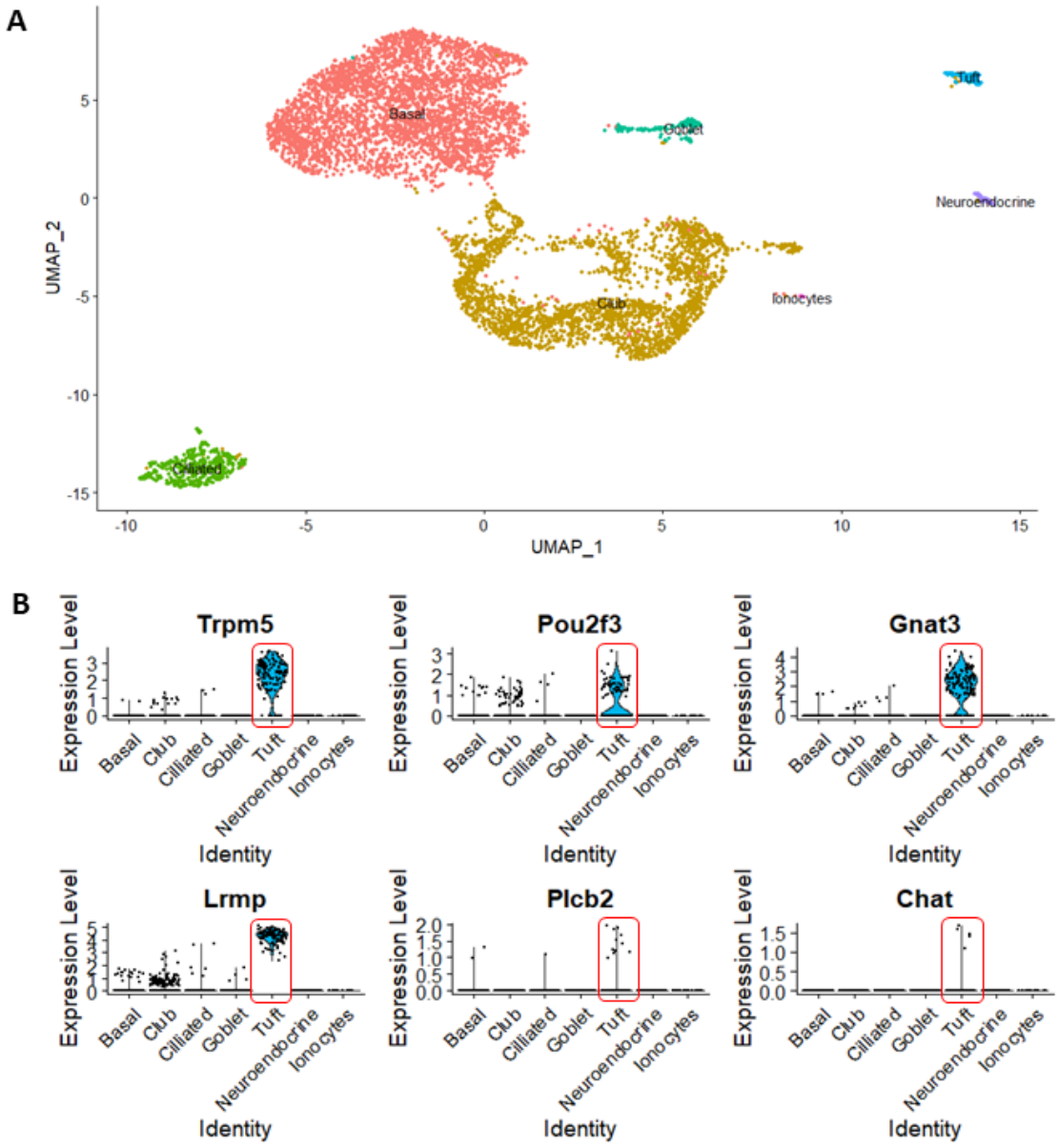

Figure 3.28*: In silico*-analysis of single cell mRNA sequencing data (GSE103354) reveals *Lrmp*-mRNA expression predominantly in brush cells in mouse tracheal epithelium.
(A) SPRING plot (Uniform Manifold Approximation and Projection, UMAP) shows eight distinct cell clusters, namely goblet, secretory, basal/club, ciliated, club, basal, basal 2, tuft and neuroendocrine/ionocyte cells. ***(B)*** Violin plots showing *Lrmp*-mRNA being predominantly expressed within the tuft cell, followed by *Gnat3*-mRNA, *Trpm5*-mRNA, *Pou2f3*-mRNA, *Plcβ2*-mRNA, and 5 cells out of 121 were expressing Chat.

Plasschaert et al. (2018) could identify eight cell clusters, namely secretory in data set GSE102580, basal, ciliated, Krt4/13, cycling basal, brush, neuroendocrine and ionocyte cells. (Figure 3.29A). We also reproduced this clustering and *Lrmp*-mRNA was expressed predominantly in brush cells followed by *Trpm5*-mRNA, *Gnat3*-mRNA, *Pou2f3*-mRNA. Three cells out of 90 were expressing *Chat* and 5 cells out of 90 were expressing *Plcβ2* (Figure 3.29B).

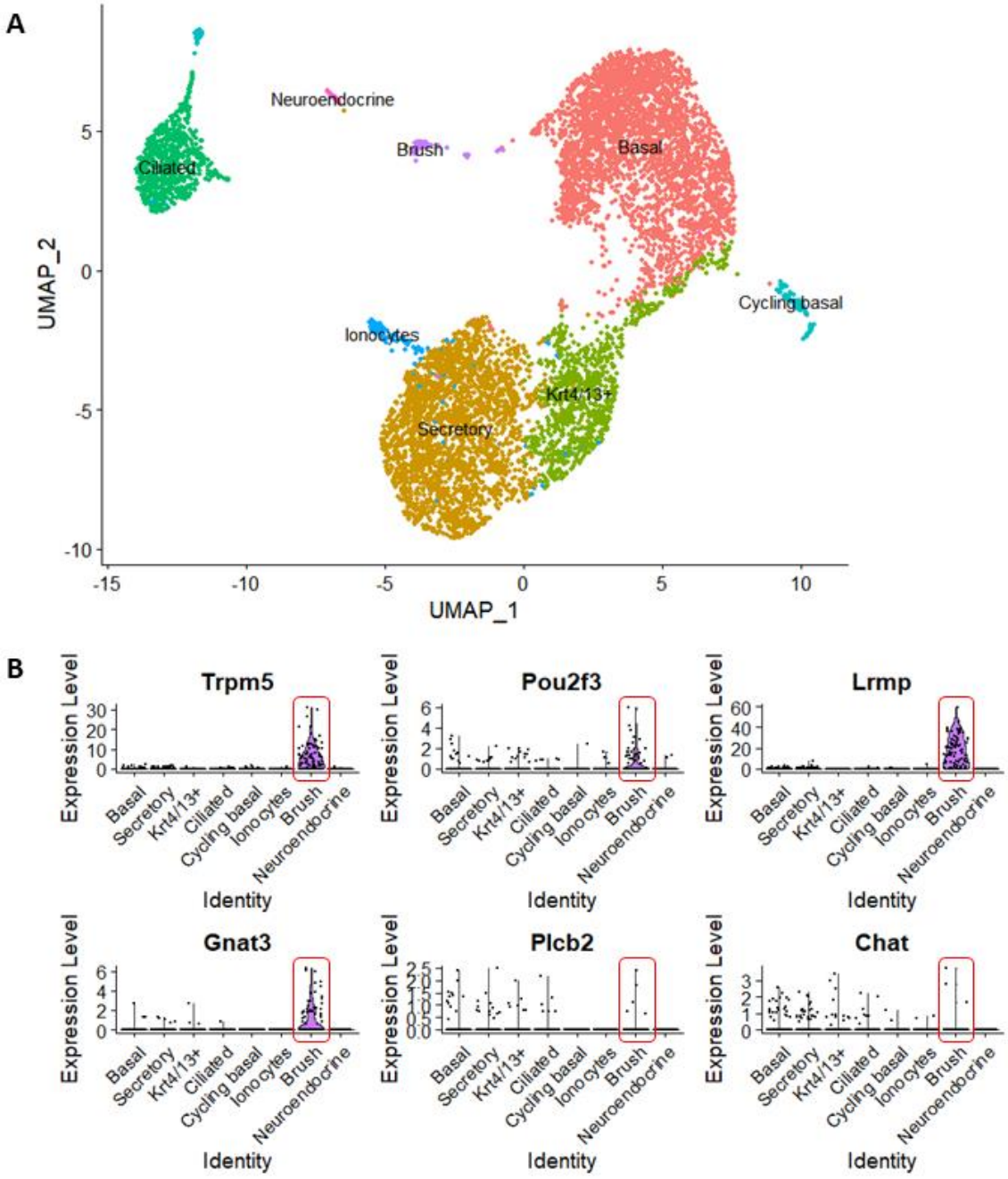

Figure 3.29*: In silico*-analysis of single cell mRNA sequencing data (GSE102580) reveals *Lrmp*-mRNA expression predominantly in brush cells in mice tracheal epithelium.
(A) SPRING plot (Uniform Manifold Approximation and Projection, UMAP) shows eight distinct cell clusters, namely secretory, basal, ciliated, Krt4/13, cycling basal, brush, neuroendocrine and ionocyte cells. ***(B)*** Violin plots showing *Lrmp*-mRNA being predominantly expressed within brush cells followed by *Trpm5*-mRNA, *Gnat3*-mRNA,

Pou2f3-mRNA. Three cells out of 90 were expressing Chat and 5 cells out of 90 were expressing Plcβ2.

3.4.2 TRPM5- and LRMP-positive brush cells were not detected in mouse intrapulmonary bronchial epithelium.

Lung cryosections from C57BL/6RJ mice (n=10) were immunolabeled with antibodies against TRMP5 and LRMP. Immunolabeling revealed that there was no immunoreactivity to TRPM5- or LRMP- antibody in intrapulmonary airways (Figure 3.30A and 3.30B), while few positive cells were found in the extrapulmonary bronchus (Figure 3.30A and 3.30B).

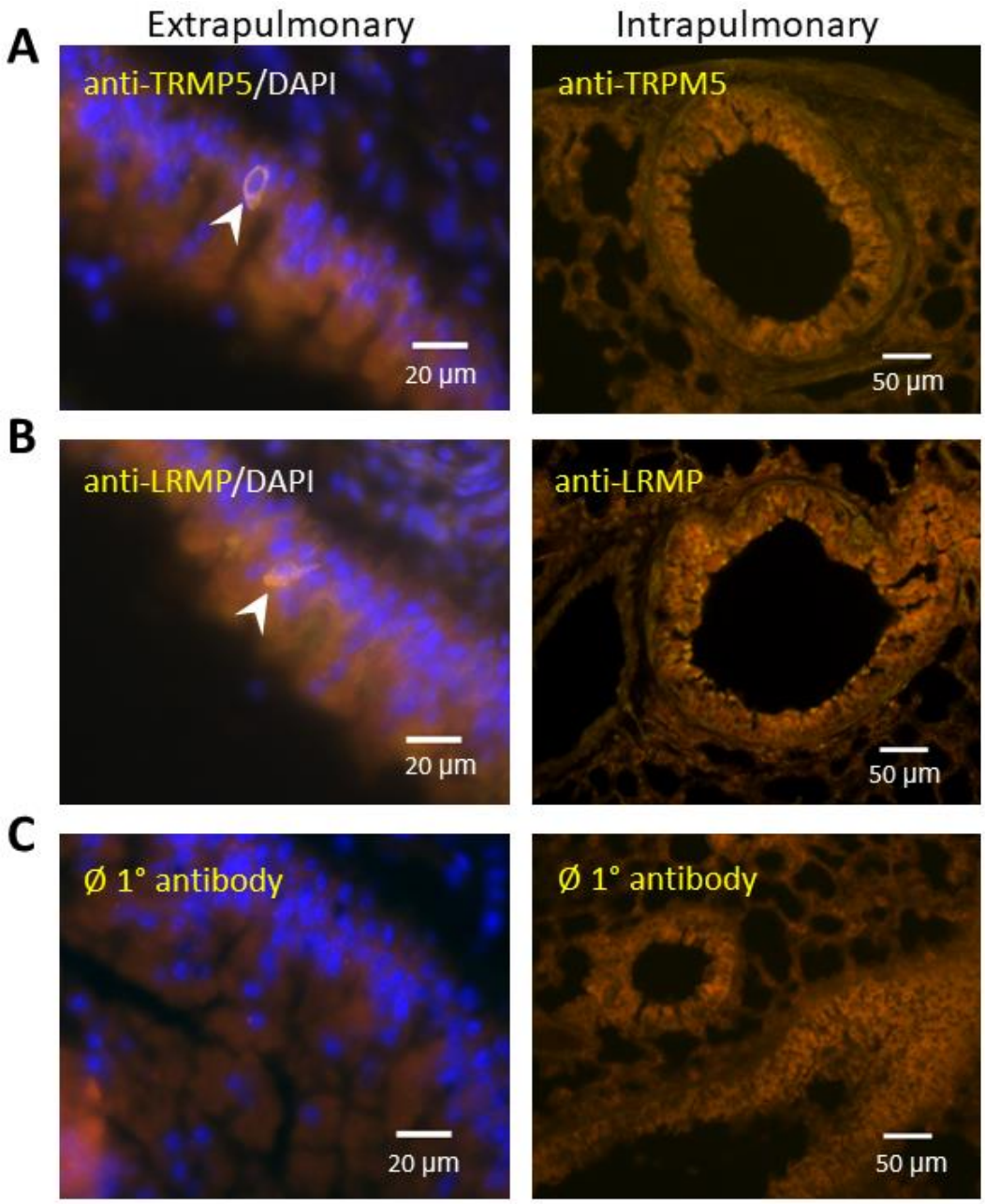

Figure 3.30: TRPM5 and LRMP immunoreactivity in bronchial epithelium.
(A-C) Immunohistochemistry of lung cryosections from C57BL/6RJ mice.
(A) Extrapulmonary bronchus immunolabeled with antibody against TRPM5 shows epithelial cell positive for TRPM5, while there is no immunoreactivity toward TRPM5 in an intrapulmonary bronchus of the same tissue section. ***(B)*** Extrapulmonary bronchus (left image) showing epithelial cell positive for LRMP. In contrast (right image) an intrapulmonary bronchus from the same tissue section shows no immunoreactivity toward LRMP. ***(C)*** No immunoreactivity is observed when primary antibodies were omitted. Images captured with color camera; true colors are shown.

4 Discussion

4.1 Human

4.1.1 The logical and first-hand approach did not work.

In this study we first tried to identify markers that can be used to locate brush cells in human. Previous studies reported ultrastructural feature of these cells using electron microscopy. These studies described cells in the trachea equipped with microvilli and with many vesicles in their cytoplasm. They constituted 0.5% of the total number of epithelial cells (Rhodin 1959; Basset et al. 1971; McDowell et al. 1978). Furthermore, these cells were reported in the main stem bronchus of a six years old child with no bronchogenic disease (Watson and Brinkman. 1964) and in the lung in a four months old infant with desquamative interstitial pneumonitis (DiMaio et al. 1988). So, previous studies in human defined brush cells by the presence of microvilli, but it remained unclear whether these cells express components of the taste transduction cascade as it is characteristic for brush cells in the murine tracheal epithelium. These signaling cascade proteins include PLCβ2, GNAT3 and TRPM5 (Krasteva et al. 2011; Tizzano et al. 2011; Saunders et al. 2013) and recently the transcription factor POU2F3 was shown to be essential for the development of $TRPM5^{+}$ cells (Yamashita et al. 2017). Antibodies against these proteins have been shown to serve as excellent immunohistochemical markers to identify brush cells in murine tracheal epithelium. These marker proteins are also expressed in murine taste cells (type II) in the tongue (Yan et al. 2001; Kinnamon and Finger 2019; Dutta Banik et al. 2018). Recent immunohistochemical studies of the sinonasal mucosa reported the presence of chemosensory cells which express taste transduction cascade markers like in murine taste cells and trachea. These cells express T2R and bitter agonists like denatonium activate these cells and cause $[Ca^{2+}]$ elevation through PLCβ2, IP3R3, and TRPM5 cascades (Lee et al. 2014).

We, thus, first attempted to locate brush cells in human airways using antibodies against PLCβ2, GNAT3, TRPM5 and POU2F3. However, we could not observe any immunoreactive cells in the nose, trachea and lung. To test for the suitability of these antibodies to label

their cognitive protein in fixed human tissue, we performed these experiments on human papilla vallata as a positive control in each incubation. These experiments revealed PLCβ2-immunoreactive cells in the taste buds, but no immunoreactivity was observed using GNAT3-, TRPM5- and POU2F3-antibodies, questioning their suitability for this type of study. The amino acid sequences are not identical between human and mice, so that the antibodies might not recognize the human proteins at all. Another possible cause for the absence of immunolabelling with PLCβ2-, GNAT3-, TRPM5- and POU2F3-antibodies in human airways might be that brush cells in human do not express these taste transduction markers and their signaling pathway is different than that in mice. Thus, we further performed *in silico*-analysis of publicly available sequencing data sets. This revealed very low expression of PLCβ2-, GNAT3-, TRPM5- and ChAT-mRNA in human trachea and bronchus, which is consistent with the lack of staining in our immunohistochemistry work. Our findings are consistent with new single cell sequencing data work on human tuft (brush) cells. The samples were obtained by brushing either from nasal polyps or ethmoid sinus. It showed that only in the allergic group tuft cells expressed the signal transduction cascade markers like TRPM5 and DCLK1. These allergic tuft cells were activated by interleukin-13 which finally lead to prostaglandin production (Kotas et al. 2022).

So, the logical first-hand approach using antisera that are well established tool to locate airway brush cells in mice did not work on human tissue and we continued with *in silico*-analysis with the aim to identify other markers.

4.1.2 LRMP expression is restricted to chemosensory cells in human airway epithelium, taste bud and colonic epithelium.

In our *in silico*-analysis we were able to reproduce the clustering reported by Goldfarbmuren et al. (2020) who could identify nine cell clusters in the tracheal epithelium, namely goblet, secretory, basal/club, ciliated, club, immune cells, basal 1, basal 2 and rare cells. The latter were subclustered into ionocytes, neuroendocrine and brush/tuft cells. scRNAseq data sets showed high expression level of mRNA coding for a

lymphoid restricted membrane protein abbreviated as LRMP in rare cells of the human tracheal and bronchial epithelium that were all signated brush (or tuft) cells because of their relatively high expression of *POU2f3*-mRNA. The difference in POU2f3 expression pattern using immunohistochemistry in our study and in this *in silico*-analysis might reflect a difference between mRNA level and protein level. POU2f3 protein level might be too low to be detected by immunohistochemistry. *LRMP* was the predominantly expressed gene in the brush cell cluster, whereas *ChAT*-mRNA was not expressed in this cluster (25 cells were used for analysis) (Goldfarbmuren et al. 2020). Additional, *in silico*-analysis of previously published scRNAseq data from human bronchial epithelial cells identified seven clusters, namely secretory, basal/secretory, ciliated, club, basal, ionocytes, and cholinergic chemosensory cells (brush/tuft) and neuroendocrine cells clustered together. Here, *LRMP* was also the predominantly expressed gene in the brush cell and neuroendocrine cell clusters and *ChAT*-mRNA was very minimally expressed (53 cells were used for analysis) (Plasschaert et al. 2018). As *ChAT*-mRNA was not expressed or only minimally expressed in brush cells, this might indicate that these cells are not cholinergic. On the other hand, levels might have been below detection limit. Our results are consistent with a previous study which identified 13 brush/tuft cells highly expressing *LRMP*. Yet, it has to be considered that the number of brush cells (13 cells) that were used for this analysis was very low (Deprez et al. 2020).

We, therefore, directed our further attention to LRMP. LRMP is an integral membrane protein of the endoplasmic reticulum with orientation in the ER membrane toward the cytosol (Behrens et al. 1994). The *LRMP* gene is expressed in healthy human lung as analyzed by using RT-PCR (Manenti et al. 2006), which fits well with our finding that LRMP is expressed in human lung including bronchus and bronchioles using immunohistochemistry. That means that LRMP is expressed in human lung both at mRNA and protein level.

Double- and triple-immunolabeling experiments in the nose, trachea and lung using antibodies against LRMP and other epithelial cell markers, including CK19 (general

epithelial cell marker which labeled epithelial cells), PGP 9.5 (neuroendocrine cell and nerve fiber marker), FOXI1 (ionocyte marker), tubulin (ciliated cell marker) and uteroglobin (secretory cell marker). These LRMP-immunoreactive cells were flask-shaped epithelial cells with apical and basal processes; they are neither neuroendocrine cells, nor ionocytes, ciliated cells or secretory cells. These findings revealed that these LRMP-immunoreactive cells are brush (chemosensory) cells and this is consistent with the publicly available single cell RNA sequencing data.

In this study, we used human colon and human taste buds as positive controls. Single-immunolabeling in the taste bud and colon using antibody against LRMP revealed that LRMP-immunoreactive cells, flask-shaped epithelial cells with apical and basal processes, are present in human colon. Our experiments are in line with previous results in the intestine which reported LRMP as a marker of tuft cells in the intestine using scRNAseq (Dye et al. 2019). Furthermore, such LRMP-immunoreactive cells, flask-shaped epithelial cells with apical and basal processes, are also located in human taste buds. This result has further strengthened our confidence in LRMP as a marker of (brush) chemosensory cells, as there are similarities between taste cells and brush cells (Höfer and Drenckhahn 1996).

The expression of LRMP in human brush cells may point towards an apparent role of this protein in the signal transduction cascade pathway; similar to its putative role in mouse taste signal transduction cascade pathway in type II cells (Shindo et al. 2010). When a substance binds to the receptor, β and γ subunits of the coupled G-proteins bind to PLCβ2, which generates IP3. IP3 might induce LRMP- and IP3R3-dependent Ca^{2+} release from the ER, which in turn causes Na^{+} influx into the cell through TRPM5. These events induce depolarization at the cell level and ACh release from the cell, which affects nearby cells (Figure 4.1).

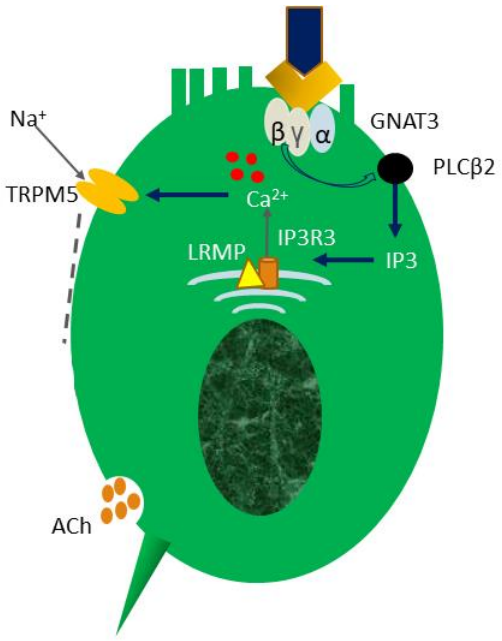

Figure 4.1: A suggested role for LRMP as part of the taste signal transduction cascade. A heterotrimeric G protein consisting of α, β and γ subunits is bound to the receptor. If a substance binds to the receptor, the G protein dissociates and a dimer of the β and γ subunits activates the enzyme PLCβ2. As a consequence, IP3 is released and binds to the IP3R3. IP3R3 and LRMP cause Ca^{2+} release from the ER into the cytosol. This leads to the activation of the cation channel TRPM5, which then induces the influx of Na^{+} into the cell. This results in depolarization of the brush cell, which then induces ACh release from the cell, acting upon nearby cells.

So, now we have a tool that allows for studying the spatial distribution of brush cells along the human airway tree. The taste signal transduction cascade in human brush cells and the main function of LRMP in these cells still need more investigations, for instance, what is the exact role of LRMP in the taste signal transduction cascade in human?

4.1.3 LRMP-immunoreactive cells extend deep into the lung.

Chemosensory cells in mice are rarely present below the tracheal bifurcation (Krasteva et al. 2011; Tizzano et al. 2011), while in human we found chemosensory cells below the tracheal bifurcation down to the bronchioles.

These cells probably correspond to those previously reported by electron microscopy in the main stem bronchus of a six years old child with no bronchogenic disease. These cells were described as having few mitochondria, few endoplasmic reticulum, many ribosomes, vesicles and vacuoles (Watson and Brinkman 1964). Additionally, an electron microscopic study revealed the presence of cells containing microvilli resembling brush cells in the trachea, bronchus and bronchioles (DiMaio et al. 1990).

Previous single cell sequencing analysis were unable to detect them in human small airways not because they were not there, but may be because they were fragile and lost during sample preparation or they were located in a discrete manner (Zuo et al. 2020). We were also unable to find these cells in every section which seems to confirm Zou et al (2020) observations. We did not observe LRMP-positive cells in the alveoli and this matches well with previous findings on the control lung. Tuft cells were not detected in the control group (without COVID-19) in human lung, but ectopically appeared in epithelial regeneration after COVID-19 (Melms et al. 2021). This is consistent with previous research on murine lung in which ectopic appearance of tuft cells was observed in epithelial regeneration after influenza infection (Rane et al. 2019).

Our quantitative analysis of LRMP-positive cells in human airways showed lowest frequency of occurrence in the trachea and the frequency increased toward the periphery, especially in the bronchioles. Under the hypothesis that brush cells serve to monitor compounds arriving with inhaled air, it would make sense to have them at the places where particles in the inhaled air will be deposited. Supportive of such a hypothesis is a recent study by Rahman et al. (2021), who reported that 30% of particles were deposited more in the small intrapulmonary bronchioles than in the trachea, main bronchus and bronchus. They used a human airway model taking into consideration

particle size (about 5 nm) and age (as age increases, particle deposition increases) (Rahman et al. 2021). These findings may provide one possible explanation for the highest density of these cells in the bronchioles (0.206/mm BM) as particles are highly deposited in that area. Thus, high exposure to these particles might promote chemosensory cells in the distal airways to initiate a protective reflex. This is in contrast, however, to earlier findings by Madsen et al. (2018), who reported that the deposition of particles (7 to 12 µm) is much higher in the primary and secondary bronchi than in terminal bronchi and alveoli (Madsen et al. 2018).

4.1.4 LRMP-immunoreactive cells are less frequent than neuroendocrine cells.

Our findings showed another rare cell type, which is the neuroendocrine cell. We found these cells which are characterized by PGP-immunoreactivity in human upper and lower tracheal epithelium. In addition, we found PGP-immunoreactive nerve fibers surrounding glands and vessels. The PGP-immunoreactive cells were flask-shaped epithelial cells with apical and basal processes. Solitary neuroendocrine cells were reported in human airway using antibodies against PGP, CGRP and GRP (Weichselbaum et al. 2005). We recorded PGP-positive cells at higher frequency of occurrence in the upper trachea (sublaryngeal) than in the lower trachea (bifurcation). The frequency ranged from 2.3 (bifurcation part) to 5.6 (sublaryngeal part) cells/mm of BM. A previous study calculated the number of these cells as 12.5 cells/cm, i.e. 1.25 cells/mm BM using chromogranin A antibody (Boers et al. 1996). In our study the frequency of these cells was slightly higher which might be caused by use of a different marker antibody, other technical aspects, or just reflects physiological variation.

In mice, the previously reported absolute numbers were higher than my data, but still in the same order of magnitude. PGP-positive cells in the upper trachea were reported as 220 cells/mm^2 (Mahmoud et al. 2021). I took the square root of this value, which is approximately 15 cells/mm in mice, while in our data it is 5.6 cells/mm. Additionally, in mice there is a gradient where neuroendocrine cells were higher in the upper trachea than the lower part (Mahmoud et al. 2021). Similarly, my data revealed a higher number

in the upper trachea than in the lower trachea, although in this material this difference was not significant.

Cutz and coworkers identified one type of K cells in human trachea in intrauterine and extrauterine life as single cells and not as neuroepithelial bodies. These cells were elongated or pyramidal with processes reaching the lumen and the basal part resting on the BM and the cytoplasm contained DCV (Cutz et al. 1975). These previous findings support our finding in human trachea using immunohistochemistry in that these cells present in the trachea as solitary cells. Endocrine-like cells were also reported in the nasal turbinate epithelium in young and adult (Thaete et al. 1981). PGP- and calbindin-immunoreactive cells were found in the respiratory epithelium of human nose in fetus and newborn. These cells had broad apical and thin basal processes. Furthermore, such cells were found in clusters (Johnson et al. 1997). Additionally, neuroendocrine cells were reported in the lung in the initial phases of fetal development (Cutz and Conen 1972). Single bombesin-immunoreactive cells and clusters of cells (NEBs) were discovered from the bronchi down to the alveolar duct (Johnson et al. 1982).

Previous scRNAseq showed that rare cells constitute 0.8% of all epithelial cells and that tuft cells are slightly more frequent than neuroendocrine cells (Goldfarbmuren et al. 2020). In contrast, our findings revealed a considerable difference in the number of chemosensory and neuroendocrine cells using immunohistochemistry. We found that PGP-positive (neuroendocrine) cells had 6-fold higher frequency than the LRMP-positive (brush) cells in the upper (sublaryngeal) trachea. This difference between PGP-positive cells and LRMP-positive cells in the upper trachea was significant. Moreover, PGP-positive cells had a 5-fold higher frequency than the LRMP-positive cells in the bronchus, and a 4-fold higher frequency in the bronchiole. Thus, the difference in the relative occurrence between my data and those data might be due to several reasons; the first one is the discrepancy between immunohistochemistry and scRNAseq, the second possible cause is that one of these antibodies could be less efficient that the other one and the third possible reason is that one of these cells could be more fragile or lost during the cell dissociation process.

4.2 Pig

4.2.1 Brush cells in pig respiratory tract epithelium.

In silico-analysis of single cell sequencing data revealed that the epithelium components in pig are ciliated cells, basal cells, secretory cells and rare cells. The later constitute less than 1%, including brush cells and ionocytes (Pezzulo et al. 2021). In the present study, we identified the poorly defined brush cells in pig, which have been reported previously in an ultrastructural study describing these cells as elongated (columnar) with a narrow nucleus located in the basal part. The suggested function for these cells was absorption. They were not detected in the alveolar epithelium (Baskerville 1970). Immunohistochemistry revealed the presence of brush cells in the porcine uterus (luminal epithelium and glands), where no direct contact with nerve fibers was observed. These cells express ChAT and markers for the canonical taste transduction cascade including TRPM5 and PLCβ2 (Sponchiado et al. 2022). Moreover, cholinergic chemosensory cells in pig urethra have been shown to express constantly TRPM5-, PLCβ2 and α-gustducin, while ChAT- and villin- (50% of samples) immunoreactivity were not constantly observed (Deckmann et al. 2015). In contrast, we found that villin and ChAT are constantly expressed in every sample we used for this study in pig airways. We performed double- and triple-immunolabeling experiments in the trachea and lung using antibodies against ChAT, villin and advillin. These experiments revealed the presence of three different phenotypes of cells in pig tracheal epithelium (all levels) and lung (bronchus and bronchioles): $ChAT^+$ $villin^+$ $advillin^+$, $ChAT^-$ $villin^+$ $advillin^+$ and $ChAT^+$ $villin^-$ $advillin^-$ cells. The cells of the first group ($ChAT^+$ $villin^+$ $advillin^+$) were flask-shaped, slender solitary epithelial cells with basal processes and apical processes reaching the lumen. Villin- and advillin-antibodies intensely stained the apical part of the cell. Interestingly, these cells extend deep into the lung down to the bronchioles and their frequency is 10-fold higher in the bronchioles that in any other region. The extension of these cells into the lung matches well with what we found in human lung, where the frequency of brush cells reaches its peak in the bronchioles. Furthermore, RT-PCR confirmed the expression of *Chat-, villin-* and *advillin*-mRNA from the trachea down to the deep part of the lung, so these markers

are expressed both at protein and mRNA level. In the second group (ChAT$^-$ villin$^+$ advillin$^+$) ChAT is not expressed in villin- and advillin-immunoreactive cells. The frequency of such ChAT$^-$ villin$^+$ advillin$^+$ cells expressed in cells/mm BM was slightly higher than that of the first group with 13-fold higher numbers in the bronchiole than in any other region. The third group consists of very few ChAT$^+$ villin$^-$ advillin$^-$ cells. They might represent triple-positive cells whose cell apex with (ad)villin-immunoreactivity might not have been included in the plane of the tissue section.

We believe that our research will serve as a base for future studies on pig and on human. As there are similarities in the anatomy of both species and in the distribution of brush cells, pig – rather than small rodents - might be a good model for human. This means that future studies might rely more on pig for closer matching to the situation in human.

4.3 Mouse

4.3.1 LRMP is restricted to brush cells in mouse trachea.

In this study we identified LRMP in mouse tracheal brush cells which express the signal transduction cascade markers including GNAT3, PLCβ2 and TRPM5 (Krasteva et al. 2011; Tizzano et al. 2011; Saunders et al. 2013). LRMP is also expressed in the taste cells of mouse papilla vallata, fungiform and foliate papillae, and it has been reported to colocalize with IP3R3 (Shindo et al. 2010). So, in this study we used mouse papilla vallata as a positive control for LRMP-immunolabeling.

LRMP$^+$ cells were identified as brush cells by double-immunolabeling with antibodies against GNAT3. Supportingly, *in silico*-analysis of publicly available scRNAseq showed that LRMP is predominantly expressed in mouse brush cells, and quantitative analysis of TRPM5-eGFP reporter mouse tracheal whole mounts showed that LRMP is colocalized with GFP in a 1:1 ratio. Our results revealed that LRMP is a predominant marker of brush cells also in mouse trachea. Our experiments corroborate a recent study in mouse intestine reporting LRMP as a p53 target gene that is expressed in tuft cells. There are two p53 binding parts in the intron of the *Lrmp* gene and p53 upregulates the transcription of *Lrmp* to keep its expression high in tuft cells (Chang et al. 2021).

The results point to the probability that LRMP has a role in the signal transduction cascade, but its exact role has not been investigated in mouse brush cells.

4.3.2 TRPM5- and LRMP-positive brush cells are not detected in mouse intrapulmonary bronchial epithelium.

Tizzano and coworkers reported that cholinergic chemosensory cells density reduces from the nose to the bronchiolar epithelium (bronchioles diameter more than 400±100 µm), and these cells are absent from smaller bronchioles and the alveoli (Tizzano et al. 2011). Our current findings principally match with this earlier report.

In contrast to the trachea, we did not detect brush cells in the intrapulmonary bronchial epithelium and only very few cells were detected in the extrapulmonary bronchial epithelium using antibodies against LRMP and TRPM5. These findings correlate satisfactorily well with those of Rane et al. (2019) and further support the idea that these cells are absent in the distal part of the lung in steady state conditions. After influenza infection, they appear only in the injured, but not in the uninjured part during regeneration suggesting a remodeling function (Rane et al. 2019).

Thus, our findings showed that chemosensory cells are absent in the intrapulmonary bronchi in mice while these cells extend deep into the lung in human and pig.

4.4 Conclusion

These data identify chemosensory cells in human airway epithelium by the presence of the protein LRMP. The distribution of these cells along the airway tree is similar to pig and markedly different from that of the most commonly used laboratory animal, the mouse. These cells are most frequent in small bronchioles in human and pig, whereas they are restricted to the trachea and extrapulmonary bronchi in mice (Figure 4.2). This suggests that pig might be a better experimental model than mice to study this cell type and its function.

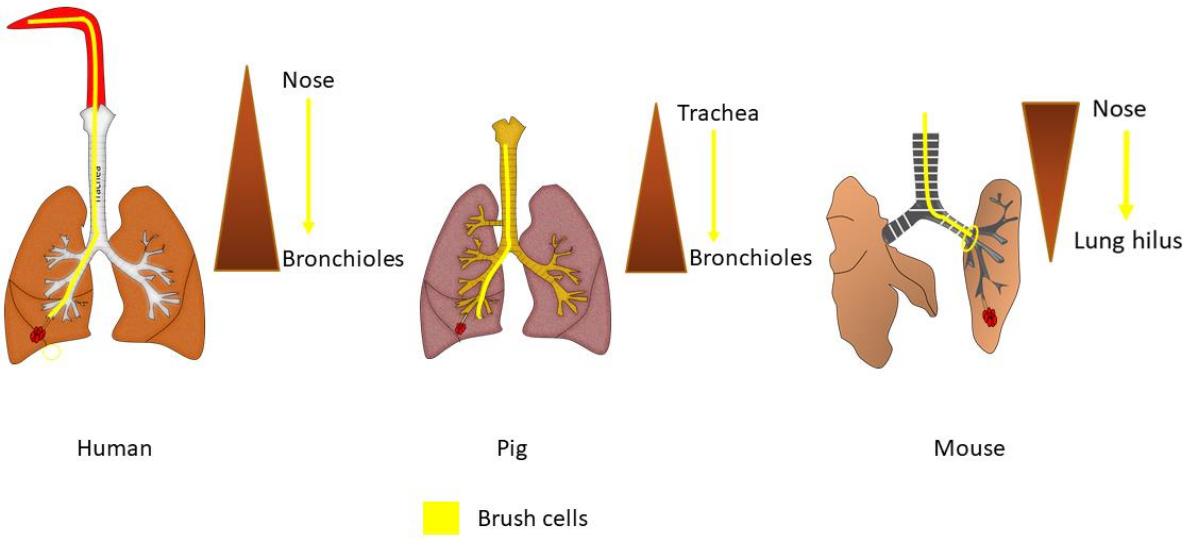

Figure 4.2: Distribution of brush cells along the respiratory tract in human, pig and mouse.

In human and pig, these cells extend deep into the lung into the bronchiolar epithelium, while in mice these chemosensory cells are restricted to extrapulmonary airways.

5 Summary

Specialized sensory epithelial cells sense potentially harmful substances and initiate protective responses. They are found along the mammalian respiratory tract. Studies in mice suggested the presence of at least two populations: 1) neuroendocrine cells (marker: PGP9.5), 2) solitary cholinergic chemosensory cells (SCCC) (synonyms: brush or tuft cells; markers: GNAT3, PLCβ2, TRPM5). Neuroendocrine cells are present in human, but the spatial distribution of SCCC remained unknown. This study aimed to provide a positional and sensory signaling pathway-focused inventory of such potentially sensory cells in the epithelium of the human and pig respiratory tract in comparison to mice (the most commonly used model organism). Single- and multiple-labelling immunofluorescence with antibodies against established marker proteins was performed on specimens of human papillae vallatae (positive control) and respiratory tract (nose, trachea, lung) obtained from anatomy body donors, lung from organ donors and lung resected from COPD patient in the course of lung transplantation; TRPM5-eGFP reporter and C57BL6/J mice served as references. Furthermore, multiple-labelling immunofluorescence with antibodies against ChAT, villin and advillin was done on specimens of pig tracheal and lung epithelium, and RT-PCR was performed for validations. Publicly available scRNAseq data of human bronchial and tracheal epithelial cells were analyzed *in silico*. Murine tracheal epithelial cells (C57BL/6 wild-type) were also analyzed *in silico*. PLCβ2-Antisera labelled cells in human taste buds, but not in the respiratory mucosa; TRPM5- and GNAT3-positive cells were not found. Accordingly, *in silico*-analysis revealed only minimal expression of these markers in human respiratory epithelial cells, in contrast to mice. Instead, scRNAseq data pointed to the endoplasmic reticulum protein LRMP (lymphoid-restricted membrane protein) as a human brush cells marker. LRMP-Antibodies labelled rare, slender epithelial cells along the entire airways reaching deep into the lung. Our quantitative analysis of LRMP-positive cells in human airways showed lowest density of occurrence in the trachea (0.003 cells/mm BM), and the density increased toward the periphery, especially in the bronchioles (0.206 cells/mm BM). Double and triple labelling showed that they form an independent population, separate from ciliated, secretory, neuroendocrine cells and

ionocytes. In pig, multiple-labelling immunofluorescence revealed the presence of three different groups: $ChAT^+$ $villin^+$ $advillin^+$, $ChAT^-$ $villin^+$ $advillin^+$ (most frequent) and $ChAT^+$ $villin^-$ $advillin^-$ (least frequent) cells. $ChAT^+$ $villin^+$ $advillin^+$ cells extend deep into the lung with predominance in small intrapulmonary airways. RT-PCR confirmed the expression of these genes along pig airway epithelium. In mice, LRMP and TRPM5 were also localized specifically to SCCC cells, which were restricted to extrapulmonary airways. These data identify chemosensory cells in human and pig airways with predominance in small intrapulmonary airways. Their distribution along the airway tree and expression of signaling pathway proteins differ markedly from the purely extrapulmonary airways in mice. Mouse trachea mimics human small airways better than human trachea. These data present LRMP as a new marker across human and mouse.

6 Zusammenfassung

Spezialisierte Epithelzellen können im Atemtrakt von Säugetieren potenziell schädliche Substanzen wahrnehmen und daraufhin Schutzreaktionen auslösen. In der Maus sind zumindest zwei solcher Zellpopulationen bekannt: 1) neuroendokrine Zellen (Marker: PGP9.5), 2) solitäre cholinerge chemosensorische Zellen (SCCC; Synonyme: Bürstenzellen = brush cells oder tuft cells; Marker: GNAT3, PLCβ2, TRPM5). Beim Menschen sind neuroendokrine Zellen auch bekannt, die räumliche Verteilung von SCCC ist hingegen ungeklärt. Ziel der vorliegenden Arbeit war die Erhebung eines auf sensorische Signalwege und auf die Positionierung innerhalb des Atemtraktes fokussierten Inventars solcher potenziell sensorischen Zellen beim Menschen und beim Schwein im Vergleich zur Maus, dem derzeit am häufigsten eingesetzten Modellorganismus. Hierzu wurden Immunfluoreszenzeinfach- und –mehrfachmarkierungen mit Antikörpern gegen etablierte Markerproteine an Gewebeproben der Papilla vallata des Menschen (Positivkontrolle) und verschiedener Abschnitte des Respirationstrakts (Nase, Trachea, Lunge) von Körperspendern für den anatomischen Unterricht sowie von Lungen von Organspendern und im von Rahmen einer Transplantation entnommener Lungen von COPD-Patienten durchgeführt; Proben von Wildtyp- und TRPM5-eGFP-Reportermäusen wurden zur Referenz herangezogen. Weitere Mehrfachmarkierungen mit Antikörpern gegen ChAT, Villin und Advillin wurden an der Trachea und der Lunge des Schweins durchgeführt; die Ergebnisse wurden über RT-PCR validiert. Publizierte, frei zugängliche Einzelzell-mRNA-Sequenzierungsdatensätze des menschlichen Bronchial- und Trachealepithels sowie des Trachealepithels der Maus wurden *in silico* analysiert. Beim Menschen markierten PLCβ2-Antikörper Zellen in der Geschmacksknospe, aber nicht im respiratorischen Epithel. TRPM5- oder GNAT3-positive Zellen wurden nicht gefunden. Entsprechend zeigte sich in der *In silico*-Analyse, im Gegensatz zur Maus, nur eine minimale Expression dieser Marker im Epithel des Menschen. Stattdessen wiesen die Einzelzellsequenzierungsdaten auf LRMP (lymphoid-restricted membrane protein), ein Protein des endoplasmatischen Retikulums, als einen Marker humaner Bürstenzellen hin.

LRMP-Antikörper markierten seltene, schlanke Epithelzellen entlang des gesamten Atemtrakts bis tief in die Lunge. Eine quantitative Analyse zeigte die geringste Dichte solcher Zellen in der Trachea (0,003 Zellen/mm Basalmembran). Zur Lungenperipherie hin nahm die Häufigkeit zu und erreichte die höchsten Wette in Bronchioli (0,206 Zellen/mm). Immunhistochemische Doppel- und Dreifachmarkierungen erwiesen diese Zellen als eigenständige Population, abgegrenzt von zilientragenden, sekretorischen, neuroendokrinen Zellen und Ionozyten. Im Schwein ergaben immunhistochemische Mehrfachmarkierungen drei verschiedene Phänotypen: $ChAT^{+}Villin^{+}Advillin^{+}$, $ChAT^{+}Villin^{+}Advillin^{-}$ (am häufigsten) und $ChAT^{+}Villin^{-}Advillin^{-}$ (am seltensten). $ChAT^{+}Villin^{+}Advillin^{+}$-Zellen waren vorwiegend intrapulmonal zu finden und reichten tief in die Lunge. Die Expression dieser Gene im Atemwegsepithel wurde durch RT-PCR bestätigt. Auch in Mäusen waren TRPM5 und LRMP spezifisch in SCCC zu finden, deren Vorkommen war aber auf extrapulmonale Atemwege beschränkt. Diese Daten identifizieren chemosensorische Zellen in den Atemwegen von Mensch und Schwein mit einer Häufung in den kleinen intrapulmonalen Atemwegen. Die Häufigkeitsverteilung entlang des Atemwegbaums und die Expression von Komponenten des Signaltransduktionswegs differieren vom rein extrapulmonalen Auftreten dieser Zellen bei der Maus. Die Trachea der Maus ähnelt hierbei mehr den intrapulmonalen Atemwegen als der Trachea des Menschen. Die Daten etablieren LRMP speziesübergreifend als Bürstenzellmarker.

7 References

Adriaensen D, Scheuermann DW (1993): Neuroendocrine cells and nerves of the lung. In *The Anatomical record* 236 (1), 70-86.

Akasaka T, Lossos IS, Levy R (2003): BCL6 gene translocation in follicular lymphoma: a harbinger of eventual transformation to diffuse aggressive lymphoma. In *Blood* 102 (4), 1443–1448.

Azad MK, Mansy HA, Gamage PT (2016): Geometric features of pig airways using computed tomography. In *Physiological Reports* 4 (20), e12995.

Bankova LG, Dwyer DF, Yoshimoto E, Ualiyeva S, McGinty JW, Raff H, von Moltke J, Kanaoka Y, Frank Austen K, Barrett NA (2018): The cysteinyl leukotriene 3 receptor regulates expansion of IL-25-producing airway brush cells leading to type 2 inflammation. In *Science immunology* 3 (28), eaat9453.

Barham HP, Cooper SE, Anderson CB, Tizzano M, Kingdom TT, Finger TE, Kinnamon SC, Ramakrishnan VR (2013): Solitary chemosensory cells and bitter taste receptor signaling in human sinonasal mucosa. In *International forum of allergy & rhinology* 3 (6), 450–457.

Barone S, Zahedi K, Brooks M, Henske EP, Yang Y, Zhang E, Bissler JJ, Yu JJ, Soleimani M (2021): Kidney intercalated cells and the transcription factor FOXi1 drive cystogenesis in tuberous sclerosis complex. In *Proceedings of the National Academy of Sciences of the United States of America* 118 (6), e2020190118.

Baskerville A (1970): Ultrastructural Studies of the Normal Pulmonary Tissue of the Pig. In *Research in Veterinary Science* 11 (2), 150–159.

Basset F, Poirier J, Le Crom M, Turiaf J (1971): Etude ultrastructurale de l'épithélium bronchiolaire humain. In *Zeitschrift fur Zellforschung und mikroskopische Anatomie (Vienna, Austria : 1948)* 116 (3), 425–442.

Behrens TW, Jagadeesh J, Scherle P, Kearns G, Yewdell J, Staudt LM (1994): Jaw1, A lymphoid-restricted membrane protein localized to the endoplasmic reticulum. In *Journal of immunology (Baltimore, Md. : 1950)* 153 (2), 682–690.

Behrens TW, Kearns GM, Rivard JJ, Bernstein HD, Yewdell JW, Staudt LM (1996): Carboxyl-terminal targeting and novel post-translational processing of JAW1, a lymphoid protein of the endoplasmic reticulum. In *The Journal of biological chemistry* 271 (38), 23528–23534.

Bensch KG, Gordon GB, Miller LR (1965): Studies on the bronchial counterpart of the Kultschitzky (Argentaffin) cell and innervation of bronchial glands. In *Journal of ultrastructure research* 12 (5-6), 668–686.

Bergeron C, Cantin AM (2019): Cystic Fibrosis: Pathophysiology of Lung Disease. In *Seminars in respiratory and critical care medicine* 40 (6), 715–726.

Bezençon C, Fürholz A, Raymond F, Mansourian R, Métairon S, Le Coutre J, Damak S (2008): Murine intestinal cells expressing Trpm5 are mostly brush cells and express markers of neuronal and inflammatory cells. In *The Journal of comparative neurology* 509 (5), 514–525.

Boers JE, den Brok JL, Koudstaal J, Arends JW, Thunnissen FB (1996): Number and proliferation of neuroendocrine cells in normal human airway epithelium. In *American journal of respiratory and critical care medicine* 154 (3 Pt 1), 758–763.

Branchfield K, Nantie L, Verheyden JM, Sui P, Wienhold MD, Sun X (2016): Pulmonary neuroendocrine cells function as airway sensors to control lung immune response. In *Science (New York, N.Y.)* 351 (6274), 707–710.

Brand-Saberi BEM, Schäfer T (2014): Trachea: anatomy and physiology. In *Thoracic surgery clinics* 24 (1), 1–5.

Bretscher A, Weber K (1979): Villin: the major microfilament-associated protein of the intestinal microvillus. In *Proceedings of the National Academy of Sciences of the United States of America* 76 (5), 2321–2325.

Bretscher A, Weber K (1980): Villin is a major protein of the microvillus cystoskeleton which binds both G and F actin in a calcium-dependent manner. In *Cell* 20 (3), 839–847.

Brown D, Lee R, Bonventre JV (1997): Redistribution of villin to proximal tubule basolateral membranes after ischemia and reperfusion. In *The American journal of physiology* 273 (6), F1003-F1012.

Burdett E, Mitchell V (2011): Anatomy of the larynx, trachea and bronchi. In *Anaesthesia & Intensive Care Medicine* 12 (8), 335–339.

Bustamante-Marin XM, Ostrowski LE (2017): Cilia and Mucociliary Clearance. In *Cold Spring Harbor Perspectives in Biology* 9 (4), a028241.

Chang CY, Wang J, Zhao Y, Liu J, Yang X, Yue X, Wang H, Zhou F, Inclan-Rico JM, Ponessa JJ, Xie P, Zhang L, Siracusa MC, Feng Z, Hu W (2021): Tumor suppressor p53 regulates intestinal type 2 immunity. In *Nature communications* 12 (1), 3371.

Chang LY, Mercer RR, Crapo JD (1986): Differential distribution of brush cells in the rat lung. In *The Anatomical record* 216 (1), 49–54.

Chaudhari N, Roper SD (2010): The cell biology of taste. In *The Journal of cell biology* 190 (3), 285–296.

Chesler AT, Szczot M, Bharucha-Goebel D, Čeko M, Donkervoort S, Laubacher C, Hayes LH, Alter K, Zampieri C, Stanley C, Innes AM, Mah JK, Grosmann CM, Bradley N, Nguyen D, Foley AR, Le Pichon CE, Bönnemann CG (2016): The Role of PIEZO2 in Human Mechanosensation. In *The New England journal of medicine* 375 (14), 1355–1364.

Clapp TR, Stone LM, Margolskee RF, Kinnamon SC (2001): Immunocytochemical evidence for co-expression of Type III IP3 receptor with signaling components of bitter taste transduction. In *BMC neuroscience* 2, 6.

Cutz E, Chan W, Wong V, Conen PE (1975): Ultrastructure and fluorescence histochemistry of endocrine (APUD-type) cells in tracheal mucosa of human and various animal species. In *Cell and tissue research* 158 (4), 425–437.

Cutz E, Conen PE (1972): Endocrine-like cells in human fetal lungs: an electron microscopic study. In *The Anatomical record* 173 (1), 115–122.

Davis JD, Wypych TP (2021): Cellular and functional heterogeneity of the airway epithelium. In *Mucosal immunology* 14 (5), 978–990.

Deckmann K, Filipski K, Krasteva-Christ G, Fronius M, Althaus M, Rafiq A, Papadakis T, Renno L, Jurastow I, Wessels L, Wolff M, Schütz B, Weihe E, Chubanov V, Gudermann T, Klein J, Bschleipfer T, Kummer W (2014): Bitter triggers acetylcholine release from polymodal urethral chemosensory cells and bladder reflexes. In *Proceedings of the National Academy of Sciences of the United States of America* 111 (22), 8287–8292.

Deckmann K, Krasteva-Christ G, Rafiq A, Herden C, Wichmann J, Knauf S, Nassenstein C, Grevelding CG, Dorresteijn A, Chubanov V, Gudermann T, Bschleipfer T, Kummer W (2015): Cholinergic urethral brush cells are widespread throughout placental mammals. In *International immunopharmacology* 29 (1), 51–56.

Delgado-Ortega M, Olivier M, Sizaret PY, Simon G, Meurens F (2014): Newborn pig trachea cell line cultured in air-liquid interface conditions allows a partial in vitro representation of the porcine upper airway tissue. In *BMC Cell Biology* 15, 14.

Deprez M, Zaragosi LE, Truchi M, Becavin C, Ruiz García S, Arguel MJ, Plaisant M, Magnone V, Lebrigand K, Abelanet S, Brau F, Paquet A, Pe'er D, Marquette CH, Leroy S, Barbry P (2020): A Single-Cell Atlas of the Human Healthy Airways. In *American journal of respiratory and critical care medicine* 202 (12), 1636–1645.

DiMaio MF, Dische R, Gordon RE, Kattan M (1988): Alveolar brush cells in an infant with desquamative interstitial pneumonitis. In *Pediatric pulmonology* 4 (3), 185–191.

DiMaio MF, Kattan M, Ciurea D, Gil J, Dische R (1990): Brush cells in the human fetal trachea. In *Pediatric pulmonology* 8 (1), 40–44.

Drevet G, Conti M, Deslauriers J (2016): Surgical anatomy of the tracheobronchial tree. In *Journal of thoracic disease* 8 (Suppl 2), S121-9.

Dutta Banik D, Martin LE, Freichel M, Torregrossa AM, Medler KF (2018): TRPM4 and TRPM5 are both required for normal signaling in taste receptor cells. In *Proceedings of the National Academy of Sciences of the United States of America* 115 (4), E772-E781.

Dye FS, Larraufie P, Kay R, Darwish T, Rievaj J, Goldspink DA, Meek CL, Middleton SJ, Hardwick RH, Roberts GP, Percival-Alwyn JL, Vaughan T, Ferraro F, Challis BG, O'Rahilly S, Groves M, Gribble FM, Reimann F (2019): Characterisation of proguanylin expressing cells in the intestine - evidence for constitutive luminal secretion. In *Scientific Reports* 9 (1), 15574.

Dziegielewska KM, Saunders NR, Evans CA, Skacel PO, Häggendal CJ, Heiwall PO, Dahalström AB (1976): Effects of colchicine and vinblastine on axonal transport of choline acetyltransferase in rat sciatic nerve. In *Acta physiologica Scandinavica* 96 (4), 486–494.

Finger TE, Kinnamon SC (2011): Taste isn't just for taste buds anymore. In *F1000 biology reports* 3, 20.

Fréchette E, Deslauriers J (2006): Surgical anatomy of the bronchial tree and pulmonary artery. In *Seminars in thoracic and cardiovascular surgery* 18 (2), 77–84.

Frizell M, Hasselgren PO, Sjöstrand J (1970): Axoplasmic transport of acetylcholinesterase and choline acetyltransferase in the vagus and hypoglossal nerve of the rabbit. In *Experimental brain research* 10 (5), 526–531.

Garciaromeu F, Maetz J (1964): The Mechanism of Sodium and Chloride Uptake by the Gills of a Fresh-Water Fish, Carassius auratus. In *The Journal of general physiology* 47(6), 1195–1207.

Goldfarbmuren KC, Jackson ND, Sajuthi SP, Dyjack N, Li KS, Rios CL, Plender EG, Montgomery MT, Everman JL, Bratcher PE, Vladar EK, Seibold MA (2020): Dissecting the cellular specificity of smoking effects and reconstructing lineages in the human airway epithelium. In *Nature communications* 11 (1), 2485.

Gordon RE, Kattan M (1984): Absence of cilia and basal bodies with predominance of brush cells in the respiratory mucosa from a patient with immotile cilia syndrome. In *Ultrastructural pathology* 6 (1), 45–49.

Gould VE, Wiedenmann B, Lee I, Schwechheimer K, Dockhorn-Dworniczak B, Radosevich JA, Moll R, Franke WW (1987): Synaptophysin expression in neuroendocrine neoplasms as determined by immunocytochemistry. In *The American Journal of Pathology* 126 (2), 243–257.

Griese M (1999): Pulmonary surfactant in health and human lung diseases: state of the art. In *The European respiratory journal* 13 (6), 1455–1476.

Gröne HJ, Weber K, Helmchen U, Osborn M (1986): Villin--a marker of brush border differentiation and cellular origin in human renal cell carcinoma. In *The American Journal of Pathology* 124 (2), 294–302.

Gu X, Karp PH, Brody SL, Pierce RA, Welsh MJ, Holtzman MJ, Ben-Shahar Y (2014): Chemosensory functions for pulmonary neuroendocrine cells. In *American Journal of Respiratory Cell and Molecular Biology* 50 (3), 637–646.

Haworth SG, Hislop AA (1981): Adaptation of the pulmonary circulation to extra-uterine life in the pig and its relevance to the human infant. In *Cardiovascular research* 15 (2), 108–119.

Hijiya K, Okada Y, Tankawa H (1977): Ultrastructural study of the alveolar brush cell. In *Journal of electron microscopy* 26 (4), 321–329.

Höfer D, Drenckhahn D (1992): Identification of brush cells in the alimentary and respiratory system by antibodies to villin and fimbrin. In *Histochemistry* 98 (4), 237–242.

Höfer D, Drenckhahn D (1996): Cytoskeletal markers allowing discrimination between brush cells and other epithelial cells of the gut including enteroendocrine cells. In *Histochemistry and cell biology* 105 (5), 405–412.

Hogan BL, Barkauskas CE, Chapman HA, Epstein JA, Jain R, Hsia CC, Niklason L, Calle E, Le A, Randell SH, Rock J, Snitow M, Krummel M, Stripp BR, Vu T, White ES, Whitsett JA, Morrisey EE (2014):

Repair and regeneration of the respiratory system: complexity, plasticity, and mechanisms of lung stem cell function. In *Cell stem cell* 15 (2), 123–138.

Hollenhorst MI, Jurastow I, Nandigama R, Appenzeller S, Li L, Vogel J, Wiederhold S, Althaus M, Empting M, Altmüller J, Hirsch AKH, Flockerzi V, Canning BJ, Saliba AE, Krasteva-Christ G (2020): Tracheal brush cells release acetylcholine in response to bitter tastants for paracrine and autocrine signaling. In *FASEB journal : official publication of the Federation of American Societies for Experimental Biology* 34 (1), 316–332.

Horvat B, Osborn M, Damjanov I (1990): Expression of villin in the mouse oviduct and the seminiferous ducts. In *Histochemistry* 93 (6), 661–663.

Huang YH, Klingbeil O, He XY, Wu XS, Arun G, Lu B, Somerville TDD, Milazzo JP, Wilkinson JE, Demerdash OE, Spector DL, Egeblad M, Shi J, Vakoc CR (2018): POU2F3 is a master regulator of a tuft cell-like variant of small cell lung cancer. In *Genes & development* 32 (13-14), 915–928.

Iwasaki A, Foxman EF, Molony RD (2017): Early local immune defences in the respiratory tract. In *Nature reviews. Immunology* 17 (1), 7–20.

Johnson DE, Lock JE, Elde RP, Thompson TR (1982): Pulmonary neuroendocrine cells in hyaline membrane disease and bronchopulmonary dysplasia. In *Pediatric research* 16 (6), 446–454.

Johnson EW, Eller PM, Jafek BW (1997): Protein gene product 9.5-like and calbindin-like immunoreactivity in the nasal respiratory mucosa of perinatal humans. In *The Anatomical record* 247 (1), 38–45.

Judge EP, Hughes JM, Egan JJ, Maguire M, Molloy EL, O'Dea S (2014): Anatomy and bronchoscopy of the porcine lung. A model for translational respiratory medicine. In *American Journal of Respiratory Cell and Molecular Biology* 51 (3), 334–343.

Kalita A, Talukdar M, Sarma K, Kalita PC, Roychoudhury P, Kalita G, Choudhary OP, Chaudhary JK, Doley PJ, Debroy S (2021): Small intestinal mucosal cells in piglets fed with probiotic and zinc: a qualitative and quantitative microanatomical study. In *Folia morphologica* 80 (3), 605–617.

Kantarci S, Donahoe PK (2007): Congenital diaphragmatic hernia (CDH) etiology as revealed by pathway genetics. In *American journal of medical genetics. Part C, Seminars in medical genetics* 145C (2), 217–226.

Kinnamon SC, Finger TE (2019): Recent advances in taste transduction and signaling. In *F1000Research* 8.

Kotas ME, Moore CM, Gurrola JG 2nd, Pletcher SD, Goldberg AN, Alvarez R, Yamato S, Bratcher PE, Shaughnessy CA, Zeitlin PL, Zhang IH, Li Y, Montgomery MT, Lee K, Cope EK, Locksley RM, Seibold MA, Gordon ED (2022): IL-13-programmed airway tuft cells produce PGE2, which promotes CFTR-dependent mucociliary function. In *JCI Insight* 7 (13), e159832.

Krasteva G, Canning BJ, Papadakis T, Kummer W (2012): Cholinergic brush cells in the trachea mediate respiratory responses to quorum sensing molecules. In *Life Sciences* 91 (21-22), 992–996.

Krasteva G, Canning BJ, Hartmann P, Veres TZ, Papadakis T, Mühlfeld C, Schliecker K, Tallini YN, Braun A, Hackstein H, Baal N, Weihe E, Schütz B, Kotlikoff M, Ibanez-Tallon I, Kummer W (2011):

Cholinergic chemosensory cells in the trachea regulate breathing. In *Proceedings of the National Academy of Sciences of the United States of America* 108 (23), 9478–9483.

Krasteva-Christ G, Soultanova A, Schütz B, Papadakis T, Weiss C, Deckmann K, Chubanov V, Gudermann T, Voigt A, Meyerhof W, Boehm U, Weihe E, Kummer W (2015): Identification of cholinergic chemosensory cells in mouse tracheal and laryngeal glandular ducts. In *International immunopharmacology* 29 (1), 158–165.

Kwan GT, Smith TR, Tresguerres M (2020): Immunological characterization of two types of ionocytes in the inner ear epithelium of Pacific Chub Mackerel (Scomber japonicus). In *Journal of comparative physiology. B, Biochemical, systemic, and environmental physiology* 190 (4), 419–431.

Lauweryns JM, Peuskens JC (1969): Argyrophil (kinin and amine producing ?) cells in human infant airway epithelium. In *Life Sciences* 8 (11), 577–585.

Lauweryns JM, Peuskens JC (1972): Neuro-epithelial bodies (neuroreceptor or secretory organs?) in human infant bronchial and bronchiolar epithelium. In *The Anatomical record* 172 (3), 471–481.

Lauweryns JM, Peuskens JC, Cokelaere M (1970): Argyrophil, fluorescent and granulated (peptide and amine producing ?) AFG cells in human infant bronchial epithelium. Light and electron microscopic studies. In *Life Sciences* 9 (24), 1417–1429.

Lauweryns JM, van Ranst L, Lloyd RV, O'Connor DT (1987): Chromogranin in bronchopulmonary neuroendocrine cells. Immunocytochemical detection in human, monkey, and pig respiratory mucosa. In *The journal of histochemistry and cytochemistry : official journal of the Histochemistry Society* 35 (1), 113–118.

Lee RJ, Kofonow JM, Rosen PL, Siebert AP, Chen B, Doghramji L, Xiong G, Adappa ND, Palmer JN, Kennedy DW, Kreindler JL, Margolskee RF, Cohen NA (2014): Bitter and sweet taste receptors regulate human upper respiratory innate immunity. In *The Journal of clinical investigation* 124 (3), 1393–1405.

Lembrechts R, Brouns I, Schnorbusch K, Pintelon I, Timmermans JP, Adriaensen D (2012): Neuroepithelial bodies as mechanotransducers in the intrapulmonary airway epithelium: involvement of TRPC5. In *American Journal of Respiratory Cell and Molecular Biology* 47 (3), 315–323.

Madsen AM, Kurdi I, Feld L, Tendal K (2018): Airborne MRSA and Total Staphylococcus aureus as Associated With Particles of Different Sizes on Pig Farms. In *Annals of work exposures and health* 62 (8), 966–977.

Mahmoud W, Perniss A, Poharkar K, Soultanova A, Pfeil U, Hoek A, Bhushan S, Hain T, Gärtner U, Kummer W (2021): CXCL13 is expressed in a subpopulation of neuroendocrine cells in the murine trachea and lung. In *Cell and tissue research* 390(1), 35-49.

Manenti G, Galbiati F, Pettinicchio A, Spinola M, Piconese S, Leoni VP, Conti B, Ravagnani F, Incarbone M, Pastorino U, Dragani TA (2006): A V141L polymorphism of the human LRMP gene is associated with survival of lung cancer patients. In *Carcinogenesis* 27 (7), 1386–1390.

Margolskee RF (2002): Molecular mechanisms of bitter and sweet taste transduction. In *The Journal of biological chemistry* 277 (1), 1–4.

Marks PW, Arai M, Bandura JL, Kwiatkowski DJ (1998): Advillin (p92): a new member of the gelsolin/villin family of actin regulatory proteins. In *Journal of cell science* 111 (15), 2129–2136.

Matsumoto I, Ohmoto M, Narukawa M, Yoshihara Y, Abe K (2011): Skn-1a (Pou2f3) specifies taste receptor cell lineage. In *Nature Neuroscience* 14 (6), 685–687.

McDowell EM, Barrett LA, Glavin F, Harris CC, Trump BF (1978): The respiratory epithelium. I. Human bronchus. In *Journal of the National Cancer Institute* 61 (2), 539–549.

Melms JC, Biermann J, Huang H, Wang Y, Nair A, Tagore S, Katsyv I, Rendeiro AF, Amin AD, Schapiro D, Frangieh CJ, Luoma AM, Filliol A, Fang Y, Ravichandran H, Clausi MG, Alba GA, Rogava M, Chen SW, Ho P, Montoro DT, Kornberg AE, Han AS, Bakhoum MF, Anandasabapathy N, Suárez-Fariñas M, Bakhoum SF, Bram Y, Borczuk A, Guo XV, Lefkowitch JH, Marboe C, Lagana SM, Del Portillo A, Tsai EJ, Zorn E, Markowitz GS, Schwabe RF, Schwartz RE, Elemento O, Saqi A, Hibshoosh H, Que J, Izar B (2021): A molecular single-cell lung atlas of lethal COVID-19. In *Nature* 595 (7865), 114–119.

Minnich DJ, Mathisen DJ (2007): Anatomy of the trachea, carina, and bronchi. In *Thoracic surgery clinics* 17 (4), 571–585.

Montoro DT, Haber AL, Biton M, Vinarsky V, Lin B, Birket SE, Yuan F, Chen S, Leung HM, Villoria J, Rogel N, Burgin G, Tsankov AM, Waghray A, Slyper M, Waldman J, Nguyen L, Dionne D, Rozenblatt-Rosen O, Tata PR, Mou H, Shivaraju M, Bihler H, Mense M, Tearney GJ, Rowe SM, Engelhardt JF, Regev A, Rajagopal J (2018): A revised airway epithelial hierarchy includes CFTR-expressing ionocytes. In *Nature* 560 (7718), 319–324.

Morroni M, Cangiotti AM, Cinti S (2007): Brush cells in the human duodenojejunal junction: an ultrastructural study. In *Journal of anatomy* 211 (1), 125–131.

Nakakuki S (1994): Bronchial tree, lobular division and blood vessels of the pig lung. In *The Journal of veterinary medical science* 56 (4), 685–689.

Narukawa M, Minamisawa E, Hayashi Y (2009): Signalling mechanisms in mouse bitter responsive taste cells. In *Neuroreport* 20 (10), 936–940.

Nonomura K, Woo SH, Chang RB, Gillich A, Qiu Z, Francisco AG, Ranade SS, Liberles SD, Patapoutian A (2017): Piezo2 senses airway stretch and mediates lung inflation-induced apnoea. In *Nature* 541 (7636), 176–181.

Oda Y (1999): Choline acetyltransferase: the structure, distribution and pathologic changes in the central nervous system. In *Pathology international* 49 (11), 921–937.

Okuda K, Dang H, Kobayashi Y, Carraro G, Nakano S, Chen G, Kato T, Asakura T, Gilmore RC, Morton LC, Lee RE, Mascenik T, Yin WN, Barbosa Cardenas SM, O'Neal YK, Minnick CE, Chua M, Quinney NL, Gentzsch M, Anderson CW, Ghio A, Matsui H, Nagase T, Ostrowski LE, Grubb BR, Olsen JC, Randell SH, Stripp BR, Tata PR, O'Neal WK, Boucher RC (2021): Secretory Cells Dominate Airway CFTR Expression and Function in Human Airway Superficial Epithelia. In *American journal of respiratory and critical care medicine* 203 (10), 1275–1289.

Ouadah Y, Rojas ER, Riordan DP, Capostagno S, Kuo CS, Krasnow MA (2019): Rare Pulmonary Neuroendocrine Cells Are Stem Cells Regulated by Rb, p53, and Notch. In *Cell* 179 (2), 403-416.

Pan J, Zhang L, Shao X, Huang J (2020): Acetylcholine From Tuft Cells: The Updated Insights Beyond Its Immune and Chemosensory Functions. In *Frontiers in cell and developmental biology* 8, 606.

Panneck AR, Rafiq A, Schütz B, Soultanova A, Deckmann K, Chubanov V, Gudermann T, Weihe E, Krasteva-Christ G, Grau V, del Rey A, Kummer W (2014): Cholinergic epithelial cell with chemosensory traits in murine thymic medulla. In *Cell and tissue research* 358 (3), 737–748.

Patel RG (2017): Nasal Anatomy and Function. In *Facial plastic surgery* 33 (1), 3–8.

Pearse AG (1969): The cytochemistry and ultrastructure of polypeptide hormone-producing cells of the APUD series and the embryologic, physiologic and pathologic implications of the concept. In *The journal of histochemistry and cytochemistry : official journal of the Histochemistry Society* 17 (5), 303–313.

Perniss A, Liu S, Boonen B, Keshavarz M, Ruppert AL, Timm T, Pfeil U, Soultanova A, Kusumakshi S, Delventhal L, Aydin Ö, Pyrski M, Deckmann K, Hain T, Schmidt N, Ewers C, Günther A, Lochnit G, Chubanov V, Gudermann T, Oberwinkler J, Klein J, Mikoshiba K, Leinders-Zufall T, Offermanns S, Schütz B, Boehm U, Zufall F, Bufe B, Kummer W (2020): Chemosensory Cell-Derived Acetylcholine Drives Tracheal Mucociliary Clearance in Response to Virulence-Associated Formyl Peptides. In *Immunity* 52 (4), 683-699.

Perniss A, Schmidt P, Soultanova A, Papadakis T, Dahlke K, Voigt A, Schütz B, Kummer W, Deckmann K (2021): Development of epithelial cholinergic chemosensory cells of the urethra and trachea of mice. In *Cell and tissue research* 385 (1), 21–35.

Peters CH, Myers ME, Juchno J, Haimbaugh C, Bichraoui H, Du Y, Bankston JR, Walker LA, Proenza C (2020): Isoform-specific regulation of HCN4 channels by a family of endoplasmic reticulum proteins. In *Proceedings of the National Academy of Sciences of the United States of America* 117 (30), 18079–18090.

Petruson B, Hansson HA, Karlsson G (1984): Structural and functional aspects of cells in the nasal mucociliary system. In *Archives of otolaryngology* 110 (9), 576–581.

Pezzulo AA, Thurman AL, Li X, Villacreses R, Yu W, Mather SE, Romano-Ibarra GS, Meyerholz DK, Stoltz DA, Welsh MJ, Thornell IM (2021): Topography-dependent gene expression and function of common cell archetypes in large and small porcine airways. In *bioRxiv*, 2021-03.

Plasschaert LW, Žilionis R, Choo-Wing R, Savova V, Knehr J, Roma G, Klein AM, Jaffe AB (2018): A single-cell atlas of the airway epithelium reveals the CFTR-rich pulmonary ionocyte. In *Nature* 560 (7718), 377–381.

Rahman MM, Zhao M, Islam MS, Dong K, Saha SC (2021): Aerosol Particle Transport and Deposition in Upper and Lower Airways of Infant, Child and Adult Human Lungs. In *Atmosphere* 12 (11), 1402.

Rane CK, Jackson SR, Pastore CF, Zhao G, Weiner AI, Patel NN, Herbert DB, Cohen NA, Vaughan AE (2019): Development of solitary chemosensory cells in the distal lung after severe influenza

injury. In *American journal of physiology. Lung cellular and molecular physiology* 316 (6), L1141-L1149.

Reid L, Meyrick B, Antony VB, Chang LY, Crapo JD, Reynolds HY (2005): The mysterious pulmonary brush cell: a cell in search of a function. In *American journal of respiratory and critical care medicine* 172 (1), 136–139.

Rhodin J (1959): LXVII Ultrastructure of the Tracheal Ciliated Mucosa in Rat and Man. In *Ann Otol Rhinol Laryngol* 68 (4), 964–974.

Rhodin J, Dalhamn T (1956): Electron microscopy of the tracheal ciliated mucosa in rat. In *Zeitschrift fur Zellforschung und mikroskopische Anatomie* 44 (4), 345–412.

Rhodin J (1966): The ciliated cell. Ultrastructure and function of the human tracheal mucosa. In *The American review of respiratory disease* 93 (3), 1-15.

Robine S, Huet C, Moll R, Sahuquillo-Merino C, Coudrier E, Zweibaum A, Louvard D (1985): Can villin be used to identify malignant and undifferentiated normal digestive epithelial cells? In *Proceedings of the National Academy of Sciences of the United States of America* 82 (24), 8488–8492.

Rock JR, Randell SH, Hogan BL (2010): Airway basal stem cells: a perspective on their roles in epithelial homeostasis and remodeling. In *Disease models & mechanisms* 3 (9-10), 545–556.

Ruppert AL, Keshavarz M, Winterberg S, Oberwinkler J, Kummer W, Schütz B (2020): Advillin is a tuft cell marker in the mouse alimentary tract. In *Journal of molecular histology* 51 (4), 421–435.

Saunders CJ, Reynolds SD, Finger TE (2013): Chemosensory brush cells of the trachea. A stable population in a dynamic epithelium. In *American Journal of Respiratory Cell and Molecular Biology* 49 (2), 190–196.

Schütz B, Ruppert AL, Strobel O, Lazarus M, Urade Y, Büchler MW, Weihe E (2019): Distribution pattern and molecular signature of cholinergic tuft cells in human gastro-intestinal and pancreatic-biliary tract. In *Scientific Reports* 9 (1), 17466.

Scudieri P, Musante I, Venturini A, Guidone D, Genovese M, Cresta F, Caci E, Palleschi A, Poeta M, Santamaria F, Ciciriello F (2020): Ionocytes and CFTR Chloride Channel Expression in Normal and Cystic Fibrosis Nasal and Bronchial Epithelial Cells. In *Cells* 9 (9), 2090.

Shindo Y, Kim MR, Miura H, Yuuki T, Kanda T, Hino A, Kusakabe Y (2010): Lrmp/Jaw1 is expressed in sweet, bitter, and umami receptor-expressing cells. In *Chemical senses* 35 (2), 171–177.

Sieber WK (1971): Growth of the alveoli and pulmonary arteries in childhood. In *Journal of Pediatric Surgery* 6 (3), 396.

Smith CP, Carroll PT (1980): A comparison of solubilized and membrane bound forms of choline-O-acetyltransferase (EC 2.3.1.6) in mouse brain nerve endings. In *Brain research* 185 (2), 363–371.

Sponchiado M, Liao YS, Reznikov LR (2022): Identification of cholinergic cells with chemosensory traits in the porcine uterus. In *Cell and tissue research* 388 (1), 33–47.

Sui P, Wiesner DL, Xu J, Zhang Y, Lee J, Van Dyken S, Lashua A, Yu C, Klein BS, Locksley RM, Deutsch G (2018): Pulmonary neuroendocrine cells amplify allergic asthma responses. In *Science* 360 (6393), 8564.

Tandon A, Bachoo M, Weldon P, Polosa C, Collier B (1996): Effects of colchicine application to preganglionic axons on choline acetyltransferase activity and acetylcholine content and release in the superior cervical ganglion. In *Journal of neurochemistry* 66 (3), 1033–1041.

Taruno A, Vingtdeux V, Ohmoto M, Ma Z, Dvoryanchikov G, Li A, Adrien L, Zhao H, Leung S, Abernethy M, Koppel J (2013): CALHM1 ion channel mediates purinergic neurotransmission of sweet, bitter and umami tastes. In *Nature* 495 (7440), 223–226.

Tedoldi S, Paterson JC, Cordell J, Tan SY, Jones M, Manek S, Dei Tos AP, Roberton H, Masir N, Natkunam Y, Pileri SA (2006): Jaw1/LRMP, a germinal centre-associated marker for the immunohistological study of B-cell lymphomas. In *The Journal of pathology* 209 (4), 454–463.

Thaete LG, Spicer SS, Spock A (1981): Histology, ultrastructure, and carbohydrate cytochemistry of surface and glandular epithelium of human nasal mucosa. In *The American journal of anatomy* 162 (3), 243–263.

Tizzano M, Cristofoletti M, Sbarbati A, Finger TE (2011): Expression of taste receptors in solitary chemosensory cells of rodent airways. In *BMC pulmonary medicine* 11, 3.

Treuting PM, Dintzis S, Montine KS (2017): Comparative Anatomy and Histology, A Mouse, Rat, and Human Atlas, Second Edition.

Van Lommel A, Bollé T, Fannes W, Lauweryns JM (1999): The pulmonary neuroendocrine system: the past decade. In *Archives of histology and cytology* 62 (1), 1–16.

Watson JH, Brinkman GL (1964): Electron microscopy of the epithelial cells of normal and bronchitic human bronchus. In *The American review of respiratory disease* 90 (6), 851–866.

Weichselbaum M, Sparrow MP, Hamilton EJ, Thompson PJ, Knight DA (2005): A confocal microscopic study of solitary pulmonary neuroendocrine cells in human airway epithelium. In *Respiratory research* 6 (1), 115.

Wenthold RJ, Mahler HR (1975): Purification of rat brain choline acetyltransferase and an estimation of its half-life. In *Journal of neurochemistry* 24 (5), 963–967.

West AB, Isaac CA, Carboni JM, Morrow JS, Mooseker MS, Barwick KW (1988): Localization of villin, a cytoskeletal protein specific to microvilli, in human ileum and colon and in colonic neoplasms. In *Gastroenterology* 94 (2), 343–352.

Wharton J, Polak JM, Bloom SR, Ghatei MA, Solcia E, Brown MR, Pearse AG (1978): Bombesin-like immunoreactivity in the lung. In *Nature* 273 (5665), 769–770.

Yamashita J, Ohmoto M, Yamaguchi T, Matsumoto I, Hirota J (2017): Skn-1a/Pou2f3 functions as a master regulator to generate Trpm5-expressing chemosensory cells in mice. In *PloS one* 12 (12), e0189340.

Yan W, Sunavala G, Rosenzweig S, Dasso M, Brand JG, Spielman AI (2001): Bitter taste transduced by PLC-beta(2)-dependent rise in IP(3) and alpha-gustducin-dependent fall in cyclic nucleotides. In *American journal of physiology. Cell physiology* 280 (4), 742-751.

Yu W, Moninger TO, Rector MV, Stoltz DA, Welsh MJ (2022): Pulmonary neuroendocrine cells sense succinate to stimulate myoepithelial cell contraction. In *Developmental cell* 57 (18), 2221-2236.

Zhao GQ, Zhang Y, Hoon MA, Chandrashekar J, Erlenbach I, Ryba NJ, Zuker CS (2003): The Receptors for Mammalian Sweet and Umami Taste. In *Cell* 115 (3), 255–266.

Zuo WL, Rostami MR, Shenoy SA, LeBlanc MG, Salit J, Strulovici-Barel Y, O'Beirne SL, Kaner RJ, Leopold PL, Mezey JG, Schymeinsky J, Quast K, Visvanathan S, Fine JS, Thomas MJ, Crystal RG (2020): Cell-specific expression of lung disease risk-related genes in the human small airway epithelium. In *Respiratory research* 21 (1), 200.

8 Declaration

"I declare that I have completed this dissertation single-handedly without the unauthorized help of a second party and only with the assistance acknowledged therein. I have appropriately acknowledged and referenced all text passages that are derived literally from or are based on the content of published or unpublished work of others, and all information that relates to verbal communications. I have abided by the principles of good scientific conduct laid down in the charter of the Justus Liebig University of Giessen in carrying out the investigations described in the dissertation."

Giessen 2023

Dima Hamarsheh

9 Acknowledgement

I acknowledge the generous financial support from Al Balqa' Applied university and Justus Liebig University Giessen.

I would like to express my warmest thanks to my supervisor, Professor Wolfgang Kummer, who made this work possible. His guidance and advice carried me through all the stages of my project.

I would like to thank my colleagues and research group. Special thanks to Dr. Alexander perniss, Dr. Krupali Poharkar, Dr. Renate Paddenberg, Dr. Uwe Pfeil, Dr. Maryam Keshavarz, Dr. Klaus Deckmann, Dr.Ulrich Gärtner, Mrs. Petra Mermer, Ms. Silke Wiegand, Mrs. Anika Seipp, Mrs. Tamara Papadakis and Mr. Martin Bodenbenner-Türich for their extraordinary cooperation.

I am deeply grateful to Ms. Patricia Berger for her remarkable support and help from the time I started my study to the end.

Very special thanks to my husband Mahmoud Lafee, for his support and assistance in every step of my thesis. I would like to thank him for making my mind relax during the hard times of my thesis.

I would also like to give special thanks to my father (Hussein), my mother (Suhair), my daughter (Rahaf), my brothers (Mohammad, Ahmad and Ibrahim) and my husband family especially my mother-in-law (Samiha) for their continuous support and understanding when undertaking my research and writing my project.

Finally, I would like to thank God, for letting me through all the difficulties. I have experienced your guidance day by day. You are the one who let me finish my degree. I will keep on trusting you for my future.

Der Lebenslauf wurde aus der elektronischen Version der Arbeit entfernt.
The curriculum vitae was removed from the electronic version of the paper.

Work experience

14th January 2019 till now	Working group: Cardiopulmonary neurobiology, Institute for Anatomy and Cell Biology- Justus Liebig University Giessen, Giessen, Germany.
January 2017- January 2019	Anatomy Department, Faculty of Medicine, Balqa Applied University, Salt, Jordan. Full time lecturer: • **Urogenital system for 3rd year medical students** • **CNS system for 3rd year medical students** • **Gastro-intestinal system for 2nd year medical students** • **MSS system for 2nd year medical students** • **General anatomy for rehabilitation Sciences** • **General anatomy for medical students** • **General histology for medical students**
December 2013- September 2015	Medical audit at Nathealth insurance company, Amman, Jordan
January 2013- December 2013	Private Sector, Zarqa, Jordan Dentist
June 2012- December 2012	Dental Center, Zarqa Hospital, Zarqa, Jordan Internship in dental clinics

Scientific conference presentaions

Solitary chemosensory cells in the respiratory tract of man, poster, **7th Anatomy Poster Party**, Institute of Anatomy and Cell Biology, Giessen, Germany, December 2022.

Solitary chemosensory cells in the respiratory tract of man, poster. **116th Annual Meeting of the Anatomical Society**, September 2022.

Solitary chemosensory cells in the respiratory tract of man, talk. **115th Annual Meeting of the Anatomical Society**, September 2021.

Solitary chemosensory cells in the respiratory tract of man, talk, **14th Annual Giessen Graduate Center for Life Sciences Conference**, September 2021.

Solitary chemosensory cells in the respiratory tract of man, talk, **6th Anatomy Video Party**, Institute of Anatomy and Cell Biology, Giessen, Germany, December 2020.

Solitary chemosensory cells in the respiratory tract of man, talk, **13th Annual Giessen Graduate Center for Life Sciences Conference**, September 2020.

Solitary chemosensory cells in the respiratory tract of man, poster, **12th Annual Giessen Graduate Center for Life Sciences Conference**, September 2019.

Courses and workshops

28th March 2019, "Designing Digital Learning Scenarios with ILIAS" workshop, Hochschulrechenzentrum (HRZ), Justus-Liebig-University Giessen, Giessen, Germany.

28th October- 29th October 2020, "Team Management for Young Scientists", Justus-Liebig-University Giessen, Giessen, Germany.

11th March- 18th March 2021, "Molecular Biology Techniques" workshop, Kerckhoff-clinic, Bad Nauheim, Germany.

14th July- 16th July 2021, “Processing and Analysis of Scientific Images”, online course.

2nd July- 10th August 2021, “Biostatistics & R”, 40 hours course, Justus-Liebig-University Giessen, Giessen, Germany.

20th October- 21st October 2022, Practical Course “Bioinformatics”, Frankfurter Straße 98, 35392 Giessen.

Research Experience

During my research, I became familiar with the following techniques:

- Tissue Fixation, processing and sectioning for electron microscopy and for histochemical techniques.
- Immunohistochemistry
- RNA isolation, reverse transcription-polymerase chain reaction (RT-PCR) and gel electrophoreses.
- Good knowledge of microscopic techniques including light microscopy, fluorescence microscopy, confocal laser scanning microscopy and transmission electron microscopy.

Knowledge and skills

- Proficient in MS Office (Word, Excel, Outlook, PowerPoint).
- Ability to work collaboratively as a team member.
- Experienced in processing and analysis of scientific images.
- A2 German level.
- Arabic language as a mother tongue.
- Very good English language.

Memberships

- Member of Jordan Dental Association since 2012.
- Member of the German Center for Lung Research (DZL) since 2019.
- Member of the Cardiopulmonary Institute (CPI) since 2019.